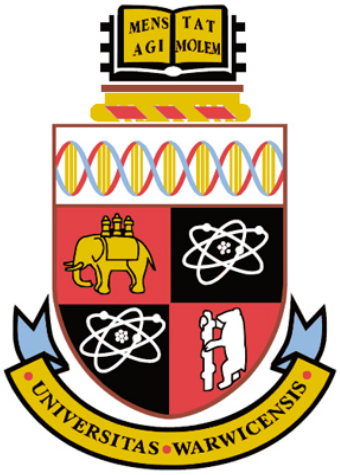

Error Correction Codes for Molecular Communication Systems

by

Yi Lu

Thesis

Submitted to the University of Warwick
for the degree of

Doctor of Philosophy

School of Engineering

October 2016

Contents

List of Tables

List of Figures

Acknowledgements

Foremost, I would like to express my deepest gratitude to my supervisors, Dr Matthew D. Higgins and Dr Mark S. Leeson for their continual guidance and support during my Ph.D. study. By working with them for the last three years, I have learnt lots of things, which I believe will benefit my future career. A special thanks to my first supervisor, Dr Matthew D. Higgins, who always believes in me, encourages me and give me the moral support during the tough times.

I would also like to thank the School of Engineering, University of Warwick for the financial support from 2013-2016. My special thanks go to Dr Yunfei Chen, Dr Adam Noel, Dr Xiayang Wang and Dr Chenyao Bai for their advice and discussions.

My sincere and warm thanks go to the members of Communication Networks Laboratory, for their help and all the happy times we spent together. I also express my thanks to my friends, especially Ying Liu and Xiaorui Zhou, for their support and care.

Last but not least, My heartfelt thanks go to my loving parents. Without their unconditional love, encouragement and support, I would not finish the Ph.D.

Declaration

This thesis is submitted in partial fulfilment for the degree of Doctor of Philosophy under the regulations set out by the Graduate School at the University of Warwick. I herewith declare that this thesis contains my own research performed under the supervision of Dr Matthew D. Higgins and Dr Mark S. Leeson, without the assistance of third parties, unless stated otherwise. No part of this thesis was previously published or submitted for a degree at any other universities.

List of Publications

Published Journals:

- **Y. Lu**, M. D. Higgins, A. Noel, M. S. Leeson, Y. Chen "The Effect of Two Receivers on Diffusion-Based Molecular Communication Systems", *IEEE Transactions on NanoBioscience*. In Press, 2016.
- **Y. Lu**, M. D. Higgins, M. S. Leeson, Y. Chen, P. Jennings "A Revised Look at the Effects of the Channel Model in Molecular Communication Systems", IET *Micro & Nano Letters*. In Press, 2016.
- **Y. Lu**, X. Wang, M. D. Higgins, A. Noel, N. Neophytou, M. S. Leeson "Energy Requirements of Error Correction Codes in Diffusion-Based Molecular Communication Systems", *Nano Communication Networks*. In Press, 2016.
- X. Wang, **Y. Lu**, M. D. Higgins, M. S. Leeson, "An Optimal Decoding Algorithm for Molecular Communications Systems with Noise, Memory, and Pulse Width", *Nano Communication Networks*, vol. 9, pp. 7-16, 2016.
- C. Bai, M. S. Leeson, M. D. Higgins, **Y. Lu** "Throughput and Energy Efficiency Based Packet Size Optimization of ARQ Protocols in Bacterial Quorum Communications", *Transactions on Emerging Telecommunications Technologies*, vol. 27, pp. 1128-1143, 2016.
- **Y. Lu,** M. D. Higgins, M. S. Leeson, "Comparison of Channel Coding Schemes for Molecular Communications Systems", *IEEE Transactions on Communications*, vol. 63, pp. 3991-4001, 2015.

Published Conferences:

- **Y. Lu**, M. D. Higgins, M. S. Leeson, "Self-Orthogonal Convolutional Codes (SOCCs) for Diffusion-Based Molecular Communication Systems", in *IEEE International Conference on Communications (ICC)*, London, 2015, pp. 1049-1053.
- **Y. Lu**, M. D. Higgins, M. S. Leeson, "Diffusion Based Molecular Communications System Enhancement Using High Order Hamming Codes", in *IEEE International Symposium on Communication Systems, Networks and Digital Signal Processing (CSNDSP)*, Manchester, 2014, pp. 438-442.

Abstract

Molecular communications (MC) is a bio-inspired paradigm that aims to utilise molecules to exchange information among nano-machines. Given the tiny devices used in a MC system and the feasibility of MC in biological environments, MC can be applied to many applications ranging from the healthcare to manufacturing fields.

In order to better realize these applications in the future, this Ph.D. research is dedicated to the investigation of a more functional, precise and reliable Diffusion-based Molecular Communications (DBMC) system. To achieve this goal, the contributions of this thesis are as follows. Firstly, the point-to-point (PTP) DBMC system with the absorbing receiver model is established and investigated. A study of the accuracy of the analytical channel model is also introduced. Secondly, dependent on different types of the transmitter (T_X) and receiver (R_X), three different communication scenarios are proposed. Thirdly, to enhance the reliability of the information at R_X, the Error Correction Codes (ECCs), as the most prominent technique is employed within the DBMC system to control or correct any errors introduced during the transmission process. Fourthly, due to the limitation of the power budget of the nano-machines, the energy efficiency of the system is also taken into account. Finally, a two-receiver broadcast DBMC system is established with an absorbing interfering receiver (R_I) and an absorbing target receiver (R_T). By analysing the performance of the communication link between T_X and R_T (target communication link), the impact of the positions of R_I on R_T is studied.

This study indicates that the application of ECCs does enhance the performance of PTP DBMC systems. In addition, the encoder and decoder design, and the BER performance are shown to be the two primary factors for selecting the most suitable ECC for the application. Finally, considering a two-receiver broadcast DBMC system with absorbing receivers, the existence of R_I does affect the performance of the target communication link which is crucial result for the field moving forward.

Nomenclature

ASK	Amplitude Shift Keying
ATP	Adenosine triphosphate
BCH	Bose, Chaudhuri and Hocquenghem
BER	Bit Error Rate
CDF	Cumulative density function
C-RM	Cyclic-Reed Muller
CSK	Concentration Shift Keying
DBMC	Diffusion-based Molecular Communications
ECC	Error Correction Code
EG-LDPC	Euclidean Geometry Low-density Parity-check
FSK	Frequency Shift Keying
GF	Galois Field
ISI	Intersymbol Interference
LCM	Lowest common multiple
MARCO	Molecular Array-based Communication
MC	Molecular communications
MEMS	Micro-electromechanical systems
MI	Mutual Information
MLG	Majority Logic Gate
MoSK	Molecule Shift Keying
MTSK	Molecular Transition Shift Keying
MIMO	Multiple-Input Multiple-Output
MUCIN	Molecular Communication Simulator
M2N	Nacro-to-nano machines
NanoNS	Nanoscale Network Simulator
NEMS	Nano-electromechanical systems
N2N	Nano-to-nano machines

N2M	Nano-to-macro machines
OOK	On-off Keying
PG-LDPC	Projective Geometry Low-density Parity-check
P-Model	Previous Model
PPM	Pulse Amplitude Modulation
PSK	Phase Shift Keying
PTP	Point to point
QAM	Quadrature Amplitude Modulation
R_I	Interfering Receiver in the two-receiver system
R_T	Target Receiver in the two-receiver system
R_X	The receiver
R-Model	Refined Model
RMSE	Root Mean Squared Error
TEC	Time-elapse Communication
T_X	The transmitter
S_1	The first receiver in the two absorbing spheres system
S_2	The second receiver in the two absorbing spheres system
SOCC	Self-orthogonal Convolutional Code
SSE	The sum of squared errors of prediction
SST	The sum of squares of the difference of the dependent variable and its mean
3D	Three-dimensional

List of Symbols

a_c	The binary value of the current symbol
$a_{c\text{-}i}$	The binary value of the i^{th} previous symbol
b	Number of input memory blocks of SOCCs
B_c	Boltzmann constant
C	Channel capacity for the system with P-Model
C_r	Channel capacity for the system with R-Model
C_{MR}	The maximum reliable transmission rate
d	Transmission distance between T_X and R_X
d_c	Critical distance
d_I	Transmission distance between T_X and R_I
d_{minH}	Minimum distance of Hamming codes
d_{minL}	Minimum distance of LDPC codes
d_{minR}	Minimum distance of C-RM codes
d_S	Transmission distance between T_X and R_X for a PTP DBMC system
d_T	Transmission distance between T_X and R_T
d_1	Transmission distance between T_X and S_1
d_2	Transmission distance between T_X and S_2
D	Diffusion coefficient
erf	Error function
erfc	Complementary error function
$erfc^{-1}$	Inverse complementary error function
E_{cH}	Error correction capability of Hamming codes
E_{cL}	Error correction capability of LDPC codes
E_{coded}	Energy consumption for an coded system
E_{cR}	Error correction capability of C-RM codes
E_{cS}	Error correction capability of SOCCs

E_{de}	Energy consumption of the decoder
E_{en}	Energy consumption of the encoder
$E_{uncoded}$	Energy consumption for an uncoded system
$g(\cdot)$	Generator polynomial
G_{coding}	Coding gain
$h(\cdot)$	Check polynomial
I	ISI length
J	Number of check sums
k_H	Information length of Hamming codes
k_L	Information length of LDPC codes
k_R	Information length of C-RM codes
k_S	Information length of SOCCs
L	Number of steps used in a majority logic decoder
m	Number of parity check bits of Hamming codes
n_E	Effective constraint length of SOCCs
n_H	Block length of Hamming codes
n_L	Block length of LDPC codes
n_R	Block length of C-RM codes
n_S	Code length of SOCCs
N_{coded}	Number of information molecules for the coded system at a chosen BER
N_i	The number of information molecules received in current time slot for the previous i^{th} emission
N_{ML}	Number of the J-input MLGs
$N_{NAND\text{-}MLGs}$	Number of NAND gates in a J-input MLG circuit
$N_{pN,i}$	The number of information molecules received in current time slot for the previous i^{th} emission for the P-Model with Normal distribution
$N_{pN,0}$	The number of molecules received in the current time slot for the current emission for P-Model with Normal distribution

$N_{\mathrm{rN},i}$	The number of information molecules received in current time slot for the previous i^{th} emission for the R-Model with Normal distribution
$N_{\mathrm{rN,T}}$	The total number of information molecules received in current time slot for the R-Model with Normal distribution
$N_{\mathrm{rN},0}$	The number of molecules received in the current time slot for the current emission for the R-Model with Normal distribution
$N_{\mathrm{rP},i}$	The number of information molecules received in current time slot for the previous i^{th} emission for the R-Model with Poisson distribution
$N_{\mathrm{rP,T}}$	The total number of information molecules received in current time slot for the R-Model with Poisson distribution
$N_{\mathrm{rP},0}$	The number of molecules received in the current time slot for the current emission for the R-Model with Poisson distribution
N_{sm}	Number of substrate molecules
$N_{\mathrm{sm\text{-}de}}$	Number of substrate molecules used in decoder
$N_{\mathrm{sm\text{-}en}}$	Number of substrate molecules used in encoder
N_{tx}	The number of molecules released at the start of each time slot
N_{T}	Total number of information molecules received in the current time slot
N_{uncoded}	Number of information molecules for the uncoded system at a chosen BER
$N_{0,i}$	The number of information molecules received during $(0, (i+1)\cdot t_s)$
N_0	The number of information molecules received in current time slot for the current emission
p_{tx}	Transmission probability of ‘1’

$P_{ca}(d,t)$	Capture probability of the information molecule at R_X
$P_{ca1,ap}$	Approximation for capture probability of S_1
$P_{ca1,ap}$	Approximation for capture probability of S_2
$P_{ca,T}$	Capture probability of R_T
P_e	Average BER
$P_{e\text{-}coded}$	BER for coded system
P_{e10}	Error probability: when a '1' is transmitted but a '0' is received
P_{e01}	Error probability: when a '0' is transmitted but a '1' is received
P_{re}	Average BER of the system with the R-Model
P_{re10}	Error probability with the R-Model: when a '1' is transmitted but a '0' is received
P_{re01}	Error probability with the R-Model: when a '0' is transmitted but a '1' is received
$P_{su}(d,t)$	Survival probability of the information molecule at R_X
P_{Te}	BER for the target communication link in the two-receiver system
Q	Number of bits transmitted used in simulation
$Q(\cdot)$	Regularized gamma function
r_H	Data rate of Hamming codes
r_L	Data rate of LDPC codes
r_R	Data rate of C-RM codes
r_S	Data rate of SOCCs
R	The radius of R_X
R_{as}	Stokes' radius of insulin
R_s^2	R-square coefficient of determination
$s(\cdot)$	Syndrome polynomial
t	Transmission time
t_s	One time slot duration
T	Absolute temperature
T_c	The condition metric of the decoding scheme

$T_{rN,c}$	The condition metrics of the decoding scheme for the R-Model with Normal distribution
$T_{rP,c}$	The condition metrics of the decoding scheme for the R-Model with Poisson distribution
$\mathbf{X}$	Binary input vector
X	Binary inputs
$\mathbf{Y}$	Binary output vector
Y	Binary outputs
z	Order of C-RM codes
τ	Pre-designed threshold
υ	Viscosity of the fluid
μ, η, ϖ	Means of the Normal distribution
σ, ς, γ	Variances of the Normal distribution
$\mathbf{B}$	The Binomial distribution
$\boldsymbol{I}$	Mutual information
$\mathbf{N}$	The Normal distribution
$\mathbf{P}$	The Poisson distribution
$\Phi(\cdot)$	Cumulative distribution function
ΔE	Energy saving for a coded system
Δt	Time step in simulation
(x_0, y_0, z_0)	Coordinate of T_X
$(0, 0, z_I)$	Coordinate of R_I
$(0, 0, z_T)$	Coordinate of R_T
∇^2	Laplace operator
'-'	Represent the positions when R_I is located to the left of both T_X and R_T
'+'	Represent the positions when R_I is between T_X and R_T
'++'	Represent the positions when R_I is located to the right of both T_X and R_T

Chapter 1
Introduction

1.1 Background

Nanotechnology is an emerging area that gives new solutions for many applications in the biomedical, environmental, industrial, military and communication engineering fields [1]. It can be viewed as the science, engineering and technology that deals with anything ranging from one to one hundred nanometers. The concept of nanotechnology was first described by the scientist Richard P. Feynman in his talk entitled “There’s Plenty of Room at the Bottom” in 1959 [2], where Feynman expresses a conjecture about how the nanotechnology will benefit people’s live. He also believed that atoms and molecules should able be controlled and manipulated by scientists, and that tiny and powerful miniaturization machines at nano-scale could be manufactured in the near future. Over a decade afterwards, the term ‘Nanotechnology’ was coined by Taniguchi, where he thinks the separation, consolidation and deformation of materials by one atom or one molecule are the main processes of the nanotechnology [3]. Then, in the 1980s, this idea was once again put forth by Drexler [4] with an in-depth explanation. In his opinion, these nano-scale machines could replicate themselves via computer control rather than human operation. Since then, the research in modern nanotechnology began to increase.

1.1.1 Nano-machines

The fabrication of machines in nano-scale is the main technique that can benefit from Nanotechnology. In general, a device that consists of nano-scale components

and able to perform a specific task, like communication, computing, sensing and data storing can be taken as a nano-machine [1]. It is also the basic functional unit for building a nanonetwork to perform more complex tasks [5].

The nano-machine can be developed by three approaches, the top-down approach, the bottom-up approach and the bio-hybrid approach [1]. For the top-down approach, the nano-machine can be built by downscaling the microelectronics without atomic level control. To achieve this, the techniques such as electron beam lithography [6] and micro-contact printing [7] are used in the manufacturing process. The components of nano-electromechanical systems (NEMS) [8] are developed by using this approach. The bottom-up approach, otherwise known as molecular manufacturing, aims to use individual molecules to build the nano-machines. Nowadays, the nano-machines, such as molecular switches and molecular shuttles are developed using this approach by the self-assembly of molecules [9]. Recently, a new manufacturing technique called the bio-hybrid approach was proposed in [10], where the existing biological nano-machines, such as nano-biosensors, nano-actuators and nano-motors are used as the basic element to develop new nano-machines. The engineered biological cell is an example that was prepared by using this approach [1].

A nano-machine can consist of one or more components dependent on its complexity level. For a functional nano-machine, the control unit, the communication unit, the reproduction unit, the power unit and the sensor and actuator unit are the five essential units [1]. The control unit can control any other components in nano-machine and gives instructions to execute the intended task [11]. The communication unit consists of a transceiver which can transmit and receive the information at the nano-level, e.g. molecules. The function of the reproduction unit is to fabricate the components using external elements and assemble these components to replicate a nano-machine. The power unit can collect energy from external sources, such as light and temperature and store it for powering all elements of the nano-machine. As the interface between the environment and the nano-machine, the sensor and actuator unit (e.g. receptors and flagellum) are used to sense the particular substance in the propagation medium and react accordingly. Several sensors and/or actuators can be included in a nano-machine.

Currently, how to handle and assemble molecular structures in a precise way is the biggest problem for developing a functional nano-machine. However, given the rapid development of manufacturing technology, the fabrication of complex nano-machines will be possible shortly.

1.1.2 Nanoscale communication

Due to the size and the simple structure of a single nano-machine, it can only execute simple tasks [1]. However, more complex tasks can be realized by the interconnection among nano-machines and allow them to cooperate and exchange information with each other, which is known as the nanonetworks [12]. The nanonetworks can enhance the functionality of the single nano-machine in several ways, such as complete more complex tasks, enhance the workspace and control the behavior of each nano-machine.

To build a nanonetwork, the communication among nano-machines must be developed. Therefore, the research regarding the communication between nano-machines has been established.

The communication between nano-machines can be realized by nano-mechanical communications [13], acoustic communications, electromagnetic communications, and molecular communications (MC) [14]. For nano-mechanical communications, the transmission of information between nano-machines is completed by mechanical contact. In this approach, a direct contact between the transmitter (T_X) and the receiver (R_X) is needed to realize the communication process. In acoustic communications, acoustic energy, such as pressure variations is used as the carrier to transmit the information from T_X to R_X. In electromagnetic communications, the information is modulated using electromagnetic waves. Finally, in MC, the molecules are used as the information carrier to be transmitted between T_Xs and R_Xs.

Of these communication schemes, MC is the most popular approach with the following advantages: firstly, the fact that the molecules have a size of the same order of magnitude as the nano-machines, thus, the emitting and collecting of molecules by nano-machines becomes feasible. Secondly, in MC, T_X and R_X do not need to be in contact like in the nano-mechanical communications. Therefore, the

transmission distance is unconstrained. Thirdly, MC, as one of the key technologies has been used in synthetic biology and bio-NEMS fields recently [15]. Finally, MC has lower heat dispersion [16], and it is more energy efficient compared with electromagnetic communications. With above reasons, the MC is becoming the most biologically suitable communication scheme and could be easily used in medical and quality control applications. Thus, the focus of this thesis is MC. More information on MC including the types of MC, related applications and current research based on MC are introduced in Chapter 2.

1.2 Open issues and challenges in MC

MC is an emerging discipline, and research in this area, both theoretical and practical, is therefore limited. In this section, the open issues and future challenges in this area are discussed in both the theoretical analysis of the MC system and the practical implementation aspects.

1.2.1 Challenges toward MC analysis

Nowadays, the mathematical modelling and theoretical analysis of the MC system have gathered lots of interest. However, the use of unrealistic assumptions and parameter settings are the main limitations of the current literature. One of the assumptions is neglecting the effects of interaction between propagation molecules on MC system performance, where the collision among propagation molecules is negligible. In that case, the factors that can affect the system performance are expected to cause an inaccurate estimation by the analytical model. Other common assumptions in this area are the precise detection and decoding mechanism at R_X and a complete synchronization mechanism between T_X and R_X [15]. Using assumptions simplifies the analysis process, but it also limits the applicability of the MC system model.

In MC system, the attenuation and distortion of the signal are the main reasons which restrict the transmission distance of MC [17]. There are several noise sources internal and external to the system because of the use of molecules as the information carrier. The internal noise sources include the interaction between the molecules, the characteristics of the molecule and extreme randomness of the

propagation route (especially for Diffusion-based MC (DBMC)). Interfering T_Xs, R_Xs and molecules are the main external noise sources. Thus, how to control or reduce the effects of the noise or how to amplify the information signal still need further investigation.

Although many mathematical MC models have been developed in recent years, the accuracy of these existing models is still unclear. What is more, the limitation of the channel capacity for MC is also unknown.

1.2.2 Challenges toward practical implementation

The implementation of MC and its application in different fields are other challenges in this field. The major concerns of this challenge are the implementation of the functional nano-machine and the implementation of the interface between different communication networks.

As a communication system, encoding, decoding, modulation, demodulation, detection and synchronization are the required functional blocks for the nano-machine to guarantee the reliability of the transmission. Furthermore, in order to maximize the utilization of the nano-machine, the techniques that can modify the functionality of the nano-machine are also required. However, due to the size of the nano-machine, the manufacturing techniques for such functional nano-machine is still in its infancy and currently does not exist.

Considering the communications between two different kinds of machines, such as the communications between nano-machine and macro/micro-machine, the hardware designs of the nano-to-macro/micro and macro/micro-to-nano interface devices are also required. These devices aim to aggregate the information that comes from nano- or macro/micro-machines, and then transmit to the macro/micro- or nano-machines, respectively. This nano-micro interfaces are considered as a hybrid devices which can enable the transmissions in both nanonetworks and conventional networks by using nano-communication techniques (e.g. molecular communication or nano-electromagnetic communication) and classical communication paradigms, respectively [18]. A potential application is a healthcare monitoring system where the nano-to-macro/micro interface device may need to transmit information from

nano-machines located in the body to an external data collection macro/micro-machine.

1.3 Motivations

As a new communication paradigm, the research in MC system has been rapidly expanding in recent years. Along with the rapid development, a series of issues, such as the accuracy of the proposed analytical model, the complexity of the system design, the lack of sufficient knowledge on MC channel, the reliability of the MC system, and in energy consumption are also exposed gradually. These problems are the main motivations of this research. On the other hand, MC may advance the existing methods in healthcare, communication technology, biological engineering, industry and environmental areas [1], [19]. Considering above reasons, MC is a convenient and beneficial research area. For now, the manufacture techniques of functional nano-machine, the design of biological circuits and the control of noise are still open problems that need time to be solved. However, it is believed that the analytical research in this area needs to be investigated early or in parallel with the practical research to get an accurate initial estimation that can benefit for future investigation.

Existing literature mostly focus on the communications between nano-machines e.g. [17, 20-25]. However, there exist the scenarios like communications between nano-machine and macro/micro-machine that can be used in the healthcare communication system. For example, the drug delivery system is such a system that a set of nano-robots guide the macro-scale drug delivery robots through emitting the specific molecules. Moreover, another example is a cardiac pacemaker as a macro-machine which communicates with nano-robots to help cardiac pacing if necessary (details are presented in Section 3.2.2).

The reliability of the transmission information at R_X is always an important concern for a communication system designer and employing Error Correction Codes (ECCs) into the communication system is an efficient way to deal with this problem. This kind of codes is widely used for improving the Bit Error Rate (BER) performance of the conventional communication system. Although the ECCs seem to be too complex to implement in a nano-machine, a substantial amount of research

is also being conducted on developing logic gates at the molecular scale or in the biological field [26], [27], [28]. Thus, the use of ECCs in the MC system is worthy of investigation, and the mathematical basis of ECCs will soon have a feasible route for implementation.

The communication model plays an important role in the theoretical analysis of the communication system. An imprecise model will cause an imprecise estimation of the system performance. Although, many communication models for the MC system have been proposed in the last few years, the investigation of the accuracy of these models is still incomplete. Thus, the accuracy of the communication model requires further study.

Given the scale of work regarding the broadcast channel in the conventional communication system, the attention to the broadcast channel in MC system is not sufficient. Recently, a lot of research focuses on the analysis of the point to point (PTP) MC system. Among current literature of broadcast MC system with absorbing receivers (description of types of receivers in MC system is given in Section 2.4), the interaction effects among receivers were not taken into account. Thus, proposing a broadcast MC system and investigating the interference among those receivers is another motivation of this research.

1.4 Objectives

This thesis aims to focus on the description of DBMC channels and evaluation of the system performance. Future studies such as improving the channel model of the MC system, enhancing the reliability of the MC system and investigating the influence between two receivers in a broadcast MC system are also the main objectives of this thesis.

The detailed description of objectives of this thesis are shown as follows:

- Performance evaluation. A PTP DBMC system is designed where the molecules are used as the information carrier to transmit information between T_X and an absorbing R_X. By investigating characteristics of the propagation and communication channels, the system performance with regards to both BER and channel capacity are evaluated.

- Intersymbol Interference (ISI) analysis. ISI as the main noise is taken into account during the theoretical analysis of the MC system. By considering an arbitrary length ISI, its effects on BER of the communication channel is investigated.
- Channel model investigation. Modeling the communication channel is one of the important parts for system performance analysis. Thus, the investigation of the MC model to provide an accurate estimation to the practical scenario is also an objective of this work.
- Reliability enhancement. In order to enhance the reliability of the MC system, ECC as a common and efficient technique is employed into the MC system. More importantly, considering the limitation in complexity and energy budget of the nano-machine, energy consumption due to the introduction of the ECCs is also need to be investigated. Through the evaluation of the BER and energy efficiency of the coded system, the designer can select the suitable codes based on their system design.
- Broadcast MC channel investigation. Another objective of this research is to provide a design of a two-receiver MC system based on a broadcast channel. The focus will be on the effect of two-receiver on broadcast MC channel and performance investigation.

1.5 Thesis outline and contributions

The structure of this thesis with a list of contributions is given as follows:

Chapter 2: State of the Art. In this chapter, a review of the existing literature of the DBMC system is provided with an overview of the topics of recent research.

Chapter 3: Point to Point Model of the Diffusion-based Molecular Communications System. In this chapter, the PTP DBMC model is provided with a description of the characteristics of the propagation and communication channel models. The contributions of this chapter are given as follows:

- The PTP DBMC system is presented with a detailed investigation of the propagation and communication channels. In addition, the discussion of the influence of parameters on the system performance is also provided in this chapter.

- Based on different types of T_Xs and R_Xs, three communication scenarios with the corresponding applications are described. This concept is applied to the analysis of the energy consumption that introduced in Chapter 4 and Chapter 6.
- An arbitrary length of ISI is introduced when analysing the channel model. The closed-form expressions of BER and channel capacity are derived, and the effect of the ISI length on the BER is also analysed.

Chapter 4: Error Correction Codes in PTP DBMC System. The use of ECCs in the PTP DBMC system is introduced in this chapter. The system performance is also investigated with regards to the BER and energy efficiency. The contributions of this chapter are given as follows:

- For the first time, the implementations of Cyclic-Reed Muller (C-RM) codes, Euclidean Geometry Low-density Parity-check (EG-LDPC) codes and Self-orthogonal Convolutional Codes (SOCCs) are introduced into MC systems.
- The Adenosine triphosphate (ATP) is used for calculating the energy consumption due to the introduction of ECCs. The expressions of energy consumption of the encoder and decoder for different ECCs are also presented.
- The performance of the coded system is also investigated with regards to the BER and energy efficiency. Moreover, the performance is compared with the uncoded system and the system that employs Hamming codes.
- Considering the system with different communication scenarios, such as the communication between nano-machine and macro/micro-machine, the energy consumption for the nano-part is also investigated.
- Finally, the critical distance, a measure of the transmission distance, at which the use of ECCs becomes beneficial is analysed under different communication scenarios.

Chapter 5: A Refined PTP DBMC Model. In this chapter, a theoretical analysis of the refined model (R-Model) for PTP DBMC is presented. In addition, the simulation process of random walk of information molecules for the three-dimensional (3D) PTP DBMC system is also described in this chapter. The contributions of this chapter are given as follows:

- A comprehensive analysis of the uncoded system performance in terms of BER is presented by introducing the refined model into the system analysis. This analysis includes an explanation, as to the issue of dependence along with a full proof from first principles of 3D diffusion.
- An arbitrary ISI length is introduced during the theoretical derivation to maximize the generality of the analysis.
- Two popular approximations of Binomial distribution – the Poisson distribution and the Normal distribution are considered in this chapter, such that the BER expressions for both approximations are provided. The Root Mean Squared Error (RMSE) is also used as a condition to determine which approximation is more suitable for a proposed PTP DBMC system.
- Finally, using those BER results obtained from theoretical analysis, the comparisons between approximations and also between the previous model (P-Model) and the R-Model are shown. The simulation results are also produced for verifying the accuracy of these channel models.

Chapter 6: A Revised Look at ECCs in PTP DBMC Systems. In this chapter, the use of ECCs in the PTP DBMC system is re-investigated by introducing the R-Model into the system analysis. The contributions of this chapter are given as follows:

- The R-Model that introduced in Chapter 5 is used for analysing the coded system to provide an accurate performance estimation.
- The system performance with respect to both BER and energy efficiency is analysed and compared with the system performance obtained in Chapter 4. The use of the R-Model is fully analysed in both uncoded system and coded system.

Chapter 7: The Effect of Two-receiver on Broadcast DBMC Systems. In order to study the effects of absorbing receivers on system performance, the broadcast MC channel is simulated and investigated in this chapter. There, the system with two absorbing receivers is introduced, one of the receivers is considered as a target receiver (R_T), and another receiver is considered as an interfering receiver (R_I). The effects of R_I on R_T can be clearly shown through the analysis of the performance of

the target link (the communication link between T_X and R_T). The contributions of this chapter are given as follows:

- A two-receiver broadcast communication channel with a 3D diffusion-based propagation model is simulated for the MC system with absorbing receivers. One of the main parameters in the performance analysis, capture probability, can be obtained via simulation.
- For the first time, the impact of the introduction of the R_I with respect to its relative location is considered by analysing the BER and channel capacity of the target communication link.

Chapter 8: Conclusions and Future Research. In Chapter 8, a summary of this thesis with an overview of the future research topics in this area is provided.

Overall, Chapter 3 focuses on the study of the performace of an un-coded PTP DBMC system and three communication scenairos and related application are introduced. Chapter 4 focuses on the study of reliablility enhancement, where the reliability of the PTP DBMC system is improved by introducing the ECCs. In order to provide an accurate estimation of system performance, in Chapter 5, an accurate communication channel model by avoding the unrealistic assumption is presented. There, an accurate channel model, R-Model, is provided by considering the dependence between the received molecules due to one transmission. In addition, the performance of an un-coded PTP DBMC system is re-analysied by considering the R-Model. Chapter 6 gives a revised look of the ECCs in PTP DBMC system by introducing the R-Model into system analysis. Considering the limited studied on broadcast model in DBMC system, in Chapter 7, a two-receiver broadcast system model is established and the analysis of the interference between receivers is also investigated.

All the programming work related to this thesis are completed by using the MATLAB simulation platform.

Chapter 2

State of the Art

2.1 Introduction

MC, as a promising area has received more and more attention in recent years, and as such the research into MC, from both theoretical and practical aspects rapidly increases. In this chapter, an overview of MC and the related literature is presented. The review focuses on four main areas that are organised as follows. In Section 2.2, the architecture of the MC system is presented. The description of selected MC mechanisms is detailed in Section 2.3. In Section 2.4, a survey of previous related work is shown. Finally, the potential application areas of MC are provided in Section 2.5.

2.2 Architecture of the MC system

A communication system aims to transmit information across space and time [16]. To achieve the communication process, a carrier signal needs to be generated and released from T_X. Then, this signal propagates through the channel to R_X where the original information can be decoded. Thus, for any communication system, it should include three main components: T_X, the communication channel, and R_X. A basic block diagram of this conventional communication system is shown in Figure 2.1.

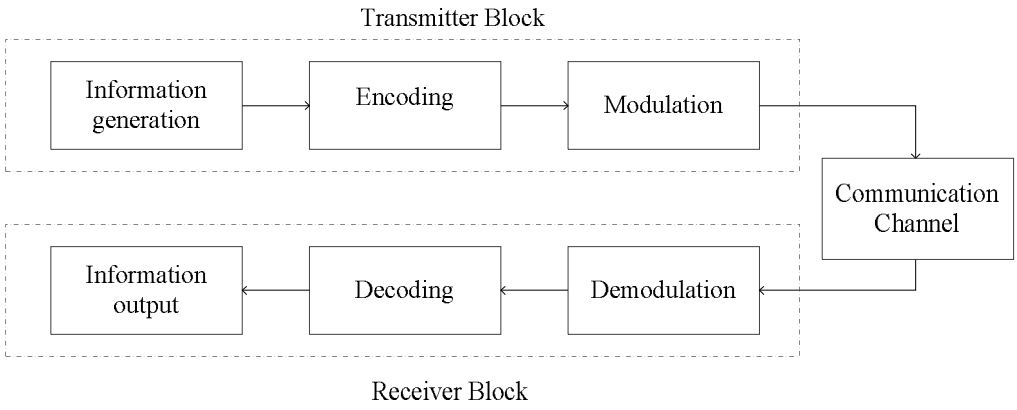

Figure 2.1: Block diagram of a basic conventional communication system.

2.2.1 Components in the MC system

In the architecture of the MC system, the three main elements can also be identified as: T_X, communication channel, and R_X. In this sense, there is no difference to a conventional system, but:

T_X: is a bio-nanomachine such as a modified living cell, a biomedical implant or a biological nano-robot, that is able to synthesise, store, and release the information molecules. The information molecules are the molecules that carry information and propagate from T_X to R_X. As an information molecule, it should have three characteristics: firstly, it will have a predefined external structure which will be easily recognised at R_X. Secondly, it should be chemically stable and be able to distinguish between the environment noise and interference molecules. Thirdly, the kind of molecules if needed should move independently in the medium. Finally, they should be easily eliminated to avoid any side-effects for the decoding process in R_X. In nature, endocrine hormones and DNA molecules [29] are the candidates of the information molecule. Another purpose of T_X is modulating the information using molecules. Many modulation techniques for the MC system have been proposed and they will be discussed in Section 2.4. At the final stage, the information molecules will be released from T_X. The releasing process is similar to the exocytosis process that is shown in Figure 2.2(a). There, the information molecules are carried by the vesicles that are located in T_X. These vesicles fuse with the surface of T_X, and then the information molecules are released into the medium.

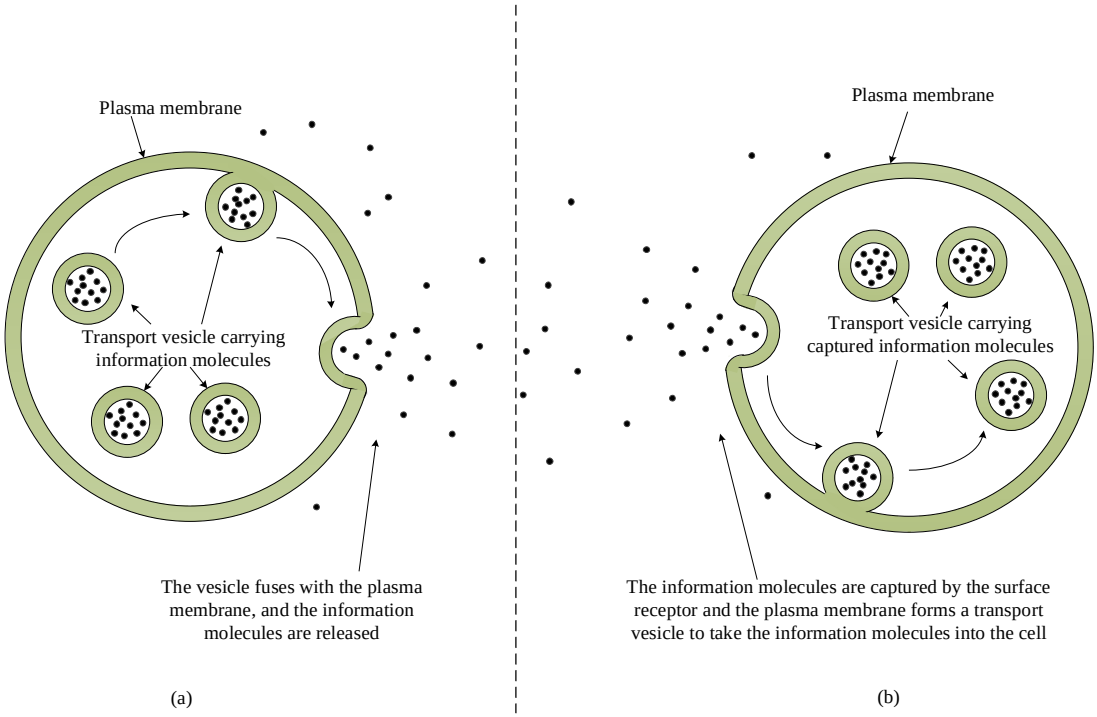

Figure 2.2: (a) Exocytosis process and (b) endocytosis process. Adapted from [30].

In addition, for a complex T_X, it may contain encoding techniques to enhance the reliability and security of the transmission information.

Communication channel: In MC, the transmission process can be realized by using different propagation mechanisms. The propagation mechanism provides a path for transmitting information molecules from T_X to R_X. Different propagation mechanisms may be used for different applications. A detailed description of three main mechanisms is discussed in Section 2.3.

R_X: is another bio-nanomachine. It aims to capture the information molecules from the surrounding area and then recover the original information. Corresponding decoding techniques to the ones used in T_X may be included. The capturing process of R_X is similar to the endocytosis process shown in Figure 2.2(b). On the surface of R_X, there are receptors to recognise a specific type of molecule, and this kind of receptors is common in most of the biological cells. When the information molecules are captured by R_X, they need to be demodulated and decoded if needed. The demodulation process can be achieved by measuring the concentration or number of captured information molecules and after these processes, the original information should be recovered.

2.2.2 Comparison between the MC system and the conventional communication system

The MC system shows different characteristics compared with conventional communication systems. A summary of main differences between the MC system and the conventional communication system is given in Table 2.1.

Table 2.1: The differences between the MC system and the conventional communication system.

Communication system / Features	Conventional Communication	MC
Information type [31]	Electronic and optical	Chemical
Information carrier [1]	Electromagnetic, acoustic or optical waves	Molecules
Devices [31]	Electronic device	Bio-nanomachine
Propagation speed [31]	Light (3×10^8 m/s)	Extremely low for DBMC (a few μm/s)
Propagation range [32]	Long (m ~ km)	Short (nm ~ m)
Propagation environment [31]	Airborne and cable	Aqueous
Noise source [1]	Electromagnetic fields and signals	Molecules in medium, diffusive
Behaviour of receivers [32]	Decoding digital information	Biochemical reaction
Energy consumption [31]	High	Extremely Low

The detailed comparisons are as follows [1], [33], [19]:

- Unlike conventional communications that utilise electromagnetic, acoustic or optical waves as the information carrier, in the MC, the information is encoded using molecules. Thus a chemical signal is carried by molecules to transmit from T_X to R_X.
- In the MC system, T_X and R_X are biological nano-machines. In contrast, the artificial devices, such as electronic circuits are used in the conventional communication system.
- The propagation speed of electromagnetic waves is much faster than the speed of propagation in pure diffusion of molecules. However, it is possible to increase the propagation speed by introducing flow into the environment

[16]. The transmission of molecules is a physical process. Thus, they are easier to be limited by the environmental conditions (e.g. temperature). The propagation speed of the MC is also dependent on the different propagation mechanisms used. In addition, due to the unpredictable movement of information molecules, the time of the molecules reach the receiver is different, and information molecules may degrade in the environment, thus they may not be received [19].

- Noise in conventional communications can be defined as an undesired signal overlapping with the information signal. In MC, the undesired signal (like molecules in the environment or released by other T_Xs) is also one of the reasons leads to an incorrect detection at R_X. Another type of noise is the interaction between the information molecules and the molecules existing in the environment. This undesired reaction may modify the structure of the information molecule. Thus, they can not be recognized by R_X. In addition, different temperatures of the environment will introduce different levels of stochastic thermal motion of bio-nanomachines and information molecules [34]. This thermal noise can affect the accuracy of the detection.
- Electrical power such as batteries, electromagnetic induction are used to drive conventional communication processes. However, in the MC, most of the communication processes are chemical processes which lead a lower energy consumption compare with the conventional communication. Furthermore, the materials and processes from the biological system can be reused to increase the energy efficiency of the MC [31].

2.3 MC types

Based on different propagation schemes, the MC types can be divided into three categories [1], which are the walkway-based MC [35], [36], [37], the advection-based MC [21] and the diffusion-based MC [23], [38], [39]. Among these schemes, the walkway-based and the diffusion-based propagations are the least and the most spontaneous process, respectively.

In walkway-based MC, the information molecules propagate through active transports. For this type of MC, the pathway between T_X and R_X is pre-designed. An

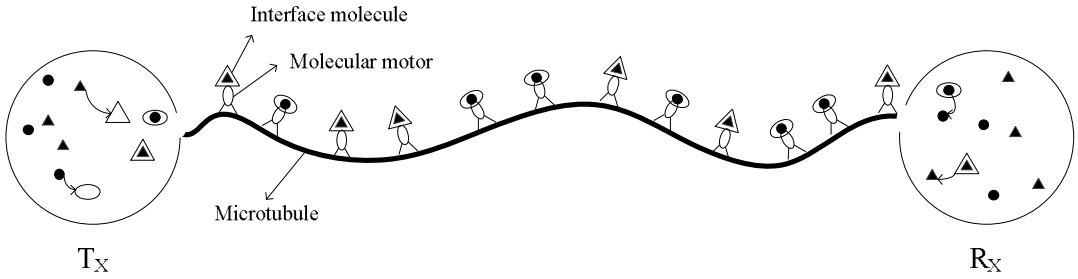

Figure 2.3: Walkway-based MC using molecular motors transport mechanism. Adapted from [30].

example is using molecular motors as the guide and transport mechanism for transmitting information molecules [36], [40], [41]. As shown in Figure 2.3, the information molecules are carried by molecular motors moving along a single protein filament chain which is made up of microtubules. There is another approach for this type of MC, where the information molecules are carried by microtubules and propelled by molecular motors and will be absorbed on a flat surface between T_X and R_X. This type of MC is normally used for intra- or inter-cell communications.

For advection-based MC, the molecules propagate through diffusion in a fluidic medium. It can be realized by using carrier entities whose motion is constrained by specific paths. The use of gap junction [42], [43], [44] (see Figure 2.4(a)) and self-propelled microorganism [45], [46], [47] (e.g. bacteria, see Figure 2.4(b)) as the transport mechanisms are two examples of the advection-based MC. The gap junction channel can transmit the diffused information molecules from T_X to R_X through contacted cells. In addition, selectivity and permeability are two properties of the gap junction channel, which can be used for realizing future functionalities, like filtering and switching. For a bacteria channel, the information is inserted into bacteria in T_X. The bacteria is guided towards to its location by attractant molecules that are released from R_X. This channel is designed based on chemotaxis phenomenon where the bacteria follow the gradient of attractant molecules, and once the bacteria reach the capturing area of R_X, the bacteria with information can be detected and the original information can be obtained.

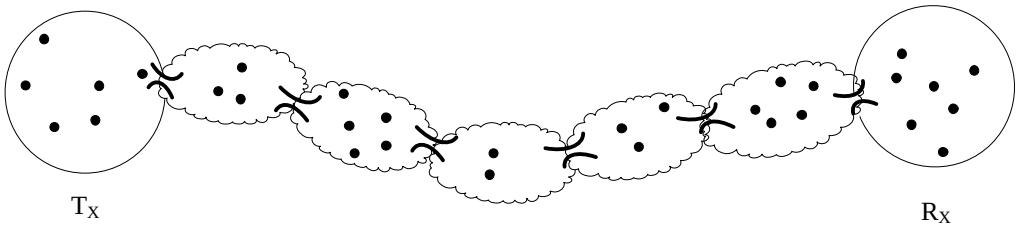

(a)

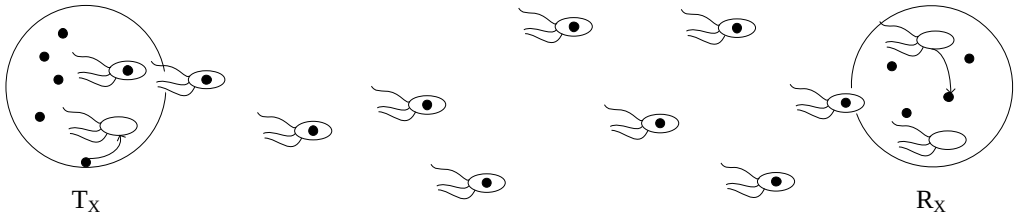

(b)

Figure 2.4: Advection-based MC (a) gap junction channel transport mechanism (b) bacteria transport mechanism. Adapted from [30].

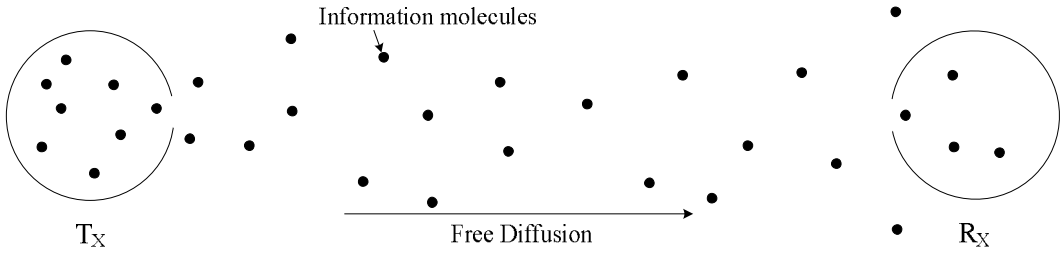

Figure 2.5: MC by the free diffusion of molecules, DBMC.

In DBMC, the information molecules propagate through their spontaneous diffusion in the medium [1], [48], [19]. This approach is illustrated in Figure 2.5, where the information molecules are emitted by T_X and then freely diffuse in the medium. The arriving information molecules will be detected and decoded at R_X, after that, the original information can be recovered.

The focus of this thesis is on DBMC, the reasons for this choice are detailed below. Amongst the above MC types, the diffusion of molecules is considered as the most basic method to describe the molecular propagation process. In the molecular motor transport mechanisms, the diffusion is considered as an unavoidable

propagation effect [41]. The bacteria in the bacteria transport mechanism are also subject to a random walk with the same rules of a biased molecular diffusion [47]. Furthermore, the DBMC exist widely in nature. For example, calcium signalling among cells [21], the synaptic transmission between neurons [49] and the pheromone communication between mammals [50]. Furthermore, unlike the molecular motor and bacteria transport mechanism, the free diffusion of molecules is not restricted to the types of the carrier.

2.4 Previous work on DBMC

A basic structure of the DBMC system is illustrated in Figure 2.5. It can be seen that the transmission process can be divided into three phases: the first phase is the emission of the information molecules. In this phase, the information molecules are released into the propagation medium. The second phase is the diffusion of the information molecules, where the information molecules spontaneously diffuse in the medium without using chemical energy. The last phase is the reception of information molecules at the receiver. The receiver used here is assumed as a perfect absorbing receiver.

In this section, a review of the existing literature and achievements of DBMC are presented. These achievements are separated into two aspects: firstly, the theoretical research on DBMC. Secondly, the implementation research on DBMC.

2.4.1 Theoretical research on DBMC

Although MC has existed in nature for billions of years, the study of MC in the communication engineering context began in 2006 [51]. Since then, the research into engineering MC systems has a rapid increase. The MC literature in theoretic analysis can be categorized into four parts: modulation techniques, channel models, types of receiver, simulation tools of MC and other related work. Each one will be presented in turn.

A. Modulation techniques

Modulation is the process that inserts the information signal into a carrier signal which can be physically transmitted in the channel. Different modulation techniques can be achieved by modifying one or more properties of the carrier signal.

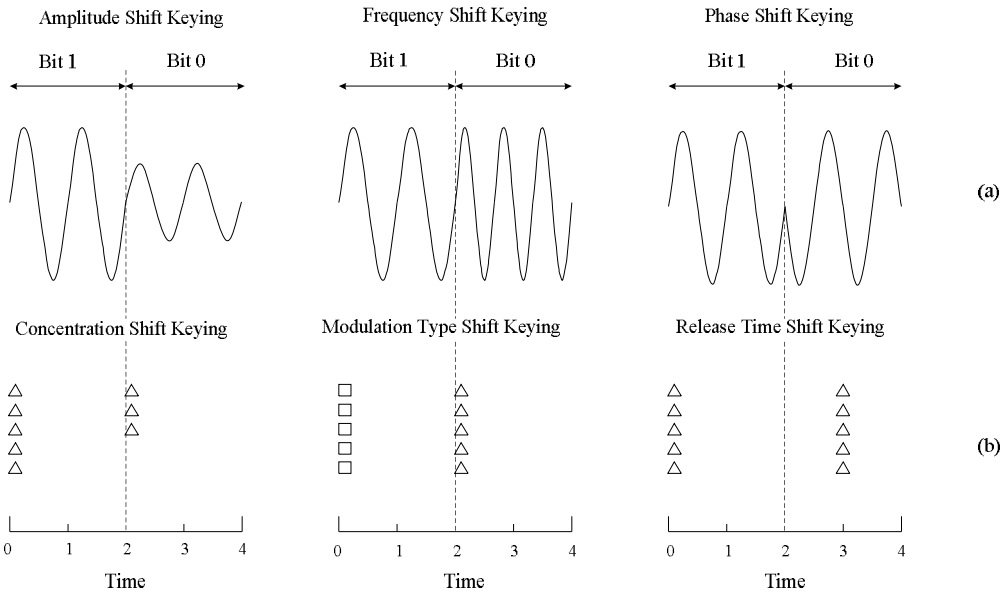

Figure 2.6: Modulation techniques for (a) conventional communications and (b) MC. Adapted from [16].

The common digital modulation schemes used in the conventional communication system are Phase Shift Keying (PSK), Frequency Shift Keying (FSK), Amplitude Shift Keying (ASK), and Quadrature Amplitude Modulation (QAM).

In MC, molecules are used as the carrier signal. Thus, the information can be modulated based on different numbers of molecules (or the concentration of molecules if the number of released information molecules is very large), different types of molecules and different release times.

Figure 2.6(a) and (b) show the modulation of binary data (0 and 1) for the conventional communication system and the MC system, respectively.

One of the first modulation schemes for MC was shown in [52]. In this work, the author presented two concentration-based modulation techniques for DBMC. In the first technique, ‘1’ and ‘0’ are presented as the ‘presence’ and ‘absence’ of a particular kind of molecules. In this case, the information is demodulated by comparing the concentration of the received signal with a pre-designed threshold level. If the concentration of the received signal is equal or larger than the pre-designed threshold, the intended symbol is demodulated as ‘1’, otherwise demodulated as ‘0’. This modulation technique is similar to the On-off Keying (OOK) that is used in a conventional communication system. In the second

modulation technique, the concentration of the information molecules is modulated based on the varying amplitude and/or frequency of a sinusoidal signal.

Two other modulation techniques called Concentration Shift Keying (CSK) and Molecule Shift Keying (MoSK) for DBMC were proposed in [25]. In CSK, the information is modulated by different numbers of the information molecules. For example, for bit '0', n_0 information molecules are released from T_X, and for bit '1', n_1 molecules are released. At R_X, the intended symbol is demodulated as '1' if the number of received information molecules during a time slot exceeds a threshold, otherwise, demodulated as '0'. This modulation technique can be extended and used to represent x bits per symbol by using 2^x different values for the number of information molecules that are released at T_X with $2^x - 1$ threshold levels. The OOK is the simplest case of CSK. For the MoSK modulation scheme, the information is represented by using different types of molecules, for x bits information per symbol, 2^x types of molecules are needed. T_X releases one type of information molecules at the start of the time slot, and at R_X, the information bit is demodulated based on the type and also the concentration of the received information molecules during a time slot. If the concentration of this type molecules exceeds the threshold, the information bit is demodulated based on the mapping table of the bit sequence and the type of information molecules. Otherwise, an error occurs if the concentration of this type of information molecules did not exceed the threshold or other types of information molecules exceed the threshold.

Pulse Position Modulation (PPM) [53] is another modulation technique based on the emission time. In PPM, the time slot is divided into two equal slots, and transmission of bit '1' and '0' are represented by a pulse released in the first or second half, respectively.

In [54] and [55], two special modulation techniques were proposed for the use of the intra-body MC system and the on-chip bacterial communication system. Aldohexose isomers, as effective information molecules are considered for the use in the intra-body MC system. Based on this idea, the authors in [54] proposed Isomer-based CSK and Isomer-based MoSK. Furthermore, a new modulation technique called Isomer-based Ratio Shift Keying was introduced, where the information bits are modulated based on the ratio of two types of isomers. The authors in [55]

presented another release timing based modulation technique called Time-elapse Communication (TEC), where the information is represented as time units to transmit in the time interval between two consecutive transmission pulses. TEC is normally used in the on-chip bacterial communication system.

Two ISI-mitigating modulation techniques were presented in [56] and [57]. In [56], the authors proposed Molecular Transition Shift Keying (MTSK) modulation technique, where the ISI can be mitigated by combining the CSK and MoSK modulation techniques. In this scheme, two types of information molecules are used for binary transmission, the choice of which type should be used is based on the current and previously transmission bits. In [57], another ISI-mitigating modulation technique called Molecular Array-based Communication (MARCO) was presented. The design of this scheme is based on the transmission order of the information molecules from T_X. For a binary version, two types of molecules 'A' and 'B' are used, to transmit '0', T_X releases the information molecule, 'A', followed by information molecule, 'B'. Conversely, to transmit '1', the T_X releases the information molecule, 'B', followed by information molecule, 'A'.

B. Channel models

Channel modelling is one of the most basic elements when analysing the communication system. The first and also the most popular channel model of DBMC was introduced in [58], where a time slotted CSK channel was represented as a binary symmetric channel. In this work, a closed-form expression for channel capacity has also been derived. However, this research did not consider the influence of ISI. The work in [59] shown the model that the current transmitted symbol can be affected by the previous symbols. In their work, the channel was modelled as a Markov chain. Other works that considered the effect of ISI on the system performance were also shown in [60] and [61]. In [60], a Z-channel was used into the DBMC system. Moreover, in this work, the author considered a simple ISI model, where the current symbol can only be effected by the first of the previous symbols. However, in [61], a more general ISI model was applied to an additive noise channel, where the noise satisfies a Poisson-Binomial probability mass function. In [62], the degradation of molecules during the propagation process was considered in the CSK-based MC channel, and the channel capacity with the different degradation rates was

also derived. Considering the limitation of the power supply of the DBMC system, an energy model for CSK-based channel system was proposed in [23]. Based on this model, an optimal communication strategy which can maximize the channel capacity has been presented.

Another kind of channel model for DBMC was built based on the continuous solution of the partial diffusion equation [63]. One of the research considering this model was presented in [17], where the attenuation and delay function of the transmission signal were also derived by employing the circuit theory for the analysis of the transmission, diffusion, and reception processes. Furthermore, an expanded work of [17] was given in [39], where a more realistic model was proposed with a detailed mathematical analysis of the noise model.

As shown in Table 2.1, the propagation speed of MC is extremely slow, and applying flow into the transmission is an efficient way to increase the speed of propagation, related research was shown in [64], [65], [66]. A release time modulation based model was presented in [64]. In that work, an additive inverse Gaussian noise was considered during the channel analysis, and the lower and upper band of the channel capacity was derived based on this noise model.

C. Types of receiver

The receiver used in a DBMC system can be classified into two broad categories: the absorbing receiver and the non-absorbing receiver. For an absorbing receiver, there are several receptors on its surface, the information molecules can be captured by these receptors and then form chemical bonds. Thus, the detection process inside the receiver can be triggered. These information molecules are absorbed and destroyed after dissociation [67]. The literature [23], [25], [68], [69] investigated the DBMC system with this kind of receiver. For a non-absorbing receiver, the receptors on the receivers' surface are used for sensing the concertation of the arrived information molecules at a specific time, and these arrived information molecules can not be absorbed by this kind of receiver. The research in [70], [71] used this type of receiver.

D. Simulation tools development

The development of simulation platforms is such an important aspect for investigating the MC system. In DBMC, there have been many works focus on this

area. Until now, the Nanoscale Network Simulator (NanoNS) developed in C++ [72], N3Sim developed in Java [73], the BINS/BINS2 developed in Java [74], [75], [76], the Molecular Communication Simulator (MUCIN) developed in Matlab [77], have been proposed for analysis the DBMC system. Among these, the NanoNS, the BINS/BINS2 and the MUCIN support 3D diffusion. 3D simulation for the N3Sim is only available under specific conditions.

E. Other research

Coding techniques are used for the conventional communication system to control and correct errors that were introduced during the transmission process. Thus, this technique is also considered as an efficient way to enhance the performance of DBMC systems. Investigating the coding techniques in DBMC is one of the main objectives of this thesis. In Chapter 4 and Chapter 6, the use of ECCs in a DBMC system is introduced with the consideration of system performance and energy consumption. The results are shown in Chapter 4 and Chapter 6. The previous works in this area are also presented and discussed in Chapter 4.

A broadcast channel is commonly used in the conventional communication system. Due to the particular characteristics of the absorbing receivers used in the DBMC system, in this thesis, the influence of these receivers in the broadcast DBMC system is also investigated. The related literature is covered in Chapter 7.

2.4.2 Practical research on DBMC

Compared to the studies of theoretical analysis of DBMC, research on the implementation of DBMC or MC is rare. One of the research on practical implementation of the MC system was shown in [78], where, the author developed a natural system to model the intercellular communication mechanisms. More research considered cell-to-cell communication was also presented in [79] and [80]. However, these systems were designed for one information transmission. In [81], the authors presented a system which can transmit an information sequence. In their work, DNA was considered as an information carrier, and by packaging the DNA message inside a bacteriophage, the information sequence can be transmitted from T_X to R_X.

The authors in [82] developed the first tabletop MC system where short text messages can be transmitted over the free air. In this system, a spray mechanism

controlled by electronic circuits was used as T_X. At R_X, the message signal can be detected by an alcohol metal-oxide sensor. This work then was further developed and can be applied in infrastructure monitoring system [83]. Furthermore, in [84], a Multiple-Input Multiple-Output (MIMO) MC system was also developed based on [82].

2.5 Application areas of MC and nanonetworks

MC has several potential applications in the medical, healthcare, the industrial, the environmental, the military and the communication engineering fields. A general overview of these applications is given in this section.

Applications in the medical and healthcare fields are the most important aspects that can be improved by MC [85], [86], [87]. Such MC system can be constructed using a group of nano-machines which can monitor the health conditions and perform a specific therapy by communicating with each other. The envisaged applications can be shown in the targeted drug delivery system [88], the healthcare monitoring system and the immune support system. In targeted drug delivery system, the drug molecules are encapsulated in a nano-capsule and propagated in the medium. This nano-capsule can be delivered to the target location under the guiding of the nano-machine located at the target side, and then the drug molecules are released. The targeted drug delivery system can reduce the influence of drugs on non-target areas. In healthcare monitoring system, a set of nano-sensors are placed at the target area in the body, and the information of target area can be delivered into another nano-robot to give a timely treatment, i.e. releasing drug molecules. On the other hand, these nano-robots can also communicate with macro/micro-machines which located outside of the body. Thus the information can be received by the observer. The immune system can be composed by several nano-machines, these nano-machines are injected into the body to protect the organism and destroy pathogens. Each nano-machine in the immune system has a specific task, for example, some of them can be used for finding pathogens, and some of them can destroy the pathogens.

MC networks may also be used in industries to develop new materials, improve the manufacturing processes and control the quality of food. MC networks in advanced fabrics and materials could provide improved functionality, for example,

antimicrobial and stain-repeller textiles [89]. In addition, the nano-actuators have been used to improve the airflow in smart fabrics by the communication between nano-actuators and nano-sensors. Food and water quality control techniques can also take advantages of nanonetworks. The little bacteria and toxic substances in food and water cannot be detected using traditional sensors. However, they can be detected by using optical nanosensors [90]. Thus the quality of food and water can be protected.

Since nanonetworks are bio-inspired, they also can be applied to environmental fields. One of the applications is using nanonetworks into the OOK biodegradation process, where the nano-actuators can be used to detect and mark different materials. The MC can also be used for monitoring environments contaminated by toxic substances [31]. To achieve this goal, the bio-nanomachines need to be integrated into macro- or micro-scale devices to form a large-scale biosensor network [91]. Like the food and water quality control system, air pollution can also be monitored and improved by connecting nano-filters to remove harmful materials from the air [92].

Another remarkable application of nanonetworks can be found in the military field. It shows that the nanonetworks can be used on the battlefield in order to detect aggressive chemical and biological agents or monitor the performance of the soldier [93].

Chapter 3
Point to Point Model of the Diffusion-based Molecular Communications System

3.1 Introduction and related work

The main focus of this chapter is to analyse the point to point (PTP) model of the diffusion-based molecular communications (DBMC) system by theoretical analysis of the propagation and communication channel models. This model contains only one transmitter and one receiver. It is also the model used for the future analysis in Chapter 4.

In the last few years, several studies of channel models and the MC system have been presented. The PTP DBMC model has been introduced first by Atakan and Akan [58], where the system performance with regards to Bit Error Rate (BER) and channel capacity had been analysed. After that, the authors in [17] illustrated a basic design of the physical end-to-end DBMC system where the emission process, the propagation process and the reception process of the information molecules have been detailed. Then, this work had been extended in [94] with the consideration of channel memory and noise. In [25] and [54], the authors focused on the modulation techniques in MC systems and provided a theoretical analysis of the system performance. Furthermore, some simulation platforms of MC systems had also been presented. In [72], a simulation platform, Nanoscale Network Simulator (NanoNS), that focuses on the physical properties of the channel and the number of received

molecules with respect to time was proposed. In [73], the N3Sim simulation framework had been proposed, where the molecular diffusion process is simulated by employing the Brownian dynamics of molecules in a fluid medium. The propagating molecules can go in and go out of R_X without any resistance. The authors in [77] further expanded the functionality, presenting an end-to-end molecular communication simulator. This simulator can analyse the MC system under different environments and modulation schemes.

In this work, the information molecules are used as the information carrier to exchange information between the transmitter (T_X) and the receiver (R_X). These information molecules move independently and do not interact with each other. The modulation technique used here is the On-off Key (OOK) modulation scheme. It represents the information data as the presence or absence of a molecule signal that can be generated by using a specific number of information molecules within T_X. The communication channel considered here is a memory limited channel, so the current symbol can only be affected by a limited number of previous symbols. Considering an absorbing R_X, the information molecules will be absorbed and removed from the environment once they reach the capturing area of R_X. Then, the information can be demodulated by counting the number of received information molecules and comparing to a pre-designed optimal threshold.

In this chapter, a basic design of the PTP DBMC system is provided with a detailed investigation of the propagation and communication models. The closed-form expressions of the BER and channel capacity is derived as a measure of the system performance. Considering an arbitrary length Intersymbol Interference (ISI) memory channel, the effect on the BER is also investigated. Furthermore, according to different kinds of T_X and R_X, three communication scenarios are proposed with a description of the related applications.

The rest of this chapter is organised as follows. The design of the PTP DBMC system is given in Section 3.2. In Section 3.3, the system performance with regards to BER and channel capacity is analysed. The theoretical results and conclusions of this chapter are given in Section 3.4 and 3.5, respectively.

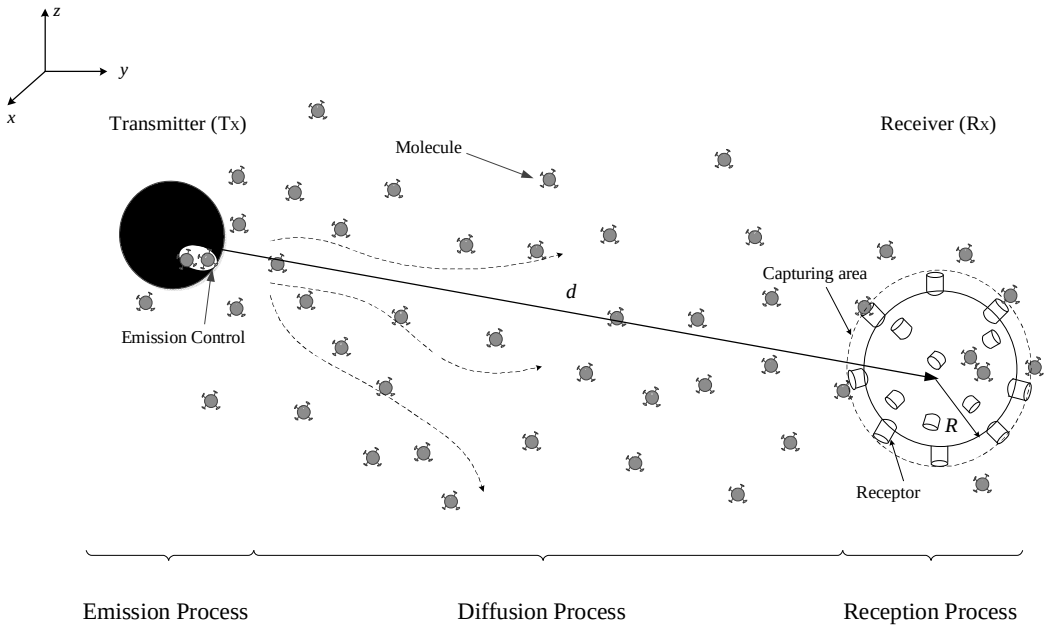

Figure 3.1: The 3D PTP DBMC system model.

3.2 The design of the PTP DBMC system

A basic design of the three-dimensional (3D) PTP DBMC system is illustrated in Figure 3.1 where only one T_X and one R_X are contained in this system. The transmitter can be considered as a functional nano-machine, where the information molecules can be modulated, encoded and released. The receiver used here is an absorbing receiver that was introduced in Section 2.4.1, when the information molecules arrive at the capturing area, they will be removed from the environment.

The transmission between T_X and R_X can be divided into three processes: the emission process, the diffusion process and the reception process, each one will be discussed in the next section.

3.2.1 Communication processes

The emission process contains two phases which are all completed in T_X. In the modulation phase, the information is translated into information molecules which can be detected by R_X. In the second phase, which is called the releasing phase, these information molecules are released from T_X into a 3D environment.

After emission from T_X, the information molecules propagate in the environment via diffusion. The diffusion of information molecules is governed by

Brownian motion. During the diffusion process, these molecules move randomly, independently and do not interact with each other.

When the information molecules arrive at the capturing area, they will be detected and absorbed by the receptor. Here, the capturing surface is considered as a sphere which has a radius the same as R_X. Within R_X, the received information molecules will be decoded and the information sent at the start of T_X can be recovered. This is known as the reception process.

3.2.2 Communication scenarios

Dependent on different types of T_X and R_X, three different communication scenarios are proposed: Scenario 1, a nano-machine communicates with a nano-machine, denoted as nano-to-nano machine (N2N) communication; Scenario 2, a nano-machine communicates with a macro/micro-machine, denoted as nano-to-macro/micro machine (N2M) communication and Scenario 3, a macro/micro-machine communicates with a nano-machine, denoted as macro/micro-to-nano machine (M2N) communication.

One of the applications that involves all three communication scenarios is the intra-body health monitoring system where the communication links are based upon the molecular diffusion process. An example is shown in Figure 3.2 which illustrates the simplified structure of an intra-body nano-network that may comprise two sizes of machines. A nano-sensor or nano-robot may be present, which is essentially a device whose components are all at the scale of a nanometre, for example targeted surgery sensors [95]. Also present may be a macro-machine which is manufactured using traditional micro-scale components, such as those found in micro-electro-mechanical systems (MEMS) [1]. For example, the macro-robot used in drug delivery mechanisms [96].

In drug delivery systems, a set of nano-robots acting as beacons located around the body, can transmit information to guide macro-scale drug delivery robots working around human blood vessels [97], [98]. Conversely, there might be applications like a macro-machine which acts as the cardiac pacemaker and needs to communicate with nano-robots. This kind of macro-machine is not designed to be

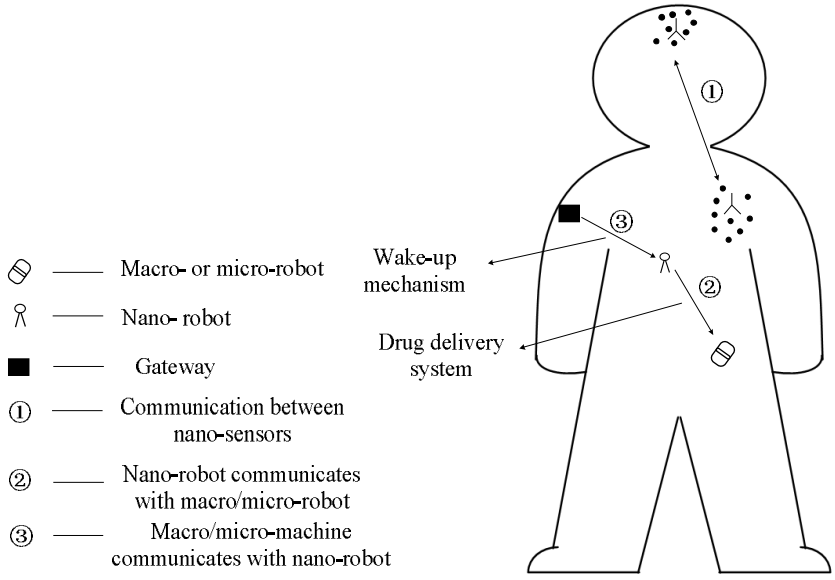

Figure 3.2: The communication scenarios of the intra-body nano-network.

mobile and most likely found on (or just under) the skin. Through emitting the information, the nano-robots can be awakened and get ready for operation.

It has been claimed that the nano-machine will most likely have to work in the nW range [99], whilst the macro-machine are effectively unconstrained in comparison.

In this thesis, three communication scenarios are considered using the same propagation and communication channel models which are introduced in the following sections.

3.2.3 Propagation model

In Section 2.3, three different MC types were described based on different propagation mechanisms. They are the walkway-based MC, the advection-based MC and the diffusion-based MC. For the first type, the information molecules propagate through a pre-designed pathway between T_X and R_X, and this pathway can be designed by using carrier substances, like molecular motors. In the advection-based MC, a fluidic medium has been used, and its flow can guide the information molecules propagation. Finally, for the diffusion-based MC, the information molecules propagate through the medium spontaneously. The focus of this thesis is towards the diffusion-based propagation model.

Considering a 3D PTP DBMC system, which is shown in Figure 3.1, the information molecules move independently, and the propagation of information molecules from T_X to R_X is governed by Brownian motion. There is the possibility that the information molecule escapes absorption by R_X, this is called the survival probability $P_{su}(d, t)$. This probability with time t satisfied the backward diffusion equation:

$$\frac{\partial P_{su}(d,t)}{\partial t} = D\nabla^2 P_{su}(d,t), \tag{3.1}$$

where ∇^2 is the Laplace operator, d is the transmission distance between the centers of the T_X and the R_X, in μm, t is the transmission time, in s, and D is the diffusion coefficient, in $\mu m^2 s^{-1}$. The value of D depends on the Boltzmann constant, the absolute temperature, the viscosity of the solution and the hydrodynamic radius of the information molecule. The initial condition and the boundary conditions of the above equation are:

$$P_{su}(d,0) = 1, \ \forall |d| > R, \tag{3.2}$$

$$P_{su}(|d| = R, t) = 0 \text{ and } P_{su}(|d| \to \infty, t) = 1 \ \forall t, \tag{3.3}$$

where, R is the radius of R_X.

Exploiting radial symmetry, the solution to (3.1) can be found at all times t:

$$P_{su}(d,t) = 1 - \frac{R}{d}\text{erfc}\left(\frac{(d-R)}{2\sqrt{Dt}}\right), \quad d > R, \ t > 0 \tag{3.4}$$

where erfc is the complementary error function.

Here, the capture ability of R_X is much more important than the survival ability of the information molecule. So the capture probability, $P_{ca}(d, t)$, can be obtained by:

$$P_{ca}(d,t) = 1 - P_{su}(d,t) = \frac{R}{d}\text{erfc}\left(\frac{(d-R)}{2\sqrt{Dt}}\right), \quad d > R, \ t > 0 \tag{3.5}$$

Figure 3.3 shows the capture probabilities for different transmission distances. The results indicate that the capture probability increases rapidly during a short time duration, and the values become stable after long time duration. Furthermore, the shorter the distance, the higher the capture probability is for a given time.

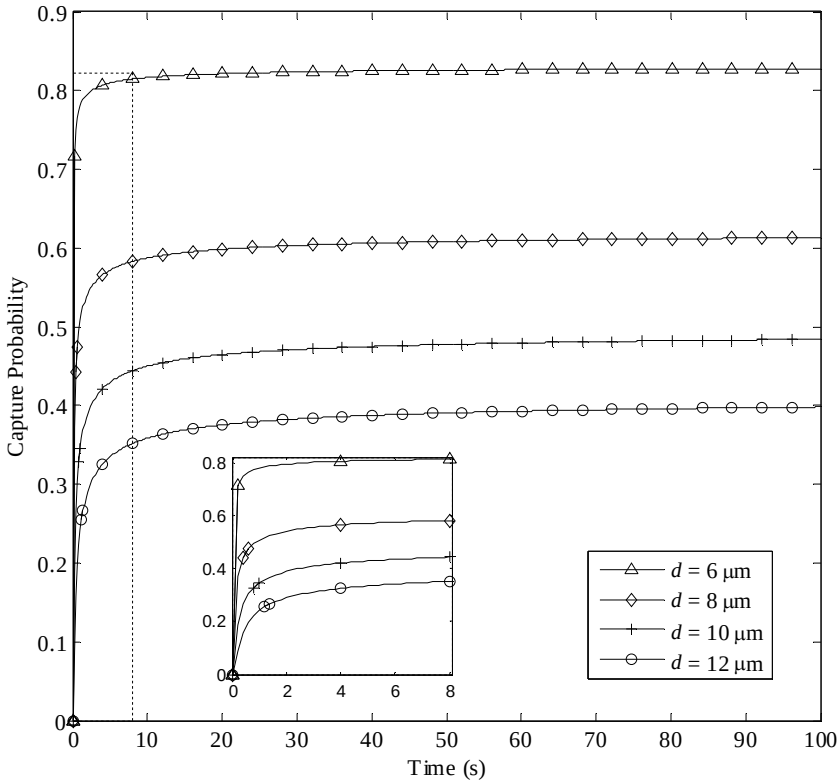

Figure 3.3: Capture probabilities with time for different transmission distance d = {6, 10, 15, 20}μm, R = 5μm and D = 79.4μm^{2}s^{-1}.

3.2.4 Communication channel model and arriving model

In agreement with the work in [23], the communication channel considered here is assumed to be a binary channel. The transmitted information is represented by a sequence of binary symbols and one symbol in each time slot, and the duration of each time slot is denoted as t_s. The modulation techniques used here is the OOK modulation scheme, for example, '1' represents a specific number of molecules released from T_X, and '0' represents no molecules released. At R_X, if the number of received molecules in an intended time slot exceeds a pre-designed threshold, τ, the symbol is denoted as '1', otherwise, it is denoted as '0' [25]. During the transmission process, errors may be introduced due to the effects of ISI which are caused by the remaining molecules from the previously transmitted symbols. Considering a memory limited channel with ISI length I, thus the current transmitted symbol can be affected by the previous I symbols.

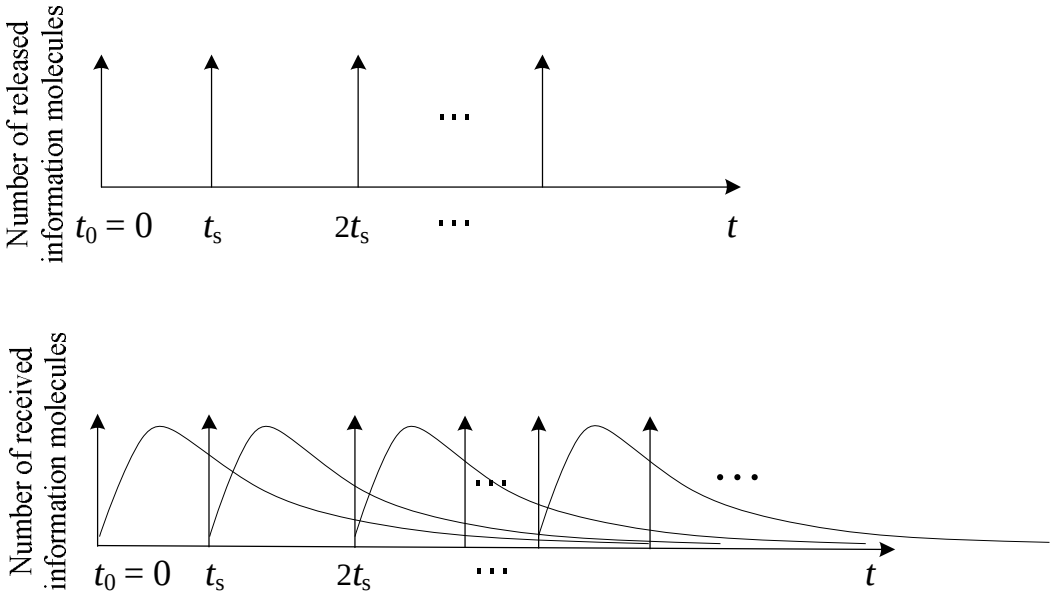

Figure 3.4: The transmission and the corresponding reception molecule signals within different time slots.

The transmission and reception molecule signals in consecutive time slots are represented in Figure 3.4. Considering that N_{tx} information molecules are released as an impulse at the start of the current time slot, and the number of molecules received among these N_{tx} molecules during the current time slot, N_0, follows a Binomial distribution given as [23]:

$$N_0 \sim \mathbf{B}\left(N_{tx}, P_{ca,0}\right), \tag{3.6}$$

where $P_{ca,0} = P_{ca}(d, t_s)$.

If N_{tx} is large enough, a Binomial distribution can be approximated by a Normal distribution, thus:

$$N_0 \sim \mathbf{N}\left(N_{tx}P_{ca,0}, N_{tx}P_{ca,0}\left(1-P_{ca,0}\right)\right). \tag{3.7}$$

The values of t_s for different distance, d, can be selected by the time at which 60% of the information molecules arrive at R_X [23].

Considering the capture probability shown in (3.5), if t goes to infinity $t \to \infty$, the capture probability gives an analytical result that an information molecule can be received by R_X:

$$P_{\mathrm{ca}}\left(d, t \to \infty\right) = \frac{R}{d}. \tag{3.8}$$

According to (3.5) and (3.8), t_s can be derived as:

$$0.6P_{\mathrm{ca}}\left(d, t \to \infty\right) = P_{\mathrm{ca}}\left(d, t_s\right),$$

$$0.6\frac{R}{d} = \frac{R}{d}\mathrm{erfc}\left(\frac{d-R}{2\sqrt{Dt_s}}\right).$$

Thus,

$$t_s = \frac{\left(d-R\right)^2}{4D\left(\mathrm{erfc}^{-1}(0.6)\right)^2}, \tag{3.9}$$

where erfc^{-1} is the inverse complementary error function.

As shown in Figure 3.4, the transmitted information molecules can not be guaranteed to reach R_X within one time slot, so the information molecules that do not reach R_X within one time slot will still exist in the environment and may arrive in future time slots.

By assuming the independence of the number of molecules received in different time slots from the same transmission. The number of information molecules that were released at the start of the i^{th} time slot before the current one and arrive in the current time slot can be denoted as N_i [23]:

$$\begin{aligned} N_i &= N_{0,i} - N_{0,i-1} \\ &\sim \mathbf{N}\left(N_{\mathrm{tx}}\left(P_{\mathrm{ca},i} - P_{\mathrm{ca},i-1}\right), N_{\mathrm{tx}}\left(P_{\mathrm{ca},i}\left(1-P_{\mathrm{ca},i}\right) + P_{\mathrm{ca},i-1}\left(1-P_{\mathrm{ca},i-1}\right)\right)\right) \\ &= \mathbf{N}\left(\eta_i, \varsigma_i\right), \end{aligned} \tag{3.10}$$

where $\eta_i = N_{\mathrm{tx}}(P_{\mathrm{ca},i} - P_{\mathrm{ca},i\text{-}1})$, $\varsigma_i = N_{\mathrm{tx}}(P_{\mathrm{ca},i}(1 - P_{\mathrm{ca},i}) + P_{\mathrm{ca},i\text{-}1}(1 - P_{\mathrm{ca},i\text{-}1}))$. $N_{0,i}$ is the number of information molecules absorbed during $(0, (i+1)\cdot t_s)$ and $N_{0,i} \sim \mathbf{N}(N_{\mathrm{tx}}P_{\mathrm{ca},i}, N_{\mathrm{tx}}P_{\mathrm{ca},i}(1 - P_{\mathrm{ca},i}))$, $P_{\mathrm{ca},i} = P_{\mathrm{ca}}(d, (i+1)\cdot t_s)$ for $i = \{1, 2, \ldots, I\}$.

Overall, the total number of information molecules received in the current time slot, N_T, composes the number of received molecules sent at the start of the current time slot, and the number of received molecules sent from the start of all I previous time slots [100]:

$$N_{\mathrm{T}} = a_{\mathrm{c}} N_0 + \sum_{i=1}^{I} a_{\mathrm{c}-i} N_i \\ \sim \mathbf{N}\left(a_{\mathrm{c}} N_{\mathrm{tx}} P_{\mathrm{ca},0} + \sum_{i=1}^{I} a_{\mathrm{c}-i}\eta_i,\ a_{\mathrm{c}} N_{\mathrm{tx}} P_{\mathrm{ca},0}\left(1-P_{\mathrm{ca},0}\right) + \sum_{i=1}^{I} a_{\mathrm{c}-i}\varsigma_i \right), \tag{3.11}$$

where $\{a_{\mathrm{c}\text{-}i},\ i = 0, 1, 2, ..., I\}$ represents the binary transmitted information sequence which includes the current and all previous I symbols.

The information is demodulated based on the number of received information molecules and the threshold, τ. For a different number of information molecules per bit, τ is different and can be selected by searching the minimum BER for $\tau \in [1, N_{\mathrm{tx}}]$. The condition metric of the demodulation scheme, $\mathrm{T_c}$, can be derived as:

$$\mathrm{T_c} = N_{\mathrm{T}} - \tau \\ \sim \mathbf{N}\left(a_{\mathrm{c}} N_{\mathrm{tx}} P_{\mathrm{ca},0} + \sum_{i=1}^{I} a_{\mathrm{c}-i}\eta_i - \tau, a_{\mathrm{c}} N_{\mathrm{tx}} P_{\mathrm{ca},0}\left(1-P_{\mathrm{ca},0}\right) + \sum_{i=1}^{I} a_{\mathrm{c}-i}\varsigma_i \right). \tag{3.12}$$

3.3 Analysis of the system performance

In this section, the BER and channel capacity are analysed based on theoretical derivation. The closed-form analytical expressions of BER and channel capacity are also presented.

3.3.1 BER analysis

The description in Section 3.2.4 shows that the ISI can introduce the errors during the transmission process. The error occurs when there is a difference between the symbol that was sent and received in the current time slot. The error can be represented in two cases: firstly, when a '0' is transmitted, but a '1' is received; and secondly, when a '1' is transmitted, but a '0' is received.

Considering the channel with an ISI length equal to I, the error patterns can be obtained by the different permutations of the previous I symbols, so the number of error patterns is 2^I. For each error pattern j, $j = \{1, 2, \ldots, 2^I\}$ is the error pattern index. The condition metric, $\mathrm{T_c}$ in (3.12) can be rewritten as:

$$\mathrm{T}_{\mathrm{c},j} = N_{\mathrm{T},j} - \tau \\ \sim \mathbf{N}\left(a_{\mathrm{c}} N_{\mathrm{tx}} P_{\mathrm{ca},0} + \sum_{i=1}^{I} a_{\mathrm{c}-i,j}\eta_i - \tau, a_{\mathrm{c}} N_{\mathrm{tx}} P_{\mathrm{ca},0}\left(1-P_{\mathrm{ca},0}\right) + \sum_{i=1}^{I} a_{\mathrm{c}-i,j}\varsigma_i \right), \tag{3.13}$$

where $\{a_{c\text{-}i,j},\ i = 1, 2, ..., I\}$ is the binary information sequence of the error pattern j, for previous I symbols.

A. When a '0' transmitted, but a '1' received

In this case, the error probability for error pattern j, $P_{e01,j}$, shows that the number of received information molecules exceeds τ, which means $T_{c,j} > 0$, so $P_{e01,j}$ can be derived as:

$$\begin{aligned} P_{e01,j} &= {p_{tx}}^{\alpha_j} \left(1 - p_{tx}\right)^{I-\alpha_j} \mathrm{P}\left(T_{c,j} > 0\right) \\ &= {p_{tx}}^{\alpha_j} \left(1 - p_{tx}\right)^{I-\alpha_j} \Phi\left(\frac{\mu_{01,j}}{\sigma_{01,j}}\right), \end{aligned} \tag{3.14}$$

where:

$$\mu_{01,j} = \sum_{i=1}^{I} a_{c-i,j}\eta_i - \tau,\ \sigma_{01,j} = \sqrt{\sum_{i=1}^{I} a_{c-i,j}\varsigma_i}. \tag{3.15}$$

p_{tx} is the transmission probability of '1' and then the transmission probability of '0' is $(1 - p_{tx})$. α_j is the number of '1's in the error pattern j. $\mathrm{P}(T_{c,j} > 0)$ is the probability of $T_{c,j} > 0$ and $\Phi(x)$ is the cumulative distribution function defined as:

$$\Phi\left(x\right) = \frac{1}{2}\left(1 + \mathrm{erf}\left(\frac{x}{\sqrt{2}}\right)\right), \tag{3.16}$$

where erf is the error function and equals to 1-erfc(x).

B. When a '1' transmitted, but a '0' received

In this case, the error probability, $P_{e10,j}$ can be derived as:

$$\begin{aligned} P_{e10,j} &= {p_{tx}}^{\alpha_j} \left(1 - p_{tx}\right)^{I-\alpha_j} \mathrm{P}\left(T_{c,j} \le 0\right) \\ &= {p_{tx}}^{\alpha_j} \left(1 - p_{tx}\right)^{I-\alpha_j} \Phi\left(-\frac{\mu_{10,j}}{\sigma_{10,j}}\right). \end{aligned} \tag{3.17}$$

where:

$$\begin{aligned} \mu_{10,j} &= N_{tx}P_{ca,0} + \sum_{i=1}^{I} a_{c-i,j}\eta_i - \tau\ , \\ \sigma_{10,j} &= \sqrt{N_{tx}P_{ca,0}\left(1 - P_{ca,0}\right) + \sum_{i=1}^{I} a_{c-i,j}\varsigma_i}. \end{aligned} \tag{3.18}$$

Thus, the average BER, P_e can be obtained by:

$$P_{\mathrm{e}} = p_{\mathrm{tx}} P_{\mathrm{e10}} + \left(1 - p_{\mathrm{tx}}\right) P_{\mathrm{e01}} = p_{\mathrm{tx}} \sum_{j=1}^{2^I} P_{\mathrm{e10},j} + \left(1 - p_{\mathrm{tx}}\right) \sum_{j=1}^{2^I} P_{\mathrm{e01},j}, \tag{3.19}$$

where P_{e01} and P_{e10} represented as:

$$P_{\mathrm{e01}} = \sum_{j=1}^{2^I} P_{\mathrm{e01},j}, P_{\mathrm{e10}} = \sum_{j=1}^{2^I} P_{\mathrm{e10},j}. \tag{3.20}$$

Table 3.1: Error probabilities for different error patterns for $I = 2$.

The previous symbols		Error pattern index	Error probabilities transmit '0', receive '1'	Error probabilities transmit '1', receive '0'
$a_{\mathrm{c-2}}$	$a_{\mathrm{c-1}}$	j	$P_{\mathrm{e01},j}$	$P_{\mathrm{e10},j}$
0	0	1	0	$\left(1-p_{\mathrm{tx}}\right)^2 \Phi\left(\frac{\tau - N_{\mathrm{tx}} P_{\mathrm{ca},0}}{\sqrt{N_{\mathrm{tx}} P_{\mathrm{ca},0}(1-P_{\mathrm{ca},0})}}\right)$
0	1	2	$p_{\mathrm{tx}}\left(1-p_{\mathrm{tx}}\right)\Phi\left(\frac{N_{\mathrm{tx}}\left(P_{\mathrm{ca},1}-P_{\mathrm{ca},0}\right)-\tau}{\sqrt{N_{\mathrm{tx}}\left[P_{\mathrm{ca},1}(1-P_{\mathrm{ca},1})+P_{\mathrm{ca},0}(1-P_{\mathrm{ca},0})\right]}}\right)$	$p_{\mathrm{tx}}\left(1-p_{\mathrm{tx}}\right)\Phi\left(\frac{\tau - N_{\mathrm{tx}} P_{\mathrm{ca},1}}{\sqrt{N_{\mathrm{tx}}\left[P_{\mathrm{ca},1}(1-P_{\mathrm{ca},1})+2P_{\mathrm{ca},0}(1-P_{\mathrm{ca},0})\right]}}\right)$
1	0	3	$p_{\mathrm{tx}}\left(1-p_{\mathrm{tx}}\right)\Phi\left(\frac{N_{\mathrm{tx}}\left(P_{\mathrm{ca},2}-P_{\mathrm{ca},1}\right)-\tau}{\sqrt{N_{\mathrm{tx}}\left[P_{\mathrm{ca},2}(1-P_{\mathrm{ca},2})+P_{\mathrm{ca},1}(1-P_{\mathrm{ca},1})\right]}}\right)$	$p_{\mathrm{tx}}\left(1-p_{\mathrm{tx}}\right)\Phi\left(\frac{\tau-N_{\mathrm{tx}}\left(P_{\mathrm{ca},2}-P_{\mathrm{ca},1}+P_{\mathrm{ca},0}\right)}{\sqrt{N_{\mathrm{tx}}\left[P_{\mathrm{ca},2}(1-P_{\mathrm{ca},2})+P_{\mathrm{ca},1}(1-P_{\mathrm{ca},1})+P_{\mathrm{ca},0}(1-P_{\mathrm{ca},0})\right]}}\right)$
1	1	4	$p_{\mathrm{tx}}^2\Phi\left(\frac{N_{\mathrm{tx}}\left(P_{\mathrm{ca},2}-P_{\mathrm{ca},0}\right)-\tau}{\sqrt{N_{\mathrm{tx}}\left[P_{\mathrm{ca},2}(1-P_{\mathrm{ca},2})+2P_{\mathrm{ca},1}(1-P_{\mathrm{ca},1})+P_{\mathrm{ca},0}(1-P_{\mathrm{ca},0})\right]}}\right)$	$p_{\mathrm{tx}}^2\Phi\left(\frac{\tau-N_{\mathrm{tx}}P_{\mathrm{ca},2}}{\sqrt{N_{\mathrm{tx}}\left[P_{\mathrm{ca},2}(1-P_{\mathrm{ca},2})+2P_{\mathrm{ca},1}(1-P_{\mathrm{ca},1})+2P_{\mathrm{ca},0}(1-P_{\mathrm{ca},0})\right]}}\right)$

Table 3.1 gives an example of different error patterns and error probabilities when $I = 2$.

3.3.2 Channel capacity

The channel capacity represents the maximum information transmission rate of a given channel. For a discrete channel, it can be computed by maximizing the Mutual Information (MI) with respect to the transmission probability of the molecular signal. Considering that the binary input and the output of the channel can be represented as $\mathbf{X} = \{X_1, X_2, \ldots, X_k\}$ and $\mathbf{Y} = \{Y_1, Y_2, \ldots, Y_k\}$. The channel capacity of a memory channel, C, can be obtained by finding the maximum value of the MI of the channel [101], [102]:

$$\mathrm{C} = \lim_{k\to\infty} \max_{p_{\mathrm{tx}}} \sum_{i=1}^{k} \frac{1}{k} \mathbf{I}\left(X_i; Y_i\right), \tag{3.21}$$

where $\boldsymbol{I}$ is the MI defined as [102]:

$$\begin{aligned} \mathbf{I}\left(X_i; Y_i\right) &= H\left(Y_i\right) - H\left(Y_i \mid X_i\right) \\ &= \mathbf{H}\left(\left(1-p_{\mathrm{tx}}\right)\left(1-P_{\mathrm{e}01}\right) + p_{\mathrm{tx}}P_{\mathrm{e}10}\right) - p_{\mathrm{tx}}\mathbf{H}\left(1-P_{\mathrm{e}10}\right) - \left(1-p_{\mathrm{tx}}\right)\mathbf{H}\left(1-P_{\mathrm{e}01}\right), \end{aligned} \tag{3.22}$$

where $\mathbf{H}(\delta) = -\delta\log_2\delta - (1-\delta)\log_2(1-\delta)$.

For a memory channel with an ISI length I, after the I^{th} symbol, the detection of emitted molecular signal will be affected by the I most recent previous signals. According to (3.14), (3.17) and (3.19), it can be deduced that the average error probability stays constant after the I^{th} symbol, thus:

$$\mathbf{I}\left(X_i; Y_i\right) = \mathbf{I}\left(X_{I+1}; Y_{I+1}\right),\ I < i \le k. \tag{3.23}$$

Therefore, for a memory limited channel, the channel capacity can be simplified as:

$$\begin{aligned} \mathrm{C} &= \lim_{k\to\infty} \max_{p_{\mathrm{tx}}} \sum_{i=1}^{k} \frac{1}{k} \mathbf{I}\left(X_i; Y_i\right) \\ &= \lim_{k\to\infty} \max_{p_{\mathrm{tx}}} \left(\sum_{i=1}^{I} \frac{1}{k} \mathbf{I}\left(X_i; Y_i\right) + \sum_{i=I+1}^{k} \frac{1}{k} \mathbf{I}\left(X_i; Y_i\right) \right) \\ &= 0 + \lim_{k\to\infty} \max_{p_{\mathrm{tx}}} \left(\frac{k-I}{k} \mathbf{I}\left(X_{I+1}; Y_{I+1}\right) \right) \\ &= \max_{p_{\mathrm{tx}}} \left(\mathbf{I}\left(X_{I+1}; Y_{I+1}\right) \right). \end{aligned} \tag{3.24}$$

Thus, by substituting (3.22) and (3.23) into (3.24), the capacity can be derived as:

$$\begin{aligned} \mathrm{C} &= \max_{p_{\mathrm{tx}}} \left(\mathbf{I}\left(X_{I+1}; Y_{I+1}\right) \right) \\ &= \max_{p_{\mathrm{tx}}} \left(\mathbf{H}\left(\left(1-p_{\mathrm{tx}}\right)\left(1-P_{\mathrm{e}01}\right) + p_{\mathrm{tx}}P_{\mathrm{e}10}\right) - p_{\mathrm{tx}}\mathbf{H}\left(1-P_{\mathrm{e}10}\right) - \left(1-p_{\mathrm{tx}}\right)\mathbf{H}\left(1-P_{\mathrm{e}01}\right) \right) \\ &= \max_{p_{\mathrm{tx}}} \Bigg(-\log_2 \Big(\left(\left(1-p_{\mathrm{tx}}\right)\left(1-P_{\mathrm{e}01}\right) + p_{\mathrm{tx}}P_{\mathrm{e}10}\right)^{\left(\left(1-p_{\mathrm{tx}}\right)\left(1-P_{\mathrm{e}01}\right) + p_{\mathrm{tx}}P_{\mathrm{e}10}\right)} \\ &\qquad \times \left(1 - \left(1-p_{\mathrm{tx}}\right)\left(1-P_{\mathrm{e}01}\right) - p_{\mathrm{tx}}P_{\mathrm{e}10}\right)^{\left(1-\left(1-p_{\mathrm{tx}}\right)\left(1-P_{\mathrm{e}01}\right) - p_{\mathrm{tx}}P_{\mathrm{e}10}\right)} \Big) \\ &\qquad + p_{\mathrm{tx}}\log_2\left(\left(1-P_{\mathrm{e}10}\right)^{\left(1-P_{\mathrm{e}10}\right)} P_{\mathrm{e}10}^{\ P_{\mathrm{e}10}}\right) + \left(1-p_{\mathrm{tx}}\right)\log_2\left(\left(1-P_{\mathrm{e}01}\right)^{\left(1-P_{\mathrm{e}01}\right)} P_{\mathrm{e}01}^{\ P_{\mathrm{e}01}}\right) \Bigg). \end{aligned} \tag{3.25}$$

3.4 Numerical results

The numerical results in terms of BER and channel capacity are presented in this section. The parameters used in the analysis are also described and analysed.

3.4.1 Parameters setup

The theoretical analysis in Section 3.3 shows that BER and channel capacity are dependent on the transmission distance, d, the radius of R_X, R, the diffusion coefficient, D, the number of released molecules per bit, N_{tx}, and the ISI length I. In this section, each parameter will be discussed in turn.

- Diffusion coefficient, D

The diffusion coefficient used during the diffusion process is considered based on insulin in water at the human body temperature [103]. Based on Stokes-Einstein equation [104], the diffusion coefficient D can be calculated as:

$$D = B_c T / 6\pi \upsilon R_{as}, \tag{3.26}$$

where the Stokes' radius of insulin R_{as} = 2.86nm, the viscosity of the fluid υ = 0.001 $kgs^{-1}m^{-1}$ and the absolute temperature T = 310K, the Boltzmann constant B_c = 1.38×10^{-23} $m^2kgs^{-2}K^{-1}$. Thus, through the calculation, D equals to 79.4μm^2s^{-1}.

- ISI length, I

As mentioned in Section 3.2.4, the previously transmitted information molecules may arrive during the current time slot which causes the ISI. Notice the complexity to compute or analyse the system performance when ISI is at infinity. Thus, a limited memory channel is considered here with an ISI length I. In order to obtain accurate results, the value of I should be taken into account.

Figure 3.5 shows the BER with number of information molecules per bit for different ISI length from 1 to 10 at a given distance and radius of R_X, where, d = 6μm and R = 5μm. As can be seen in Figure 3.5, the longer the ISI length I, the higher the BER. It can also be noted that as the ISI length increases considerably, the effect it has upon the BER becomes less prominent, i.e. the BER value begins to converge. Therefore, choosing I = 10 for analysis the channel is enough to produce an accurate result. Therefore, the following results are computed based on a limited memory channel with I = 10.

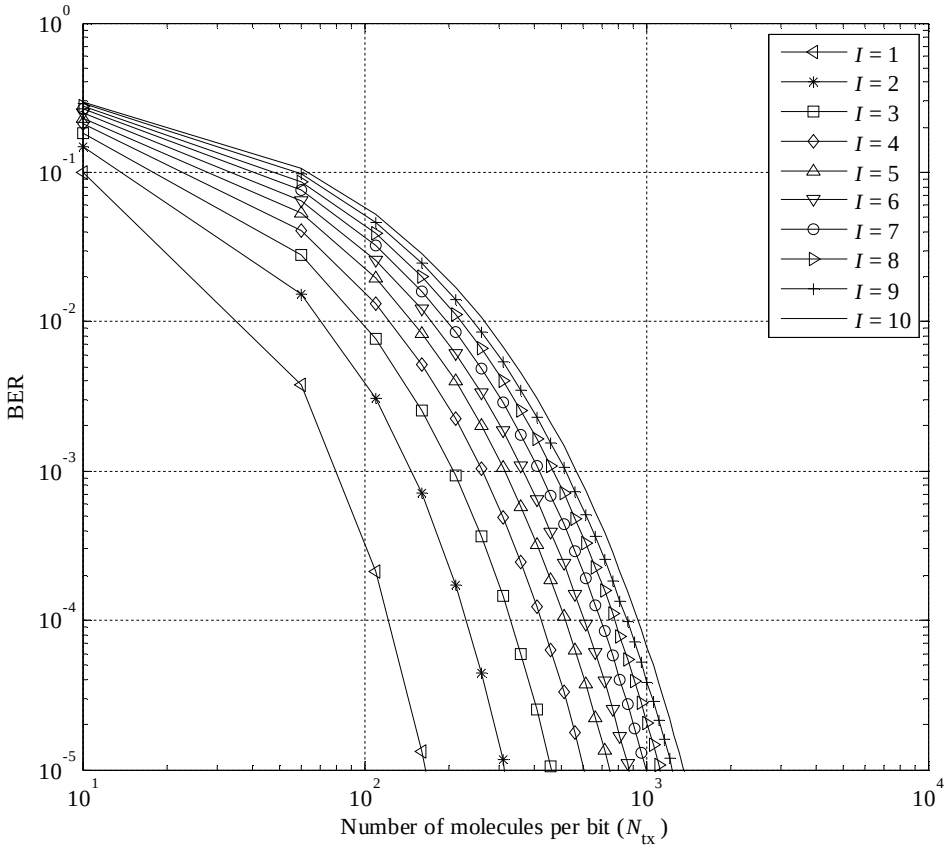

Figure 3.5: BER for different ISI length $I = \{1, 2, \ldots, 10\}$ at $d = 6\mu m$, $p_{tx} = 0.5$.

- Time slot duration, t_s

t_s is another important parameter which can affect the performance of the system. The expression of t_s is given in (3.9), where the time in which 60% of molecules arrive at R_X has been used as t_s. The advantage of this decision method is the value of t_s should be different for different transmission distances, d. Thus, it can provide an accurate result compare with the method that using a flat t_s for all transmission distances.

- Pre-designed threshold, τ

The value of the threshold used at R_X is a pre-designed threshold. It can be obtained by searching the minimum BER for a specific N_{tx} in a range $\tau \in [1, N_{tx}]$. Figure 3.6 show the values of threshold versus number of information molecules for $d = \{6, 8, 10, 12\}\mu m$ with $R = 5\mu m$, $I = 10$. It indicates that for a fixed value of N_{tx}, the value of threshold decreases as the distance increases.

Above all, the system performance presented in the following section is based on a set of parameters which are shown in Table 3.2.

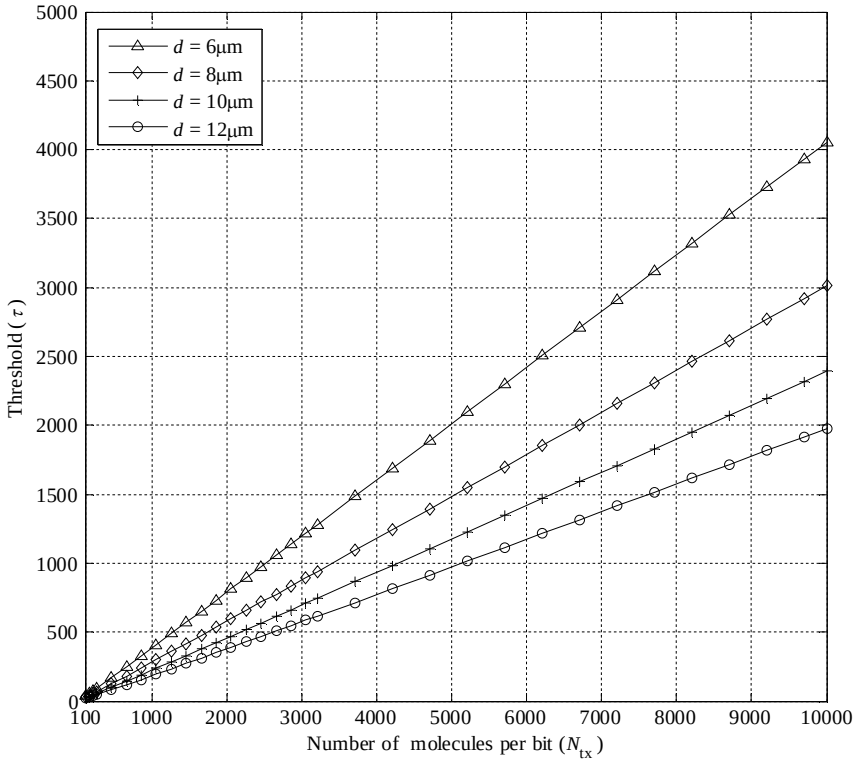

Figure 3.6: The values of threshold with number of information molecules per bit for different *d*.

Table 3.2: Parameter Setting.

Parameter	Definition	Value
R	Radius of the R_X	5μm
d	Transmission distance	{6, 8, 10, 12}μm
D	Diffusion coefficient	$79.4\mu m^2 s^{-1}$
N_{tx}	Number of molecules per bit	$100\sim10^4$
I	ISI length	10

3.4.2 BER and channel capacity

In this section, the BER and channel capacity of the PTP DBMC system are studied in two aspects: firstly, when $0 < p_{tx} < 1$ (the BERs when $p_{tx} = 1$ and 0 are extremely low, thus here these two cases have been ignored); secondly, when $p_{tx} = 0.5$ which is also the value that gives the channel capacity (This is proven by the first study).

A. $0 < p_{tx} < 1$

The BER and MI for different d and N_{tx} show in Figure 3.7. The results clearly show that increasing the transmission distance leads to a lower MI and higher BER. Conversely, the increasing in number of information molecules per bit causes an increasing in MI and decreasing in BER. The increase of d causes a decreasing of the capture probability at R_X, which is known from (3.5). Thus, the number of received information molecules and the corresponding threshold also be reduced. The reduction of the threshold leads to a more sensitive decoding scheme, which means a slightly changes in the number of received information molecules will raise the error probability during the decoding process.

Channel capacity represents the maximum transmission rate that can be achieved over the communication channel. Referring to (3.25), the channel capacity is selected as the maximum value of MI in a range of p_{tx}, where $0 < p_{tx} < 1$. The MI results in Figure 3.7 indicate that with the increasing of p_{tx}, the MI increases first, and when it reaches the maximum value, it starts decreases. The maximum MI, which is the channel capacity, is obtained when p_{tx} is equal to 0.5.

The results also indicate that the transmission probability that gives the maximum mutual information can not derive the lowest BER. This is because the PTP DBMC channel considered here is a non-symmetric memory channel, thus the value of p_{tx} that gives the miminum BER and also the maximum channel capacity does not exist. This indicates that there is the relationship of restriction between the the maximum reliable tranmsission rate and the relability of a given PTP DBMC.

In order to balance the MI and BER performance, a optimal, p_{tx} can be obtained by finding the maximum reliable transmission rate in a range $0 < p_{tx} < 1$:

$$\begin{aligned} C_{MR} &= \max_{p_{tx}} \left(\mathbf{I}\left(X_{I+1};Y_{I+1}\right)\left(1-P_e\right)\right) \\ &= \max_{p_{tx}} \Bigg[\Bigg(-\log_2 \Big(\left(\left(1-p_{tx}\right)\left(1-P_{e01}\right)+p_{tx}P_{e10}\right)^{\left((1-p_{tx})(1-P_{e01})+p_{tx}P_{e10}\right)} \\ &\qquad \times \left(1-\left(1-p_{tx}\right)\left(1-P_{e01}\right)-p_{tx}P_{e10}\right)^{\left(1-(1-p_{tx})(1-P_{e01})-p_{tx}P_{e10}\right)} \Big) \\ &\qquad + p_{tx}\log_2\left(\left(1-P_{e10}\right)^{\left(1-P_{e10}\right)} P_{e10}^{\ P_{e10}}\right) + \left(1-p_{tx}\right)\log_2\left(\left(1-P_{e01}\right)^{\left(1-P_{e01}\right)} P_{e01}^{\ P_{e01}}\right) \Bigg) \\ &\qquad \times \left(1-p_{tx}P_{e10}-\left(1-p_{tx}\right)P_{e01}\right) \Bigg]. \end{aligned} \tag{3.27}$$

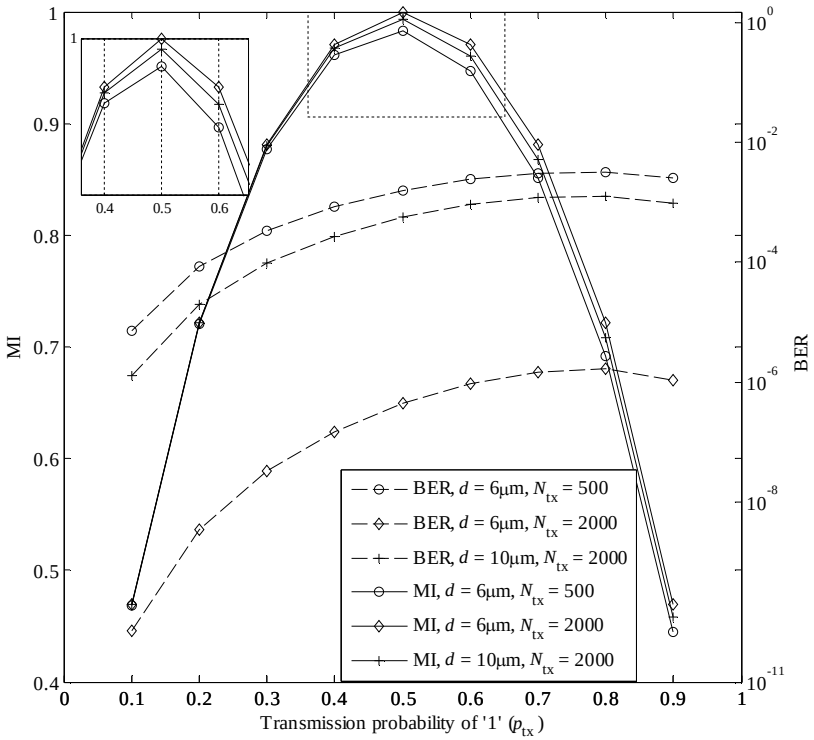

Figure 3.7: BER and MI versus p_{tx} for different d and N_{tx}.

The maximum value can be obtained by using MATLAB programming. The optimal p_{tx} for the system with d = 6μm, N_{tx} = {500, 2000} and a system with d = 10μm, N_{tx} = 2000 are all equal to 0.5.

B. p_{tx} *= 0.5*

Considering the transmission probability of '1' equals to 0.5. The BER and channel capacity with number of molecules per bit for different transmission distance d are given in Figure 3.8 and Figure 3.9, respectively. The results indicate that as the number of molecules increases, the system performance is getting better and it can be reflected in both BER and capacity. On the other hand, for a specific number of molecules per bit, the increase in d leads to the increase in BER and decrease in capacity, respectively.

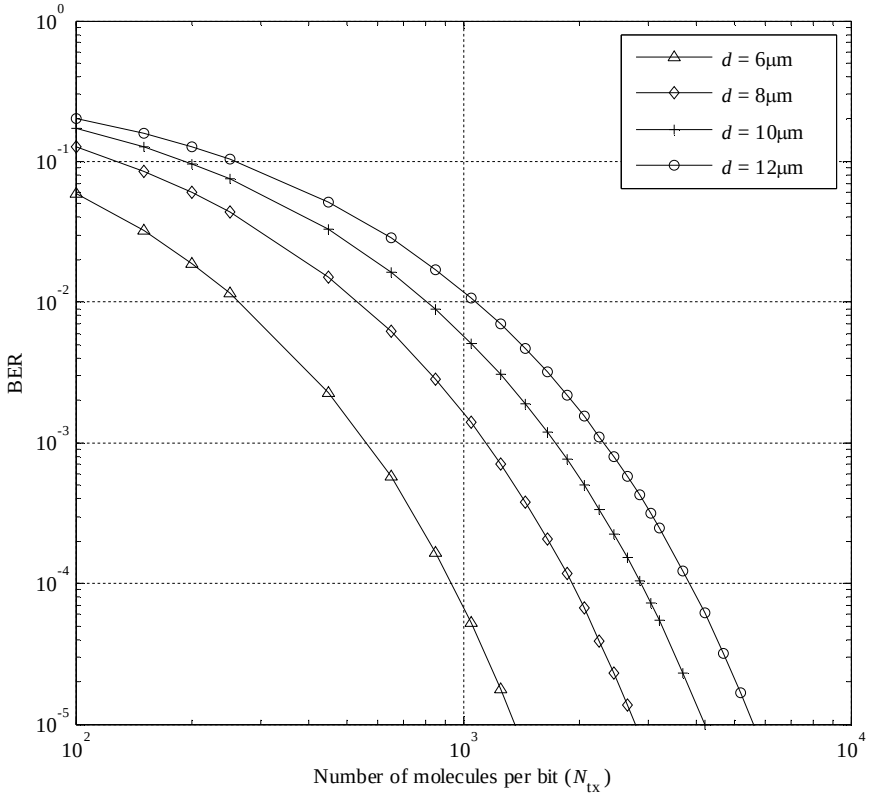

Figure 3.8: BER with number of information molecules per bit for different *d*.

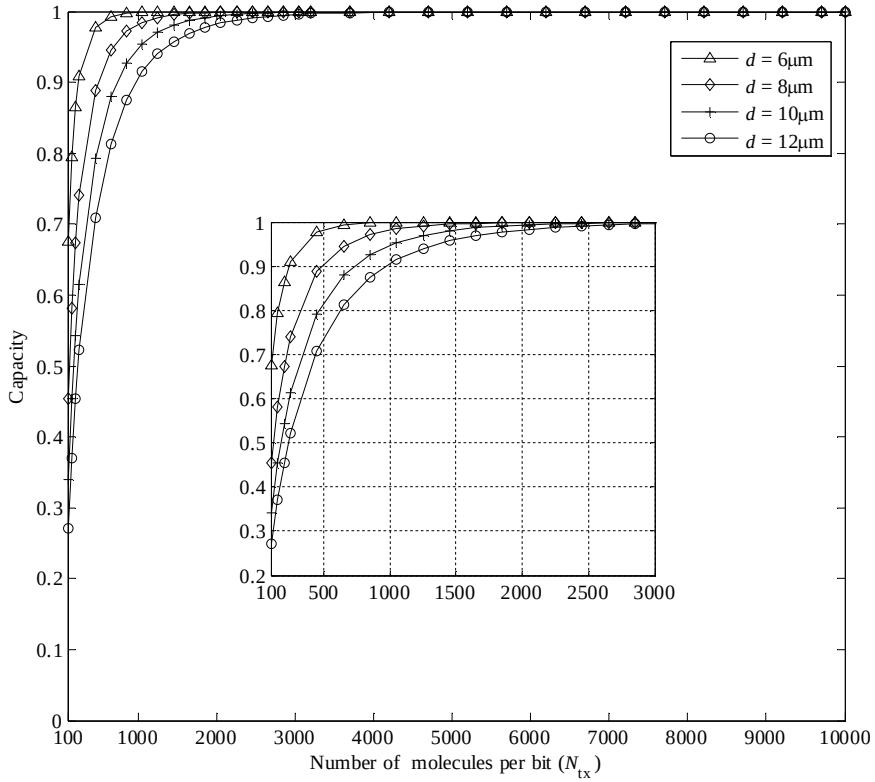

Figure 3.9: Channel capacity for the DBMC with different *d*.

3.5 Conclusions

In this section, a basic design of the PTP DBMC system model is introduced with a detailed analysis of the propagation and communication models. The concept of three different communication scenarios is also proposed in this chapter.

In this system, the information molecules are released as a pulse at T_X, and the propagation of information molecules from T_X to R_X is modeled by Brownian motion. When these molecules reach the capturing area of R_X, they will be absorbed and removed from the environment. At R_X, the information is demodulated by counting the number of arrived information molecules. This value is compared with the pre-designed threshold to determine whether '1' or '0' is sent by T_X. Through the investigation, the ISI length, number of molecules per bit, and transmission distance have a significant influence on a communication system with a fixed diffusion coefficient and R_X's radius. The system performance is analysed under the consideration of a memory limited channel with an ISI length 10. The theoretical results are obtained for both BER and channel capacity which show that the number of molecules per bit and the transmission distance has significant effects on the system performance. The improvement of the system performance can be achieved by increasing the number of molecules per bit or decreasing the transmission distance.

Chapter 4
Error Correction Codes in PTP DBMC System

4.1 Introduction and related work

The reliability of the transmission data is always the major concern for the communication system designer. In the conventional communication system, employing Error Correction Codes (ECCs) is a fast and efficient way to deal with this issue. In this chapter, this idea is taken forward into the MC system, and due to the energy limitation of the nano-machine, the energy consumption caused by the introduction of the ECCs will also be considered.

Only a small amount of literature in the area of ECCs applied to MC systems. One of the early works that considered ECCs for MC system was presented in [68], where the Hamming code as a simple block code was proposed for MC systems. The key results in that paper show that the use of Hamming codes can improve the system performance. Further work followed in [105], where the author proposed a molecular coding distance function that considers the transition probability between codewords. The suitable code for MC system can be constructed by using this distance function. The authors in [106] focused on the need to introduce simple codes due to the issue of energy use. The use of minimum energy codes in the MC systems was presented in [107], where the energy consumption can be reduced by minimizing the average code weights. These works all present that the employment of coding techniques into the MC system can improve the BER performance compared to the uncoded system.

Here, four ECCs are introduced. Three of them are from block code family, they are Hamming codes, Cyclic Reed-Muller (C-RM) codes and Low-density Parity-check (LDPC) codes. One of them is from the convolutional codes family which is Self-orthogonal Convolutional Codes (SOCCs). A brief review of each code is given in the following paragraphs.

Hamming codes, as the first optimum class of linear codes devised for error correction, have been widely used in the conventional communication systems [108]. Although these simple block codes can only correct a single error and not powerful codes for the conventional communication system, they are easy to encode and decode and very efficient in terms of the energy budget for the MC system. Here, the Hamming codes, as the most basic coding techniques are employed into the MC system and also provided as a comparison.

RM codes [109], [110] are a class of linear codes over a Galois Field of two ($GF(2)$). In this work, the RM codes are constructed as cyclic codes to show it is also a subset of Bose, Chaudhuri and Hocquenghem (BCH) codes. This kind of RM codes is denoted as C-RM codes which can be easily encoded and decoded using the shift-register encoder and majority logic decoder, respectively. From the perspective of energy, the main advantage of C-RM codes is that the encoder is simpler than the original RM codes, thus may hold benefits for the applications above [111], [112] [113].

LDPC codes have an extensive taxonomy [114-117], to be in a large scale it can be branched into either Random or Structured LDPC codes. The former are sometimes known as Gallager or Makay Random codes [114], [116]. Based on different structures of LDPC codes, the latter type can be divided into Euclidean Geometry LDPC (EG-LDPC) codes and Projective Geometry LDPC (PG-LDPC) codes. Several advantages over Random LDPC codes are shown in EG-LDPC and PG-LDPC codes, such as the existence of several decoding algorithms (cyclic or quasi-cyclic), a simpler decoding scheme and the ability to extend (or shorten) the code in order to adapt to an application [118], [119], [120]. It has been shown in [117] that both EG-LPDC codes and PG-LDPC codes have almost identical error performance. Furthermore, a comprehensive account of the implementation of a

cyclic EG-LDPC code has been shown in [121] such that in this work, the focus will be placed on one specific construction, namely the cyclic EG-LDPC code.

SOCCs is a kind of convolutional code which has the property of being easy to implement, thus satisfying one of the key design requirements, simplicity [122], [123]. The further motivation of this study is that this kind of convolutional code has been shown to have an equal, or superior, performance to block codes in low cost and low complexity applications. Examples can be found detailing their competitiveness in practical applications [124-127].

The contributions of this work are that for the first time, the implementations of a C-RM code, an SOCC and an EG-LDPC code are shown for use in the MC system. In addition, the overall complexity of the encoder and decoder circuits such that the amount of energy required is taken into account. The critical distance [128], a measure of the transmission distance at which the use of ECCs become beneficial is also introduced as a metric of the energy consumption. The performance of the coded system is evaluated with regards to both BER and critical distance. This presents a system designer with two metrics to evaluate the effectiveness of applying the code if, the transmission distances of the target application are known. In situations where raw energy consumption is required, the third metric of absolute energy requirements for the codes is shown with associated target BERs. The performance of the coded system is compared to an uncoded system and a system that employs Hamming codes. Furthermore, considering the system that includes the interaction between nano-machine and macro-machine, the energy consumption for the nano-part is also investigated.

The remainder of this chapter is organised as follows. Section 4.2 gives an introduction of logic circuits in the biological field. In Section 4.3, the energy model used within the MC is discussed. The introduction and construction of different coding schemes are given in Section 4.4 and Section 4.5, respectively. Section 4.6 shows the BER analysis for coded PTP DBMC systems. The energy consumption for different coding schemes is presented in Section 4.7. Section 4.8 then provides the numerical results, followed by the conclusions in Section 4.9.

4.2 Logic circuits in biological field

In the conventional communication system, the coding and decoding techniques can be implemented using digital electronic circuits which are composed of large numbers of transistors. By interconnecting these transistors, the function of Boolean logic like AND, NAND, OR, XOR and NOR can be realized. However, in MC systems, due to the size of T_X and R_X, the complexity of the electronic circuits is too overwhelming to employ. Thus, the realization of logic gates needs to be investigated from the biological field.

The authors in [28] considered the protein-based signaling networks within biological cells. It is shown that the fundamental motif in all signaling networks is based on the protein phosphorylation and dephosphorylation cycle which is also called a cascade cycle via kinases and phosphatases respectively. In addition, for logic gates, a fasting changing concentration needs to exist in one of two states, and the cascade cycle can complete this process when operating in ultrasensitive mode. Thus it is possible to construct various control and computational analogue and digital circuits by combining these cascade cycles. Coupled with the notion that these kinds of networks are of a similar scale to those needed for any future artificial nano-networks, they can also be used to estimate the energy requirements of the encoding and decoding circuits used here.

Figure 4.1 shows how a NAND gate could be formed from a cascade cycle. ‘A’ and ‘B’ are the inputs to the kinase step that can cause the cascade cycle to switch. NAND gate is a universal gate, so it is clearly possible to build all future logical circuits. In [28], the authors also presented a basic memory unit, the binary counter and NOT gate by combining cascade cycles.

In the traditional electronic circuit design, a clear low or high voltage level at the output stage is needed for ensuring the reliability of the transmission data. However, the thermal noise and intrinsic distortion of the transistors exist in the circuits which cause an unstable level of the output signal.

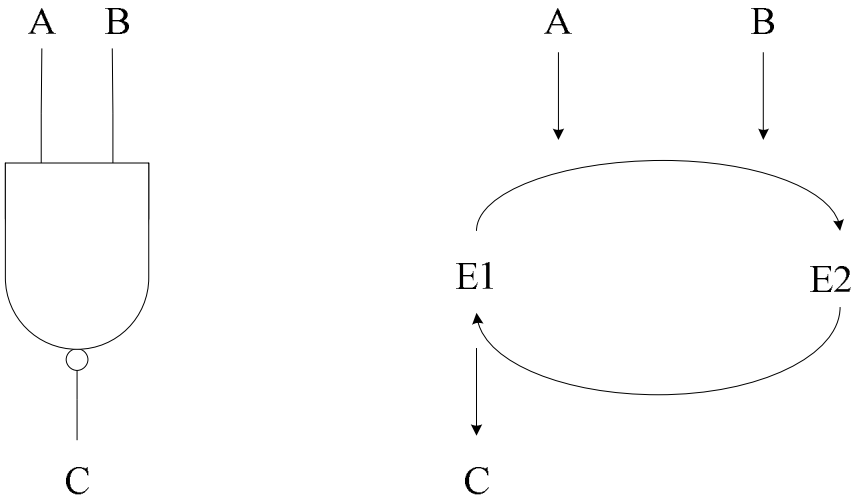

Figure 4.1: NAND gate formed from a cascade cycle [28].

Similar to electronic circuits, the circuits that are formed of cascade cycles are also suffered from the cascade cycle's intrinsic fluctuations distortion [129]. The way to reduce this kind of noise is to increase the signal intensity by increasing the number of substrate molecules, N_{sm}. These substrate molecules are the input signal of the cascade cycle. Here, these substrate molecules can be looked as the code generation molecules required to encode and decode the data. They are considered different to the information molecules that were introduced in Chapter 3, as they are internal molecules and only used for the encoding and decoding process within T_X and R_X and do not suffer from any effects caused by diffusion.

An investigation of the impact of the number of substrate molecules on the performance of the cascade cycle has been given in [129]. Each substrate molecule is either unmodified or modified at the output of cascade cycle. The cascade cycle system is given in Figure 4.2 for different N_{sm}. Figure 4.2 (A) indicate that when the N_{sm} is small (N_{sm} = 30), the high and low outputs overlap and blur due to the cascade cycle's intrinsic fluctuation distortion, when N_{sm} increases to 300 (Figure 4.2 (B)), a clear transmission output pulse is given. A further increase of N_{sm} will cause a slow output response and information loss (Figure 4.2 (C), (D)). Overall, the selected value of N_{sm} = 300 is sufficient to reduce the effects that come from the biochemical intrinsic distortion.

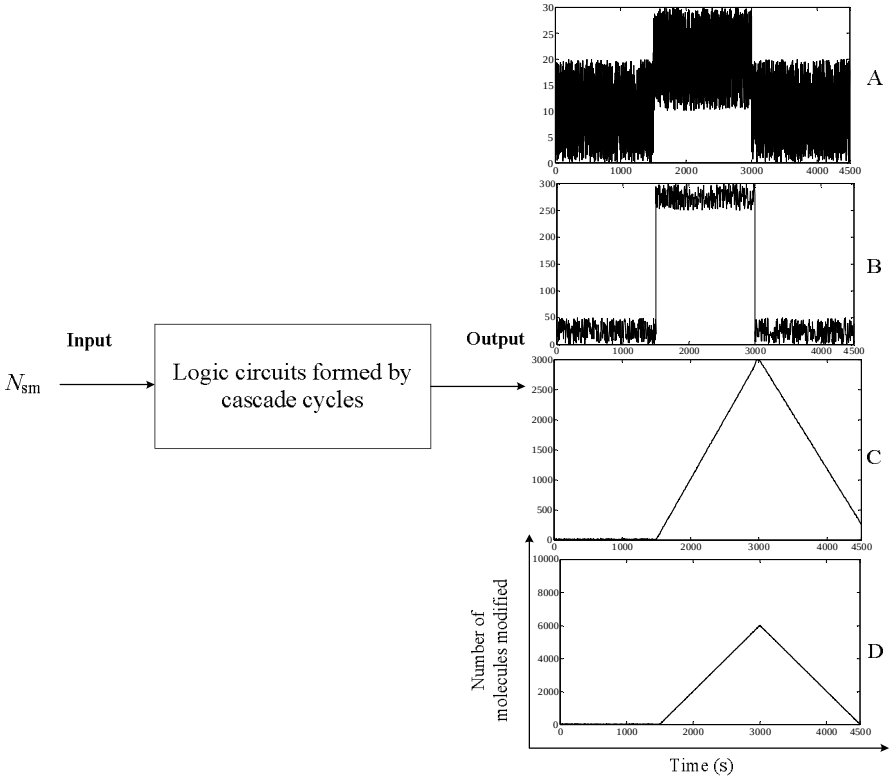

Figure 4.2: Cascade cycle system and the output signal when (A) N_{sm} = 30, (B) N_{sm} = 300, (C) N_{sm} = 3000, (D) N_{sm} = 10000 [129].

4.3 Energy model

In Section 3.2.2, it was mentioned that the most pertinent application that contains the three communication scenarios is an intra-body network that collects and monitors vital biological activity [130]. In the healthcare domain, the quality of the data and the energy efficiency are two key metrics for the analysis process.

Introducing coding techniques can improve the performance of the communication system, but there will be an extra cost in energy due to the encoding and decoding process at T_X and R_X. This extra energy is proportional to the complexity of the encoder and decoder circuits.

Adenosine triphosphate (ATP) [49] is used to measure the energy transfer between cells in living organisms, and here, it is used to calculate the energy requirements of the proposed coding systems. The energy consumption during the encoding and decoding processes can be composed of two parts: energy cost to drive

the operation of biological circuits, and the energy cost for generating the substrate molecules.

For a NAND gate, the suitable measure of the energy required for the cascade cycle to complete was equal to a single ATP reaction[49], [131]. The energy cost from one ATP reaction, in Joules, is approximately equal to 8.3×10^{-20} J. Considering such small quantities, here, the energy is worked in B_cT. Thus the energy cost for one ATP reaction is 20 B_cT, where B_c is the Boltzmann constant and it is assumed here that the system is operating at an absolute temperature, T = 300K. As mentioned in Section 4.2, all further logic circuits can be devised from combinations of NAND gates based on the principles of Boolean algebra [23]. So the total energy cost for the logic circuits can be computed.

Synthesizing the substrate molecules also results in energy consumption. The energy cost of synthesizing a molecule is approximately 2450 B_cT [23]. In this case, the total energy cost of synthesizing the substrate molecules is $2450N_{sm}\ B_cT$.

4.4 Block codes in MC system

Block codes are an important family of ECCs. In block coding, the transmission binary information sequence is segmented into information block with a fixed length, k. The encoder aims to transforms each information block into an n bits codeword [125] by inserting ($n - k$) parity check bits to improve the reliability of the information, these bits can be used to recover the original information during the decoding process. Most known block codes belong to the class of linear codes. This class of codes has a strong structural property and usually used in practice. In addition, the famous cyclic codes are also a subclass of the linear codes. Compare with the normal linear block codes, the cyclic codes can be obtained by imposing an additional strong structural on the codes [132].

In this section, the Hamming codes, C-RM codes and EG-LDPC codes as the cyclic codes are considered to be used for the MC system. The communication channel model used here is the model that was introduced in Chapter 3. Each code will be described in turn.

4.4.1 Hamming codes

A Hamming code is one of the simple linear block codes used in many applications. For any integer $m \geq 2$, the Hamming codes has the following parameters:

Block length: $$n_{\mathrm{H}} = 2^m - 1, \tag{4.1}$$

Information length: $$k_{\mathrm{H}} = n_{\mathrm{H}} - m, \tag{4.2}$$

Number of parity check bits: $$m = n_{\mathrm{H}} - k_{\mathrm{H}}, \tag{4.3}$$

Data rate: $$r_{\mathrm{H}} = k_{\mathrm{H}} / n_{\mathrm{H}}, \tag{4.4}$$

Error correction capability: $$E_{\mathrm{cH}} = \lfloor d_{\mathrm{minH}} - 1 \rfloor / 2, \tag{4.5}$$

where $\lfloor x \rfloor$ returns to the largest integer not greater than x. d_{minH} is the minimum distance between any two codewords of the code. For Hamming codes, $d_{\mathrm{minH}} = 3$, therefore, it can correct one error in each block. Hamming codes can be represented as (n_{H}, k_{H}).

As one of the cyclic codes [119], Hamming code can be encoded by multiplying the information polynomial with the generator polynomial. In this work, (7,4), (15,11) and (31,26) Hamming codes are introduced in the DBMC system.

For (7,4), (15,11) and (31,26)Hamming codes, the generator polynomial are given by:

$$g_{m=3}(x) = x^3 + x + 1, \tag{4.6}$$

$$g_{m=4}(x) = x^4 + x + 1, \tag{4.7}$$

$$g_{m=5}(x) = x^5 + x^2 + 1. \tag{4.8}$$

The simplest decoder for this kind of code is the Meggitt decoder. Using the Maggitt Theorem, the syndrome polynomial for testing the error patterns for above Hamming codes are configured as:

$$s_{m=3}(x) = x^2 + 1, \tag{4.9}$$

$$s_{m=4}(x) = x^3 + 1, \tag{4.10}$$

$$s_{m=5}(x) = x^4 + x. \tag{4.11}$$

Figure 4.3 shows an example of encoder and decoder for (15,11)Hamming code.

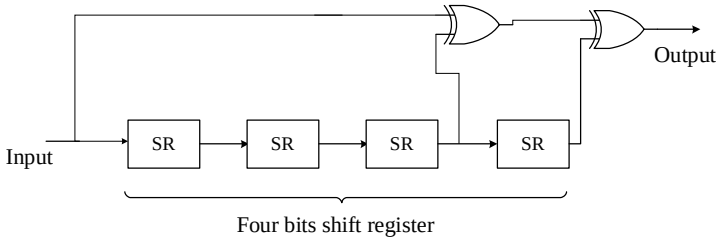

(a)

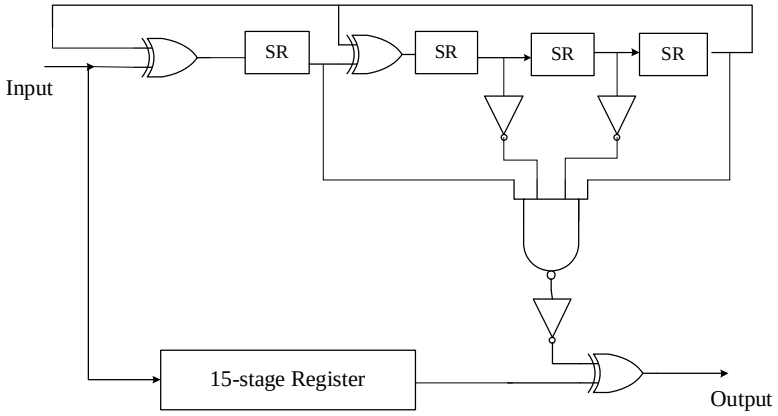

(b)

Figure 4.3: Nonsystematic encoder [132] (a) and Meggitt decoder (b) [132] for (15,11)Hamming code.

4.4.2 C-RM codes

RM codes are a class of binary codes with multiple error correction capabilities. Here the way in which they are constructed as cyclic codes is introduced which are termed C-RM codes.

For any integer, $l \geqslant 2$ and $0 \leqslant z < l - 1$, the z^{th} order C-RM codes can be represented as (z, l)C-RM with the following parameters [132]:

Block length: $$n_{\mathrm{R}} = 2^{l} - 1, \tag{4.12}$$

Information length: $$k_{\mathrm{R}} = 1 + \binom{l}{1} + \binom{l}{2} + \cdots + \binom{l}{r} = n_{\mathrm{R}} - \sum_{i=1}^{l-z-1} \binom{l}{i}, \tag{4.13}$$

Data rate: $$r_{\mathrm{R}} = k_{\mathrm{R}} / n_{\mathrm{R}}, \tag{4.14}$$

Error correction capability: $$E_{\mathrm{cR}} = \lfloor d_{\mathrm{minR}} - 1 \rfloor / 2, \tag{4.15}$$

where the minimum distance $d_{\mathrm{minR}} = 2^{l-z} - 1$.

Given a nonnegative integer q, where $1 \le q \le 2^l - 2$, the number of 1's in the binary expansion of q can be denoted as $w_2(q)$, and α^q are the roots of the generator polynomial $g_{\text{C-RM}}(x)$ if and only if [133]:

$$1 \le w_2(q) \le l - z - 1. \tag{4.16}$$

α^q are the roots of the check polynomial $h(x)$ if and only if:

$$l - z \le w_2(q) \le l - 1. \tag{4.17}$$

The generator and check polynomials for the C-RM codes are:

$$g_{\text{C-RM}} = \prod_{\substack{1 \le w_2(q) \le l-z-1 \\ 1 \le q \le 2^l - 2}} M^{(q)}(x), \tag{4.18}$$

$$h_{\text{C-RM}}(x) = (\text{x}+1) \prod_{\substack{l-z \le w_2(q) \le l-1 \\ 1 \le q \le 2^l - 2}} M^{(q)}(x), \tag{4.19}$$

where $M^{(q)}(x)$ is the minimal polynomial of α^q.

Considering the (1,4)C-RM code, all integers q satisfying (4.16) and (4.17) are {1, 2, 3, 4, 5, 6, 8, 9, 10, 12} and {7, 11, 13, 14}, respectively. Thus, the roots of the generator polynomial can be represented as:{α^1, α^2, α^3, α^4, α^5, α^6, α^8, α^9, α^{10}, α^{12}}, where α^1, α^2, α^4, α^8 have the same minimal polynomial: $M_1(x) = x^4 + x + 1$, and α^3, α^6, α^9, α^{12} have the same minimal polynomial: $M_2(x) = x^4 + x^3 + x^2 + x + 1$, and the minimal polynomial of α^5 and α^{10} is $M_3(x) = x^2 + x + 1$. According to (4.18), the generator polynomial can be computed as:

$$g_{(1,4)\text{C-RM}}(x) = M_1 \cdot M_2 \cdot M_3 = x^{10} + x^8 + x^5 + x^4 + x^2 + x + 1. \tag{4.20}$$

Similarly, the roots of the check polynomial are: {α^7, α^{11}, α^{13}, α^{14}}, where α^7, α^{11}, α^{13}, α^{14} have the same minimal polynomial: $M_1(x) = x^4 + x^3 + 1$. According to (4.19), the check polynomial is given as:

$$h_{(1,4)\text{C-RM}}(x) = (x+1) \cdot (x^4 + x^3 + 1) = x^5 + x^3 + x + 1. \tag{4.21}$$

By using the same method, the generator and check polynomials for the (1,3), (2,4), (2,5), and (3,5)C-RM codes are given by:

$$g_{(1,3)\text{C-RM}}(x) = x^3 + x + 1. \tag{4.22}$$

$$h_{(1,3)\text{C-RM}}(x) = x^4 + x^2 + x + 1. \tag{4.23}$$

$$g_{(2,4)\text{C-RM}}(x) = x^4 + x + 1. \tag{4.24}$$

$$h_{(2,4)\text{C-RM}}(x) = x^{11} + x^8 + x^7 + x^5 + x^3 + x^2 + x + 1. \tag{4.25}$$

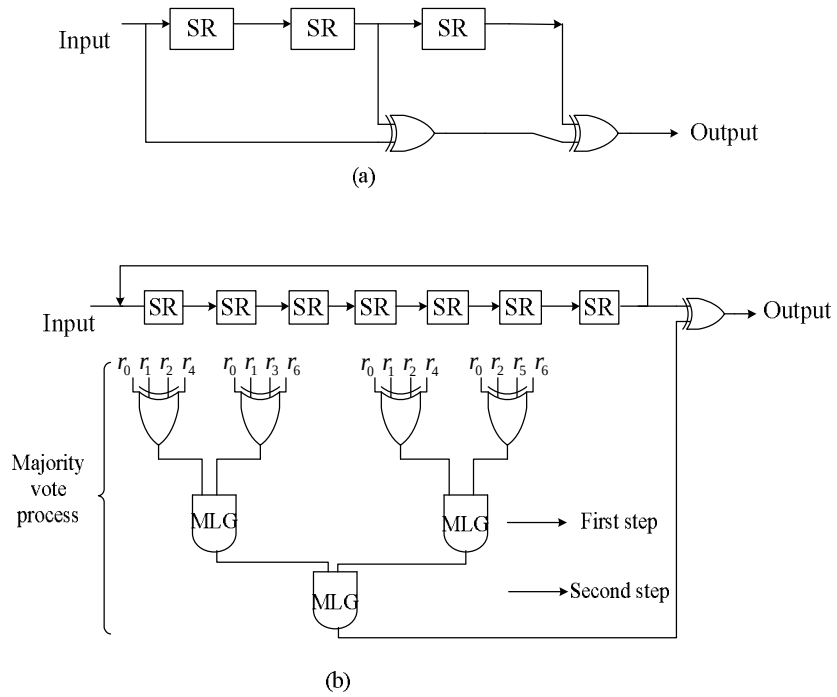

Figure 4.4: (a) Non-systematic feedback encoding circuit and (b) a two-step majority logic decoder for the (1,3)C-RM codes [133].

$$g_{(2,5)\text{C-RM}}(x) = x^{15} + x^{11} + x^{10} + x^9 + x^8 + x^7 + x^5 + x^3 + x^2 + x + 1. \tag{4.26}$$

$$h_{(2,5)\text{C-RM}}(x) = x^{16} + x^{12} + x^{11} + x^{10} + x^9 + x^4 + x + 1. \tag{4.27}$$

$$g_{(3,5)\text{C-RM}}(x) = x^5 + x^2 + 1. \tag{4.28}$$

$$\begin{aligned} h_{(3,5)\text{C-RM}}(x) = {} & x^{26} + x^{25} + x^{24} + x^{23} + x^{22} + x^{21} + x^{18} + x^{14} \\ & + x^{13} + x^{12} + x^8 + x^7 + x^6 + x^5 + x^2 + 1. \end{aligned} \tag{4.29}$$

Considering the C-RM hardware requirements, as shown in Figure 4.4, the encoding process can be achieved using simple feedback shift registers and subsequently decoded using a multiple-step majority logic method.

4.4.3 EG-LDPC codes

An EG-LDPC code can be constructed based on the lines and points of the Euclidean geometry. In this chapter, a special case: cyclic two-dimensional EG-LDPC codes are considered [118], [134]. To simplify the nomenclature, the LDPC codes mentioned below are all assumed to be cyclic and two-dimensional [118], [135].

In general terms, LDPC codes can be represented as (n_L, k_L), and for any integer, s, $s \geq 2$, the LDPC codes can be generated using following parameters [118]:

Block length: $$n_L = 2^{2s} - 1, \tag{4.30}$$

Information length: $$k_L = 2^{2s} - 3^s, \tag{4.31}$$

Data rate: $$r_L = k_L / n_L, \tag{4.32}$$

Error correction capability: $$E_{cL} = \lfloor d_{minL} - 1 \rfloor / 2, \tag{4.33}$$

where the minimum distance $d_{minL} = 2^s+1$. The number of 1's for row and column also as the weights of the parity-check matrix which are given as $\rho = 2^s$ and $\theta = 2^s$ respectively [118].

Before describing EG-LDPC codes, the finite field is introduced. Finite field, also called Galois Field (*GF*) is a finite set of elements which can be added, multiplied and divided with the results being an element of the set. The ECCs that could be constructed based upon these fields can be efficiently encoded and decoded [134], which for molecular communications, is a major concern.

EG(*o*,*q*) is an *o* - dimensional Euclidean geometry over *GF*(*q*), where *o* is a positive integer greater than one, $q = p^{\kappa}$, $\kappa \geq 1$and *p* is a prime number [133]. An EG-LDPC code can be constructed based on the lines and points of Euclidean geometry.

Considering that *EG*(2,2^s) is a Euclidean geometry on *GF*(2^s), where each point is a 2-tuple over *GF*(2^s) and where an all zero 2-tuples can be called the origin. Thus, this geometry contains 2^{2s} points and $2^s(2^{2s} - 1)/(2^s - 1)$ lines. *GF*(2^{2s}) is an extended field *GF*(2^s), so each element in *GF*(2^{2s}) can be referred as a 2-tuple over *GF*(2^s), which means that 2^{2s} elements in *GF*(2^{2s}) can be regarded as 2^{2s} points in *EG*(2, 2^s) [118], [136], [137]. Assuming α is a primitive element of *GF*(2^{2s}) means all the non-zero elements in *GF*(2^{2s}) can be represented as α^i, where *i* is a positive integer. Let α^j be a non-origin point, so a line in *EG*(2, 2^s) can be formed from the 2^s points in *EG*(2, 2^s), shown as:

$$\left\{\lambda\alpha^j\right\} \triangleq \left\{\lambda\alpha^j : \lambda \in GF\left(2^s\right)\right\}. \tag{4.34}$$

Then let α^i and α^j be two independent points, so a line passing through α^j can be formed as:

$$\left\{\alpha^i + \lambda\alpha^j\right\} \triangleq \left\{\alpha^i + \lambda\alpha^j : \lambda \in GF\left(2^s\right)\right\}. \tag{4.35}$$

Each line in $EG(2, 2^s)$ can be represented as a vector of length 2^{2s}. For this LDPC code, the rows of the parity check matrix $H_{EG}(2, s)$ correspond with the $2^{2s} - 1$ lines that do not pass through the origin in $EG(2, 2^s)$, and the columns correspond with the $2^{2s} - 1$ non-origin points in $EG(2, 2^s)$.

Therefore the parity check matrix, $H_{\mathrm{LDPC}}(2, s)$ is a $(2^{2s} - 1) \times (2^{2s} - 1)$ square matrix, and it can be constructed by taking the incidence vector of a line in $EG(2, 2^s)$ that does not pass through the origin and then cyclically shifting this vector $2^{2s} - 2$ times. This LDPC code is a kind of cyclic code [118], so the generator polynomial $g_{\mathrm{LDPC}}(x)$ can be obtained from the roots in $GF(2^{2s})$. u, a non-negative integer, can be expressed in radix – 2^s form as:

$$u = \delta_0 + \delta_1 2^s, \tag{4.36}$$

where $u < 2^{2s}$ and $0 \le \delta_i < 2^s$, $0 \le i < 2$. $W_2{}^s(u)$ denotes the 2^s weight of u, shown as:

$$W_{2^s}(u) = \delta_0 + \delta_1. \tag{4.37}$$

For a non-negtive integer l, let $u^{(l)}$ be the remainder of $2^l u/(2^{2s} - 1)$, where $0 \le u^{(l)} < 2^{2s} - 1$ then α^u is a root of $g_{\mathrm{LDPC}}(x)$ if and only if:

$$0 < \max_{0 \le l < s} W_{2^s}\left(u^{(l)}\right) \le 2^s - 1. \tag{4.38}$$

Three LDPC codes are shown in this chapter, which are (15,7), (63,37) and (255,175)LDPC codes. For the (15,7)LDPC code, consider $EG(2,2^s)$ and let α and β be the primitive elements of $GF(2^{2\times 2})$ and $GF(2^2)$ respectively. Given $p(x) = x^4 + x + 1$ is the primitive polynomial of $GF(2^{2\times 2})$, it is easy to prove that $\beta = \alpha^5$ because of $\beta^3 = \alpha^{15} = 1$. Therefore $\lambda \in \{0, 1, \beta, \beta^2\}$ or $\{0, 1, \alpha^5, \alpha^{10}\}$ constitute $GF(2^2)$. Let $\alpha^i = \alpha^{14}$ and $\alpha^j = \alpha$, so one of the lines of $EG(2, 2^2)$ can be obtained from (4.35) as:

$$\left\{\alpha^7, \alpha^8, \alpha^{10}, \alpha^{14}\right\} \in \left\{\alpha^{14} + \lambda\alpha : \lambda \in \left\{0, 1, \alpha^5, \alpha^{10}\right\}\right\}. \tag{4.39}$$

These four points in a line do not pass through the origin, so the parity check matrix H_{LDPC} can be formed using the corresponding binary incidence vector (0 0 0 0 0 0 0 1 1 0 1 0 0 0 1) and its $2^{2s} - 2 = 14$ circulations.

From (4.36), (4.37) and (4.38), the roots of the generator polynomial can be obtained as:$\{\alpha^1, \alpha^2, \alpha^3, \alpha^4, \alpha^6, \alpha^8, \alpha^9, \alpha^{12}\}$. α^1, α^2, α^4, α^8 all have the same minimal polynomial: $M_1(x) = x^4 + x + 1$, whilst α^3, α^6, α^9, α^{12} all have the same minimal polynomial: $M_2(x) = x^4 + x^3 + x^2 + x + 1$, then the lowest common multiple (LCM) can be obtained as the generator polynomial:

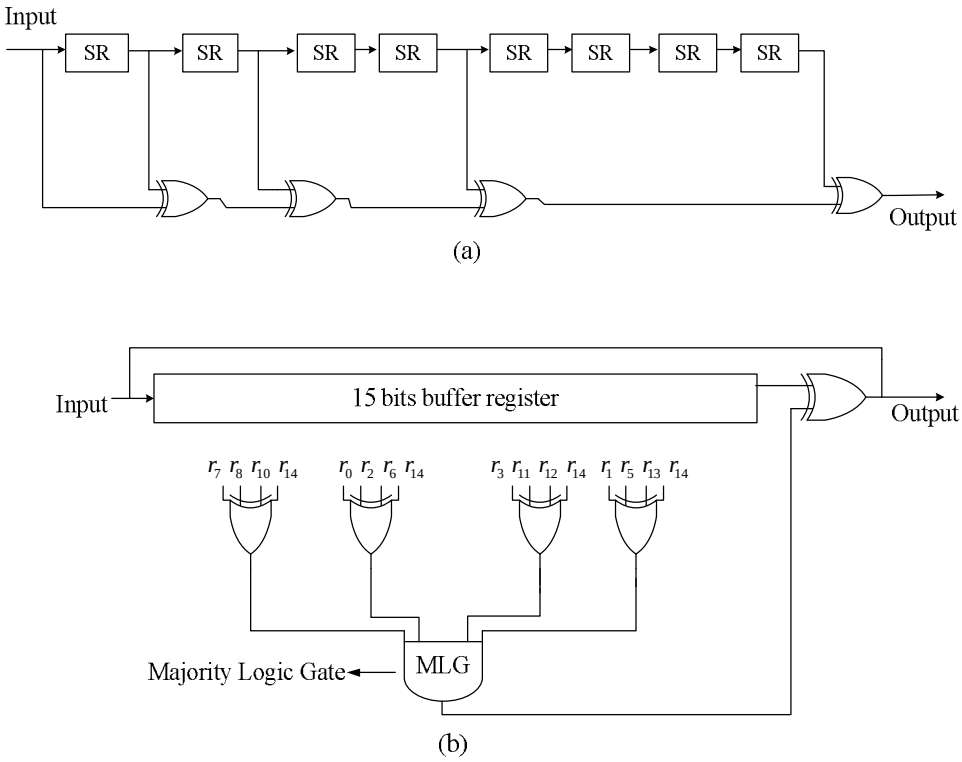

Figure 4.5: Nonsystematic encoding circuit (a) and one-step majority logic decoder (b) [121] for the (15,7)LDPC codes.

$$g_{(15,7)\mathrm{LDPC}}(x) = LCM\left[M_1(x), M_2(x)\right] = x^8 + x^7 + x^6 + x^4 + 1. \qquad (4.40)$$

In the same way, the generator polynomials for the (63,37) and (255,175)LDPC codes are given by:

$$g_{(63,37)\mathrm{LDPC}}(x) = x^{26} + x^{24} + x^{16} + x^{15} + x^{14} + x^{13} + x^{12} + x^{10} + x + 1. \qquad (4.41)$$

$$\begin{aligned} g_{(255,175)\mathrm{LDPC}}(x) = {} & x^{80} + x^{78} + x^{76} + x^{74} + x^{71} + x^{69} + x^{68} + x^{67} \\ & + x^{66} + x^{64} + x^{63} + x^{61} + x^{59} + x^{58} + x^{55} + x^{54} + x^{51} \\ & + x^{49} + x^{47} + x^{45} + x^{42} + x^{40} + x^{39} + x^{38} + x^{37} \\ & + x^{36} + x^{27} + x^{26} + x^{25} + x^{23} + x^{22} + x^{21} + x^{19} \\ & + x^{18} + x^{17} + x^{16} + x^{15} + x^{14} + x^{13} + x^{11} + x^{10} \\ & + x^{9} + x^{7} + x^{6} + x^{3} + 1. \end{aligned} \qquad (4.42)$$

Considering the LDPC hardware requirements, as shown in Figure 4.5, the encoding process can be achieved using simple feedback shift registers and subsequently decoded using a one-step majority logic decoding method.

4.5 Convolutional codes

The convolutional code, a kind of linear codes that was first proposed by Elias [138] as an alternative to block codes. The main difference between the block codes and the convolutional codes is the encoder design. In convolutional codes, the encoder contains b memory blocks and at any given time, the n_S bits codeword is produced not only dependent on the k_S message bits but also dependent on the b previous input blocks. Therefore, the convolutional codes are looked as the stream code, and the corresponding encoder operates on continuous streams of the information not the information blocks [119]. The (n_S, k_S, b) convolutional codes can be implemented using a k_S-input n_S-output linear sequential circuit with a b-bits memory block. Comparing with block codes, the convolutional codes are preferred to be used in the practice, this is because with same complexity of the encoder and decoder design, the convolutional codes provide better performance.

One of the convolutional codes considered here is the self-orthogonal convolutional code (SOCC). An SOCC is a kind of convolutional code which has the property of being easy to implement thus satisfying one of the key design requirements of code simplicity [122], [123].

For an (n_S, k_S, b) SOCC, n_S is the code length, k_S is the information length and b is the number of input memory blocks. $r_S = k_S/n_S$ is the code rate [125]. The error correction capacity, E_{cS}:

$$E_{cS} = \lfloor J/2 \rfloor, \tag{4.43}$$

where J is the number of check sums that orthogonal on one error.

The effective constraint length, n_E, represents the total number of channel error bits checked by the orthogonal check sum equations, where:

$$n_E = \frac{1}{2}\left(J^2 + J\right)k_S + 1. \tag{4.44}$$

In this work, only SOCCs with an information length $k_S = n_S - 1$ are considered. This chapter represents four SOCCs: they are (2,1,6) and (2,1,17)SOCCs, both with $r_S = 1/2$, and (3,2,2) and (3,2,13)SOCCs, both with $r_S = 2/3$.

The generator polynomials of (2,1,6) and (2,1,17)SOCCs are:

$$g_{(2,1,6)\mathrm{SOCC},1}^{(2)}(x) = x^6 + x^5 + x^2 + 1, \tag{4.45}$$

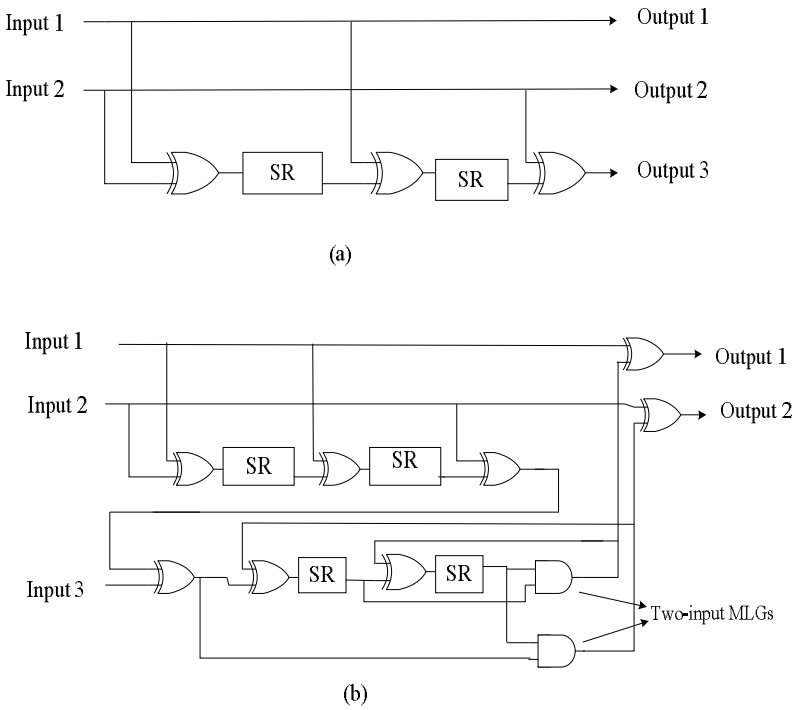

Figure 4.6: The (a) encoder and (b) decoder for a (3,2,2)SOCC [125].

$$g_{(2,1,17)\mathrm{SOCC},1}^{(2)}(x) = x^{17} + x^{16} + x^{13} + x^{7} + x^{2} + 1, \tag{4.46}$$

where $g_{\mathrm{SOCC},i}^{(n\mathrm{s})}$ is the generator polynomials with $i = 1, 2, \ldots, k_{\mathrm{S}}$.

For (3,2,2) and (3,2,13)SOCCs, the generator polynomials pairs are:

$$g_{(3,2,2)\mathrm{SOCC},1}^{(3)}(x) = x+1, \tag{4.47}$$

$$g_{(3,2,2)\mathrm{SOCC},2}^{(3)}(x) = x^{2} + 1, \tag{4.48}$$

$$g_{(3,2,13)\mathrm{SOCC},1}^{(3)}(x) = x^{12} + x^{9} + x^{8} + 1, \tag{4.49}$$

$$g_{(3,2,13)\mathrm{SOCC},2}^{(3)}(x) = x^{13} + x^{11} + x^{6} + 1. \tag{4.50}$$

The encoder and feedback majority-logic decoder for (3,2,2)SOCC is shown in Figure 4.6.

4.6 BER analysis for coded PTP DBMC systems

The BER for the uncoded PTP DBMC system has been analysed in Chapter 3. In order to compare the coded and the uncoded system performance, in this chapter, the BER for the coded system is investigated.

4.6.1 BER for system with linear block codes

Considering that the decoder can correct all errors less or equal to the error correction capacity, the decoded BER for the system with linear block codes can be expressed by the following approximation:

$$P_{\text{e-coded}} \approx \frac{1}{n} \sum_{j=E_c+1}^{n} j \binom{n}{j} \left(P_e^*\right)^j \left(1-P_e^*\right)^{n-j}, \tag{4.51}$$

where n is the block length, E_c is the error correction capacity. P_e^* is the one bit error probability in the uncoded case. Aiming to use the same number of molecules as an uncoded system, the number of molecules used for the calculation of P_e^* for the coded system should be evaluated with a reduction of the number of molecules used for an uncoded system, (3.19), by multiplying with the code rate.

4.6.2 BER for system with convolutional codes

For the convolutional code with a feedback majority-logic decoder, the BER can be upper bounded by [125]:

$$P_{\text{e-coded}} \le \frac{1}{k} \sum_{j=E_c+1}^{n_E} j \binom{n_E}{j} \left(P_e^*\right)^j \left(1-P_e^*\right)^{n_E-j}, \tag{4.52}$$

where k is the information length of the code. $P_{\text{e-coded}}$ can be approximated as [125]:

$$P_{\text{e-coded}} \approx \frac{1}{k} \binom{n_E}{E_c+1} \left(P_e^*\right)^{E_c+1}. \tag{4.53}$$

4.6.3 Coding gain

The coding gain is also introduced as a way to measure the BER performance. For MC systems, the coding gain aims to measure the difference between number of molecules for the uncoded and coded system required to reach the same BER level. It can be directly obtained as:

$$G_{\text{coding}} = 10 \times \log\left(\frac{N_{\text{uncoded}}}{N_{\text{coded}}}\right). \tag{4.54}$$

where N_{uncoded} and N_{coded} are the number of information molecules for the uncoded and the coded system at a chosen BER level.

4.7 Energy consumption analysis

Combining the energy model introduced in Section 4.3, the mathematical derivation of energy consumption for different coding techniques is investigated in this section. The total energy consumption for the encoder or decoder circuits can be composed of two parts: the first part is the energy cost to drive logic gates operation and the second part is the energy cost of synthesizing the substrate molecules.

Table 4.1: Logic gates and corresponding ATPs' consumptions.

Logic gate	Number of cost ATPs
NAND	1
NOT	1
XOR	4
Shift-register unit	4

Table 4.1 shows four basic logic gates and the corresponding ATPs' consumptions.

4.7.1 Energy consumption of encoding and decoding process

A. Energy consumption for Hamming codes

With reference to Figure 4.3, for m = {3, 4, 5} Hamming codes, two XOR gates and m shift-register units are needed for each encoder circuit, which implies the energy consumption of the encoder circuits is:

$$E_{\text{en-H}} = 20N_{\text{sm-en}}(4m+8) + 2450N_{\text{sm-en}}. \tag{4.55}$$

Three XOR gates, (m + n_{H}) shift-register units, (m – 1) NOT gates and one multi-input NAND gate are needed for each decoder circuits which implies the energy cost of the decoder is:

$$\begin{aligned} E_{\text{de-H}} &= 20N_{\text{sm-de}}(4(m+n_{\text{H}}) + (m-1+1) + 12) + 2450N_{\text{sm-de}} \\ &= 20N_{\text{sm-de}}(5m+4n_{\text{H}}+12) + 2450N_{\text{sm-de}}. \end{aligned} \tag{4.56}$$

where $N_{\text{sm-en}}$ and $N_{\text{sm-de}}$ are the numbers of substrate molecules used for encoder and decoder respectively. As refers in Section 4.2, $N_{\text{sm-en}} = N_{\text{sm-de}} = 300$.

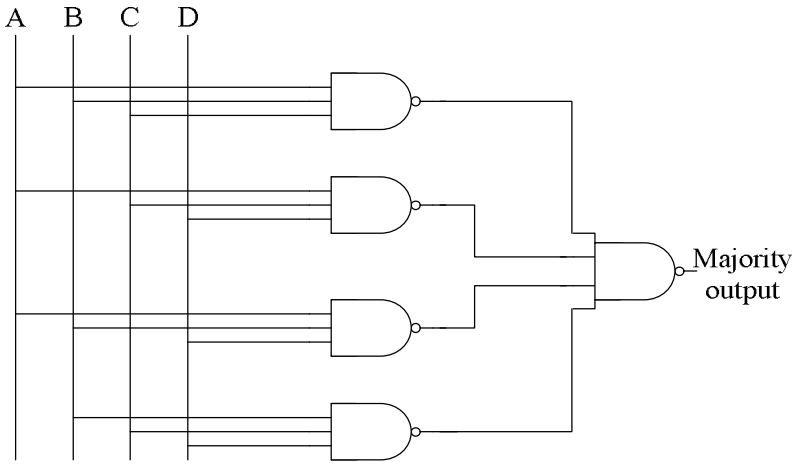

Figure 4.7: Four-input MLG implementation circuit.

B. Energy consumption for C-RM codes

Considering the C-RM hardware requirements, as shown in Figure 4.4, the encoding process can be achieved using simple feedback shift registers and subsequently decoded using a multiple-step majority logic method. An output one is produced when more than half of its inputs are equal to one, otherwise, the output is zero. An example of four-input Majority Logic Gate (MLG) is shown in Figure 4.7.

For any J-input MLG, the number of NAND gates can be calculated as:

$$N_{\text{NAND-MLGs}} = \begin{cases} \sum_{i=J/2+1}^{J-1} \binom{J}{i} + 1, & J \neq 2 \\ 2, & J = 2 \end{cases} \tag{4.57}$$

For C-RM codes, $(n_R - k_R)$ shift registers are used, and the number and the location of the two-input XOR gates in the circuits are dependent upon the generator polynomial of each code. The energy cost of encoding is therefore:

$$E_{\text{en-(1,3)RM}} = 20N_{\text{sm-en}}\left(4\left(n_R - k_R\right) + 8\right) + 2450N_{\text{sm-en}}, \tag{4.58}$$

$$E_{\text{en-(1,4)RM}} = 20N_{\text{sm-en}}\left(4\left(n_R - k_R\right) + 24\right) + 2450N_{\text{sm-en}}, \tag{4.59}$$

$$E_{\text{en-(2,4)RM}} = 20N_{\text{sm-en}}\left(4\left(n_R - k_R\right) + 8\right) + 2450N_{\text{sm-en}}, \tag{4.60}$$

$$E_{\text{en-(2,5)RM}} = 20N_{\text{sm-en}}\left(4\left(n_R - k_R\right) + 40\right) + 2450N_{\text{sm-en}}, \tag{4.61}$$

$$E_{\text{en-(3,5)RM}} = 20N_{\text{sm-en}}\left(4\left(n_R - k_R\right) + 8\right) + 2450N_{\text{sm-en}}. \tag{4.62}$$

In general, the z^{th} order C-RM code can be decoded with a (z + 1)-step majority logic decoder. For these decoding circuits, the total number, N_{ML}, of the J-input MLGs used in the circuit can be analysed as [125]:

$$N_{\text{ML}} = 1 + \sum_{i=1}^{L-1} J^i, \tag{4.63}$$

where $J = d_{\text{minR}} - 1$, and $L = z + 1$ is the number of steps used in the majority logic decoder.

The multi-input XOR gates used in majority vote process can be obtained by using the combination of multiple two-input XOR gates, and the number of inputs of the XOR gate is dependent on the check polynomial. In this work, the two-input MLGs are used in (1,3)C-RM, (2,4)C-RM and (3,5)C-RM decoders' design, six-input MLGs are used in the (1,4)C-RM and (2,5)C-RM decoders' design. According to (4.57), the two-input MLG and the six-input MLG can be formed by 2 and 22 NAND gates.

In addition, n_{R}-stage buffer registers and an extra two-input XOR gate are also needed. Here for C-RM codes, the energy cost of decoding is therefore:

$$E_{\text{de-(1,3)RM}} = 20N_{\text{sm-de}}\left(4n_{\text{R}} + 58\right) + 2450N_{\text{sm-de}}, \tag{4.64}$$

$$E_{\text{de-(1,4)RM}} = 20N_{\text{sm-de}}\left(4n_{\text{R}} + 590\right) + 2450N_{\text{sm-de}}, \tag{4.65}$$

$$E_{\text{de-(2,4)RM}} = 20N_{\text{sm-de}}\left(4n_{\text{R}} + 242\right) + 2450N_{\text{sm-de}}, \tag{4.66}$$

$$E_{\text{de-(2,5)RM}} = 20N_{\text{sm-de}}\left(4n_{\text{R}} + 6998\right) + 2450N_{\text{sm-de}}, \tag{4.67}$$

$$E_{\text{de-(3,5)RM}} = 20N_{\text{sm-de}}\left(4n_{\text{R}} + 994\right) + 2450N_{\text{sm-de}}. \tag{4.68}$$

C. Energy consumption for LDPC codes

For (15,7), (63,37) and (255,175)LDPC codes, ($n_{\text{L}} - k_{\text{L}}$) shift registers are used, and the number of two-input XOR gates in the circuits is dependent upon the generator polynomial of each code. The energy cost of encoding is therefore:

$$E_{\text{en-(15,7)LDPC}} = 20N_{\text{sm-en}}\left(4\left(n_{\text{L}} - k_{\text{L}}\right) + 16\right) + 2450N_{\text{sm-en}}, \tag{4.69}$$

$$E_{\text{en-(63,37)LDPC}} = 20N_{\text{sm-en}}\left(4\left(n_{\text{L}} - k_{\text{L}}\right) + 40\right) + 2450N_{\text{sm-en}}, \tag{4.70}$$

$$E_{\text{en-(255,175)LDPC}} = 20N_{\text{sm-en}}\left(4\left(n_{\text{L}} - k_{\text{L}}\right) + 180\right) + 2450N_{\text{sm-en}}. \tag{4.71}$$

In addition, for different LDPC codes, the decoding circuits can be modified with ρ-input XOR gates, θ-input MLGs, and n_{L} buffer registers. The multi-input XOR gate can be obtained by using the combination of multiple two-input XOR gates. Here for (15,7), (63,37) and (255,175)LDPC codes, the energy cost of decoding is therefore:

$$E_{\text{de-(15,7)LDPC}} = 20N_{\text{sm-de}}\left(4n_{\mathrm{L}} + 57\right) + 2450N_{\text{sm-de}}, \tag{4.72}$$

$$E_{\text{de-(63,37)LDPC}} = 20N_{\text{sm-de}}\left(4n_{\mathrm{L}} + 321\right) + 2450N_{\text{sm-de}}, \tag{4.73}$$

$$E_{\text{de-(255,175)LDPC}} = 20N_{\text{sm-de}}\left(4n_{\mathrm{L}} + 27297\right) + 2450N_{\text{sm-de}}. \tag{4.74}$$

D. Energy consumption for SOCCs

Referring the description of SOCCs in Section 4.5. For each encoder, the number of shift register units for the encoder is b, and number of the XOR gates is dependent upon on the generator polynomials. The energy cost of the encoding is thus:

$$E_{\text{en-(2,1,6)SOCC}} = 20N_{\text{sm-en}}\left(4b + 12\right) + 2450N_{\text{sm-en}}, \tag{4.75}$$

$$E_{\text{en-(2,1,17)SOCC}} = 20N_{\text{sm-en}}\left(4b + 20\right) + 2450N_{\text{sm-en}}, \tag{4.76}$$

$$E_{\text{en-(3,2,2)SOCC}} = 20N_{\text{sm-en}}\left(4b + 12\right) + 2450N_{\text{sm-en}}, \tag{4.77}$$

$$E_{\text{en-(3,2,13)SOCC}} = 20N_{\text{sm-en}}\left(4b + 28\right) + 2450N_{\text{sm-en}}. \tag{4.78}$$

The decoder can be separated into two parts, one is the same as the encoder, and then another part contains b register units, k_{S} MLGs, the MLGs used here are two-input MLGs, where each one can be looked as an AND gate. The number of XOR gates is dependent on the polynomial generator and the information length. So the energy cost of the decoding is:

$$E_{\text{de-(2,1,6)SOCC}} = 20N_{\text{sm-de}}\left(8b + 37\right) + 2450N_{\text{sm-de}}, \tag{4.79}$$

$$E_{\text{de-(2,1,17)SOCC}} = 20N_{\text{sm-de}}\left(8b + 70\right) + 2450N_{\text{sm-de}}, \tag{4.80}$$

$$E_{\text{de-(3,2,2)SOCC}} = 20N_{\text{sm-de}}\left(8b + 36\right) + 2450N_{\text{sm-de}}, \tag{4.81}$$

$$E_{\text{de-(3,2,13)SOCC}} = 20N_{\text{sm-de}}\left(8b + 74\right) + 2450N_{\text{sm-de}}. \tag{4.82}$$

4.7.2 Critical distance

In order to analyse when the coding becomes beneficial, the critical distance [128] as a measure of the actual transmission distance at which the coding gain matches the extra energy requirements introduced by the ECCs.

The total energy cost for an uncoded system, E_{uncoded} and coded system, E_{coded} can be calculated as:

$$E_{\text{uncoded}} = 2450 N_{\text{uncoded}}. \tag{4.83}$$

$$E_{\text{coded}} = 2450 N_{\text{coded}} + E_{\text{en}} + E_{\text{de}}. \tag{4.84}$$

where N_{uncoded} and N_{coded} are the numbers of molecules used for the uncoded and coded system at a chosen BER level. E_{en} and E_{de} are the energy consumption for the encoding and decoding process.

For reaching the same BER level, the energy saving (or loss) for a coded system compare with uncoded system can be defined as:

$$\begin{aligned} \Delta E &= E_{\text{uncoded}} - E_{\text{coded}} \\ &= 2450\left(N_{\text{uncoded}} - N_{\text{coded}}\right) - E_{\text{en}} - E_{\text{de}}. \end{aligned} \tag{4.85}$$

It is clear to see that when $\Delta E \geq 0$, the use of ECC is beneficial to the MC system. When $\Delta E = 0$, (4.85) reduces to:

$$N_{\text{uncoded}} - N_{\text{coded}} = \left(E_{\text{en}} + E_{\text{de}}\right)/2450. \tag{4.86}$$

Thus, the critical distance can be found by searching the transmission distance, d, that satifies the equation (4.86), this process can be completed by using MATLAB programming. The relationship between N_{uncoded} and N_{coded} can be obtained by substituting the energy consumption values for different coding schemes that introduced in Section 4.7.1.

4.8 Numerical results

The performance of MC system is evaluated via two aspects: one is the BER, and the other is the energy efficiency i.e. critical distance and total energy consumption under three different communication scenarios.

The coded schemes are applied based on the uncoded system that introduced in Chapter 3. The BER and energy efficiency results are presented based on a set of parameters in Table 4.2 and Table 4.3, respectively.

Table 4.2: Simulation parameters for BER.

Parameter	Definition	Value
R	Radius of the R_X	5μm
d	Transmission distance	{6 ~ 15}μm
D	Diffusion coefficient	$79.4\mu m^2 s^{-1}$
I	ISI length	10
N_{tx}	Number of molecules per bit	100 ~ 4000
Q	Number of transmitted bits	10^{15}

Table 4.3: Simulation parameters for energy efficiency.

Parameter	Definition	Value
R	Radius of the R_X	5μm
d_c	critical distance	Variance
D	Diffusion coefficient	$79.4\mu m^2 s^{-1}$
I	ISI length	10

4.8.1 BER performance of coded DBMC system

The BER results for both uncoded and coded systems are given in this section. The results are presented in two methods. Firstly, the values of BER for the coded system are given based on the theoretical analyses introduced in Section 4.6. Secondly, the values of BER are obtained based on the simulation of encoding and decoding processes.

A. Theoretical results

The BER performance results are shown in Figure 4.8(a) and (b). It indicates that increasing the number of molecules per bit leads to a smaller BER for uncoded and coded systems. For the system with block codes and SOCCs, when the number of molecules per bit greater than 250 and 300 respectively, the performance of the coded system is better than the uncoded system.

Using the equation (4.54), the coding gain for (7,4), (15,11), (31,26) Hamming code, (1,3), (1,4), (2,4), (2,5), (3,5) C-RM codes, (15,7), (63,37) (255,175) LDPC codes and (2,1,6), (2,1,17), (3,2,2), (3,2,13) SOCCs are shown to be 1.33dB, 1.68dB, 1.66dB, 1.33dB, 1.89dB, 1.68dB, 2.30dB, 1.66dB, 1.73dB, 2.50dB, 2.59dB, 1.51dB, 1.73dB, 1.49dB, 1.88dB respectively at the BER level of 10^{-3}. At a BER level of 10^{-9}, the coding gain for above codes are shown to be 1.70dB, 2.52dB,

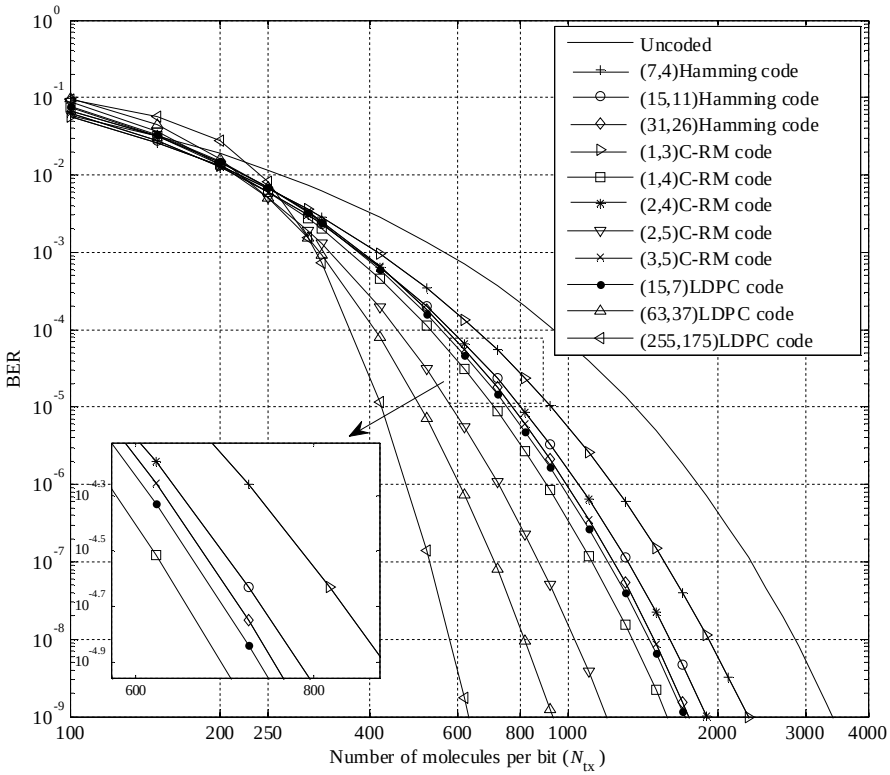

(a)

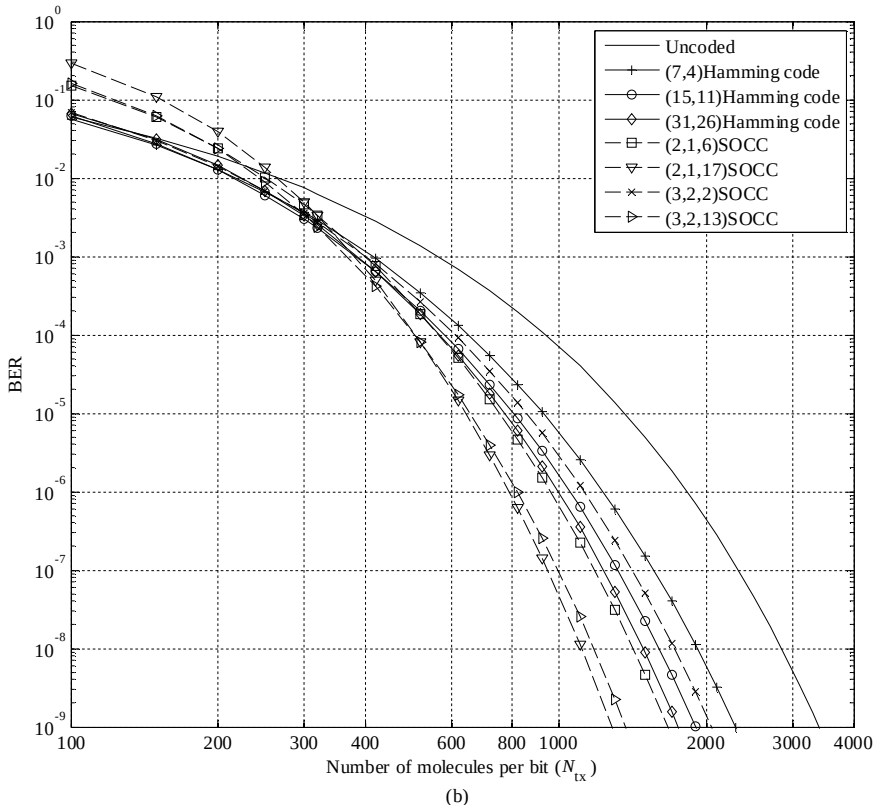

(b)

Figure 4.8: (a) BER comparison for a coded system with block codes and uncoded system. (b) BER comparison for a coded system with SOCCs, Hamming codes and uncoded system.

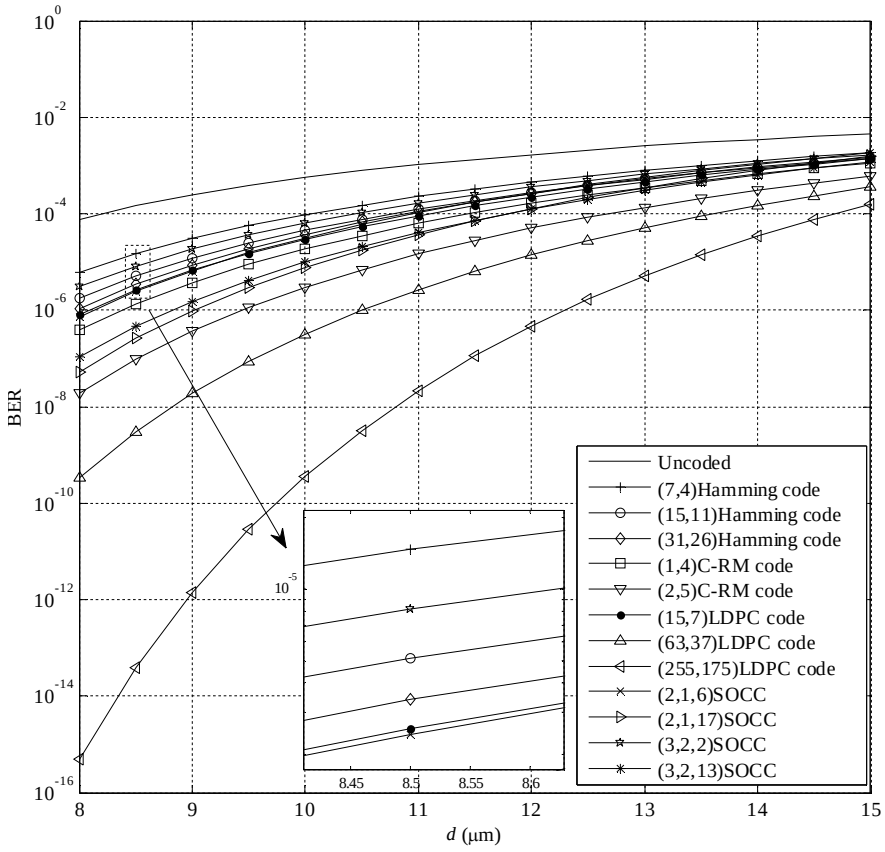

Figure 4.9: BER vs transmission distance for coded and uncoded system, N_{tx} = 2000.

2.88dB, 1.70dB, 3.31dB 2.52dB, 4.54dB, 2.88dB, 2.96dB, 5.62dB, 7.30dB, 3.09dB, 4.24dB, 2.20dB, and 3.95dB. The results indicate that of all these error correction schemes considered, the (255,175) LDPC code will provide the highest system performance. In addition, it also shows that three pairs of coding schemes have the same BER curves. These are (1,3) C-RM code with (7,4) Hamming code, (2,4) C-RM code with (15,11) Hamming code and (3,5) C-RM code with (31,26) Hamming code. This is because C-RM codes with E_{cR} = 1 are equivalent to Hamming codes, such that the Hamming code is also the simplest example of a C-RM code [132].

Figure 4.9 shows the BER with different transmission distance for coded and uncoded system when N_{tx} = 2000. It can be seen that the increases of transmission distance lead to a higher BER for both coded and uncoded system. The BER performance can be improved by introducing coding techniques in the MC system. It also noticed that the lowest and highest BERs are given by (255,175)LDPC code and (7,4)Hamming code respectively.

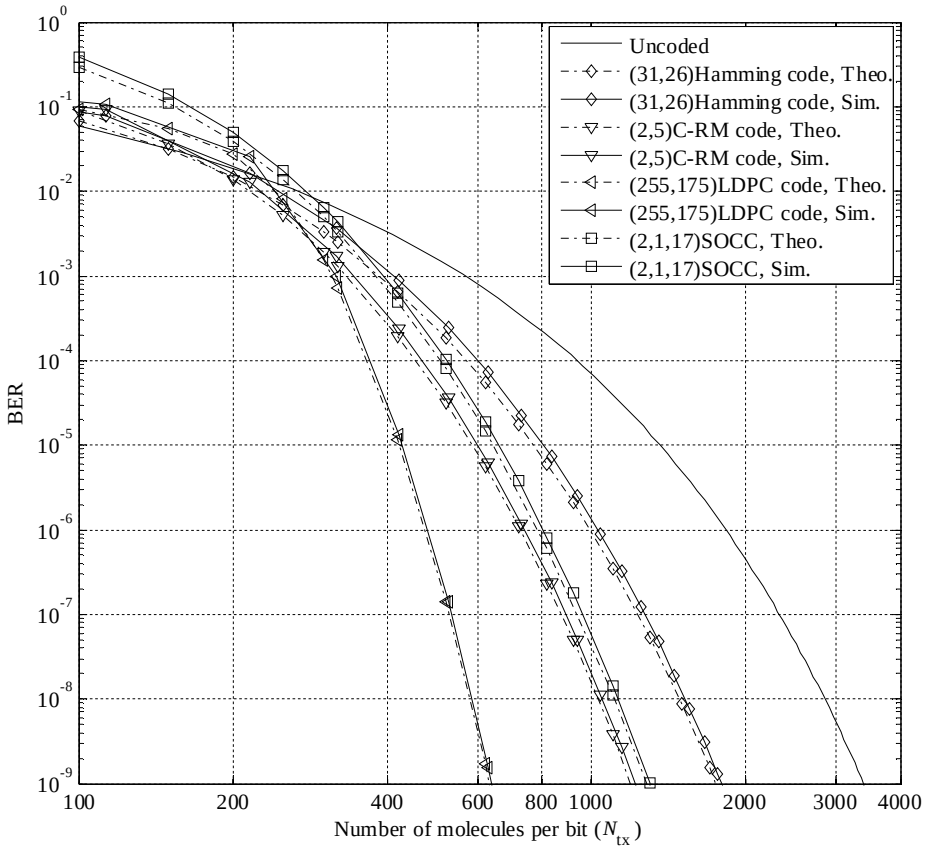

Figure 4.10: Theoretical BER and Simulation BER for different coding schemes, d = 6μm.

B. Simulation results

In the simulation process, in order to achieve a 10^{-9} BER level, 10^{15} consecutive information bits are encoded at T_X based on different encoding schemes, and then 10^{15}/(Information length) blocks are transmitted through the MC channel. At R_X, the information is decoded, and the BER for the coded system can be obtained.

Here, the comparison between the theoretical and simulation results for (31,26)Hamming code, (2,5)C-RM code, (255,175)LDPC code and (2,1,17)SOCC are given in Figure 4.10. It can be noticed that the BER results from theoretical analysis and simulation are very similar and differ only slightly from each other.

4.8.2 Energy efficiency

Two ranking systems are shown in analysing the energy efficiency of the ECCs. The main ranking system is the critical distance which introduced in Section 4.7.2.

However, there are cases where is no critical distance as in fact, in those cases, the use of ECC is always beneficial. In these cases, the ECC is ranked purely depended on the total energy consumption, (4.84) for the coded system.

Here, the two ranking system are considered under three communication scenarios, which are N2N, N2M, and M2N communications. For N2N communication, the extra energy requirements introduced by the encoder and decoder need to be taken into account. For N2M communication, the T_Xs are considered much simpler than the R_Xs, so when calculating the energy, only the encoder consumption needs to be taken into account by setting $E_{de} = 0$ in (4.86). Moreover, for M2N communication, the R_X needs to be much simpler than the T_X, so only the decoder consumption need to be included, so E_{en} set to zero in (4.86).

As the (4.86) shows, the critical distance is affected by two factors. Firstly, an obvious relationship in the system performance exists for the different coding schemes at different distances, as shown in Figure 4.8. Secondly, the encoder and decoder circuitry for each of the codes is different, with varying levels of complexity such as those in Figure 4.3, Figure 4.4, Figure 4.5 and Figure 4.6.

Figure 4.11 to Figure 4.16 provide the main critical distance and energy consumption results for different communication scenarios and different coding techniques. The critical distance for each code can be treated as a ground level. When the designed parameters fall in the left side of the ground level, this code is worth to apply into the designed system, otherwise not. This means the code is worth applied into the system only when the application with a transmission distance equal or larger than the critical distance. On the other hand, for each communication scenario, there exist a lowest critical distance level for BERs from 10^{-9} to 10^{-3}, and the corresponding code is considered as a best-fit ECC. The best-fit ECC is the code that has a wider application range. For another metric, energy consumption, the lower the better.

Figure 4.11 provides the critical distance and energy consumption results for N2N communication scenario with different Hamming, C-RM and LDPC codes over a BER range of 10^{-9} to 10^{-3}. Clearly from the results shown in Figure 4.11(a), the critical distance of (15,11)Hamming and (15,7)LDPC codes exist in a small BER

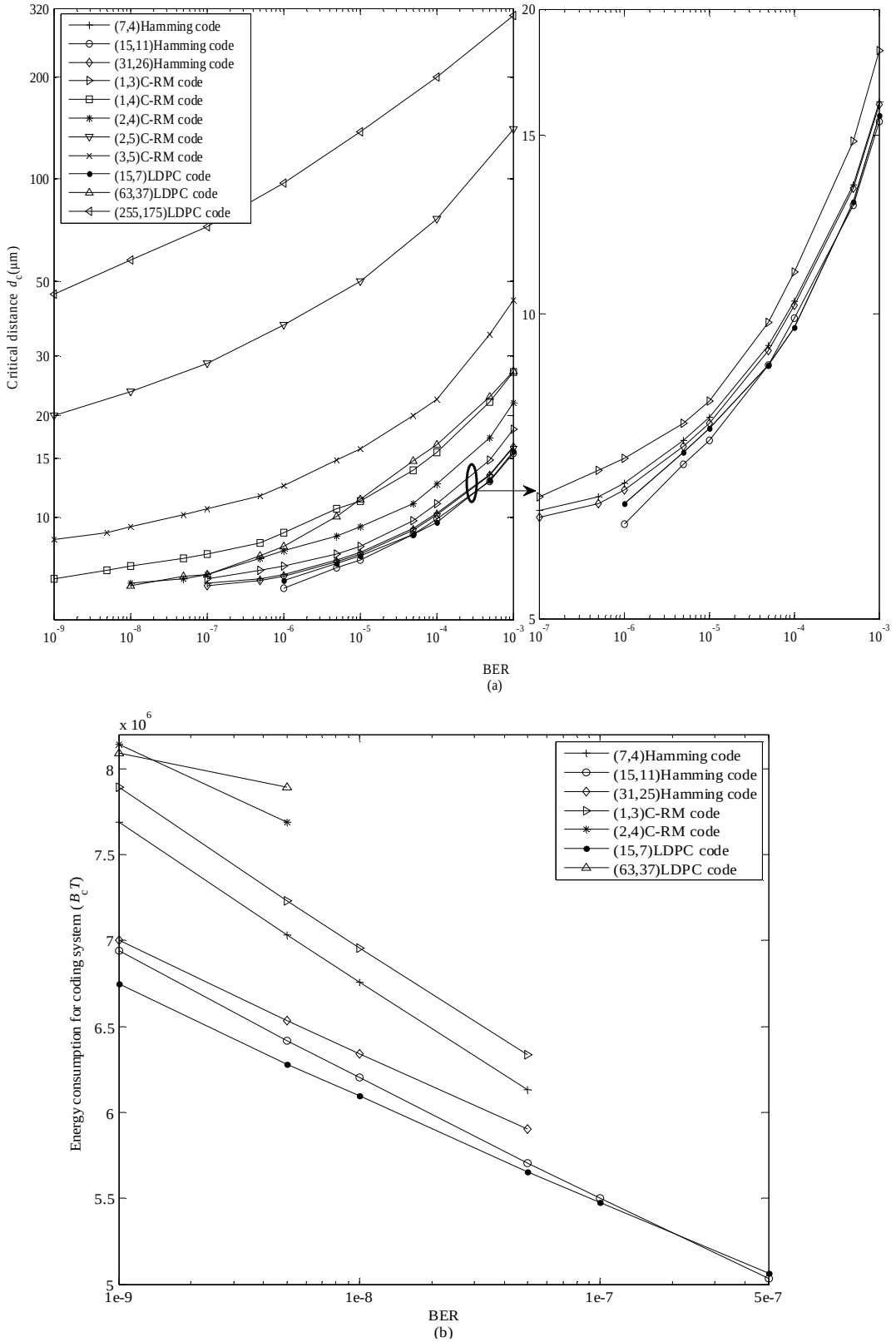

Figure 4.11: (a) critical distance and (b) energy consumption with BER for (7,4), (15,11),(31,26)Hamming codes, (1,3), (1,4), (2,4), (2,5), (3,5)C-RM codes and (15,7), (63,37), (255,175)LDPC codes when considering N2N communication.

range from 10^{-6} to 10^{-3}, and the lowest critical distance belongs to (15,11)Hamming code. Under the same communication architecture, Figure 4.11(b) shows the energy cost for the coded system at those BER levels where the critical distance does not exist. It is clearly shown that (15,7)LDPC code gives the lowest energy cost of the coded system. So under this communication scenario, when the system operates at 10^{-6} to 10^{-3} BER levels, (15,11)Hamming code is the first choice, otherwise, (15,7)LDPC code with the lowest energy cost should be selected.

There also exists another nano-communications architecture that a nano-machine transmits information to macro-machine which is not constrained by the same power budget. Therefore, if one considers such a system, and assumes the extra energy comes from the encoder only, then the critical distance and energy consumption results can be seen in Figure 4.12(a) and (b). Here, the interesting observation is most codes are beneficial for N2M communication system. In this case, the analysis should focus on the energy cost shown in Figure 4.12(b), when considering the system operating at 10^{-9} to 10^{-6} BERs, the (63,37)LDPC should be considered as the designer's first choice with the lowest energy cost. For BER levels from 10^{-4} to 10^{-3}, the (15,11)Hamming has the lowest critical distance.

Similarly, there may be system designs whereby a macro/micro-machine is communicating with a nano-machine, M2N communication, such that, it is critical to minimize the decoding energy costs with an assumption for now that the encoding costs can be contained within a larger energy budget. Under this scenario, only the energy cost of the decoder is considered as an extra energy, the results are shown in Figure 4.13(a) and (b). Here, if the system is operating at 10^{-5} to 10^{-3} BERs, then the (15,7)LDPC provides the shortest critical distance for which coding becomes beneficial. For operating BERs lower than 10^{-5}, Figure 4.13(b) shows that the lowest energy cost for the coded system which also belongs to (15,7)LDPC code. In this case, the (15,7)LDPC code becomes the best choice for a molecular communication system that is operating between 10^{-9} and 10^{-3} BER levels.

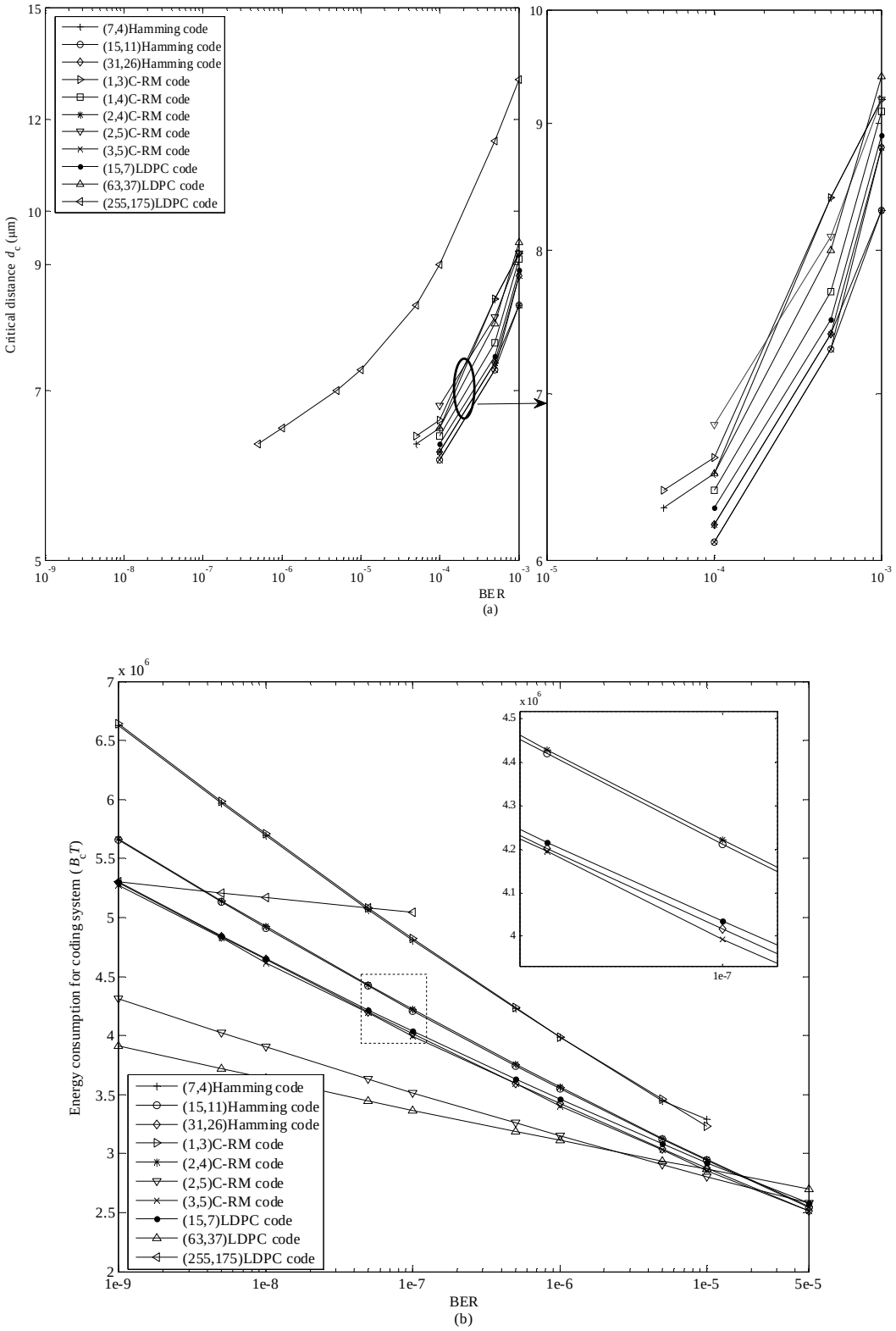

Figure 4.12: (a) critical distance and (b) energy consumption with BER for (7,4), (15,11),(31,26)Hamming codes, (1,3), (1,4), (2,4), (2,5), (3,5)C-RM codes and (15,7), (63,37), (255,175)LDPC codes when considering N2M communication.

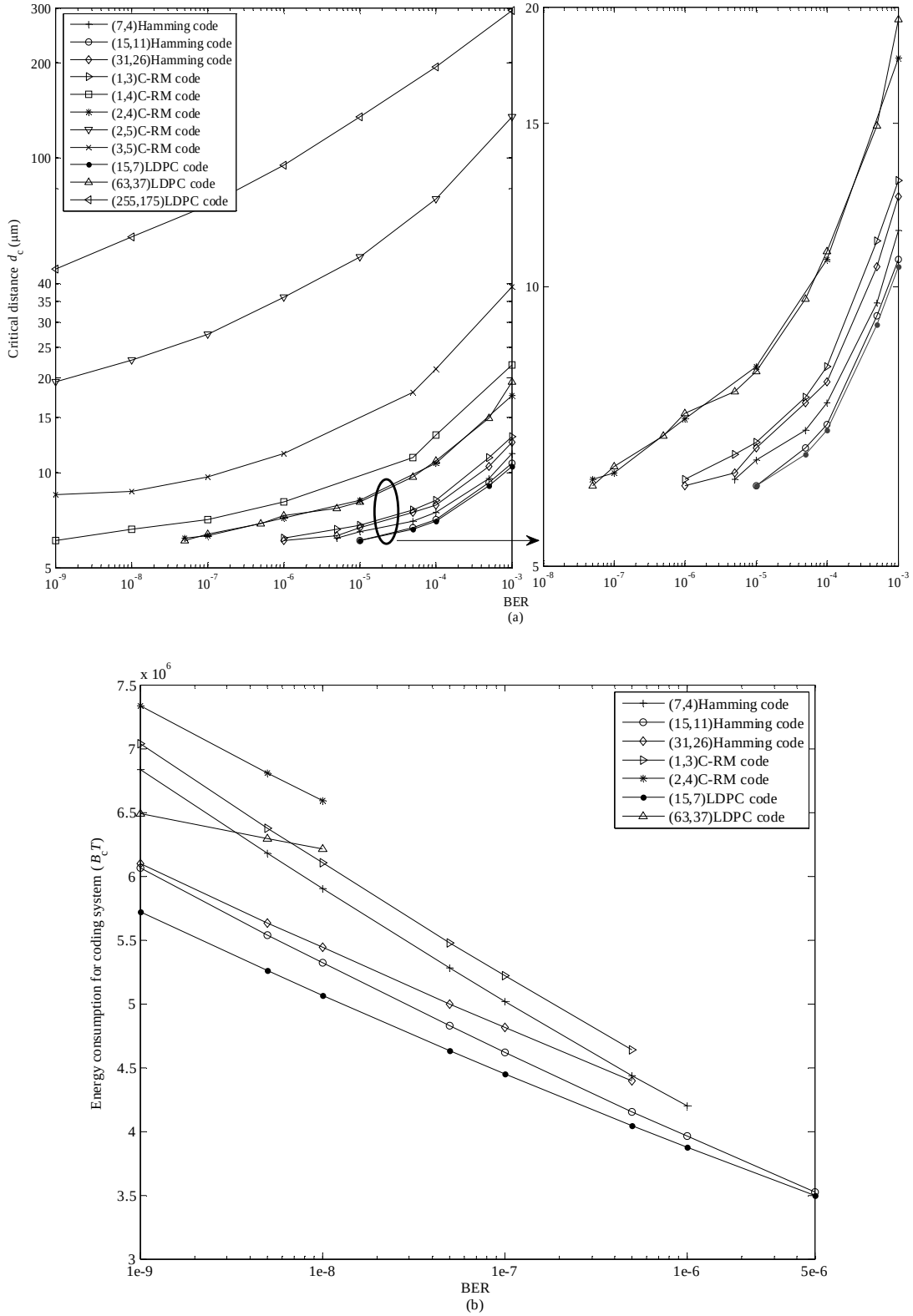

Figure 4.13: (a) critical distance and (b) energy consumption with BER for (7,4), (15,11),(31,26)Hamming codes, (1,3), (1,4), (2,4), (2,5), (3,5)C-RM codes and (15,7), (63,37), (255,175)LDPC codes when considering M2N communication.

From the above analysis, the best-fit ECCs from the select block codes are (15,11)Hamming and (15,7)LDPC codes for N2N communication scenario, (15,11)Hamming and (63,37)LDPC codes for N2M communication scenario, and (15,7)LDPC code for M2N communication scenario. Thus, these block codes are considered to be compared with the critical distance and energy consumption for SOCCs.

Figure 4.14 shows the comparisons between the best fitting block codes and the SOCCs for N2N communication system. It indicates that the SOCC codes show the better results in both critical distance and energy consumption compare with the best fitting block codes. The critical distance results are given in Figure 4.14(a), where (2,1,6) and (3,2,2) SOCCs are all better than (15,11)Hamming code and the (2,1,6)SOCC gives the lowest energy cost which shows in Figure 4.14(b). Thus, for the system operating between 10^{-9} to 5×10^{-5} and 5×10^{-5} to 10^{-3} BERs, the (2,1,6) and (3,2,2)SOCC apply a wider transmission range respectively.

Figure 4.15 shows another scenario which is N2M communication. When considering the system operating at 10^{-9} to 5×10^{-6}, the (63,37)LDPC code is still the best choice with the lowest energy cost. For a system operating at 10^{-4} to 10^{-3}, the critical distance of (15,11)Hamming is the same as (2,1,6)SOCC, the designer can have either. The results for M2N communication scenario is shown in Figure 4.16. Here, the (3,2,2) SOCC get the lowest critical distance between a BER level of 5×10^{4} to 10^{-3}. Considering the energy cost from 10^{-9} to 10^{-5}, the (2,1,17)SOCC own the lowest energy cost when the system operating at 10^{-9} to 10^{-8} BERs, and for those systems working at 5×10^{-7} to 10^{-5}, the (15,7)LDPC is the best choice with the lowest energy cost.

All the results present from Figure 4.11 to Figure 4.16 indicate that the increasing in operating BER leads to a longer critical distance and lower energy consumption. With the increasing of the level of operating BER, the coding gain is reduced. Thus, a longer critical distance is needed to guarantee the extra energy is equals to the coding gain. However, the increasing in BER level will cause a reducing of number of molecules that needed for the coded system. Thus, with a fixed coding technique, the equation, (4.84) indicates that the total energy consumption decreases.

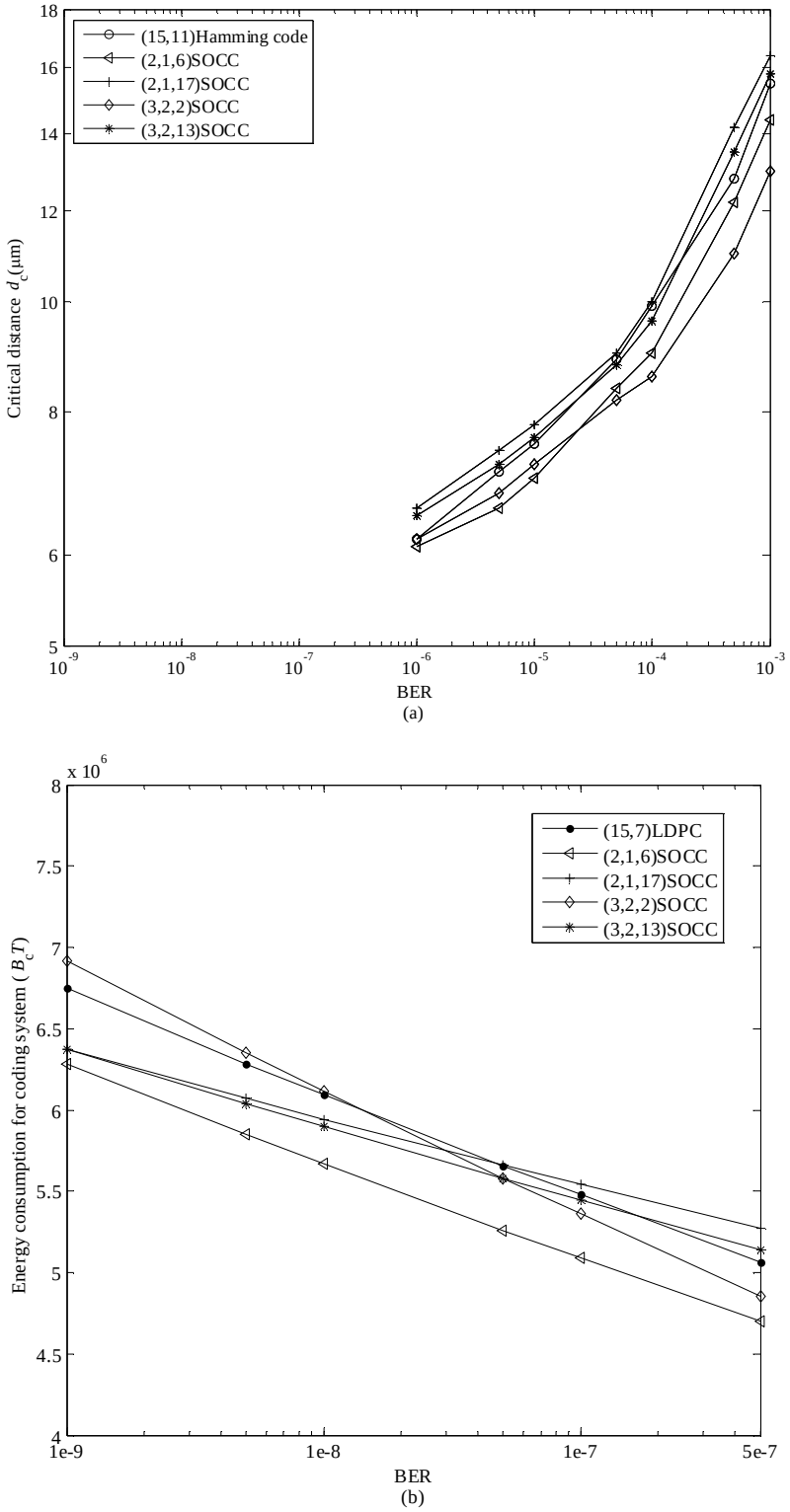

Figure 4.14: (a) critical distance and (b) energy consumption comparisons between the best-fit block codes and (2,1,6), (2,1,17), (3,2,2), (3,2,13)SOCC codes when considering N2N communication.

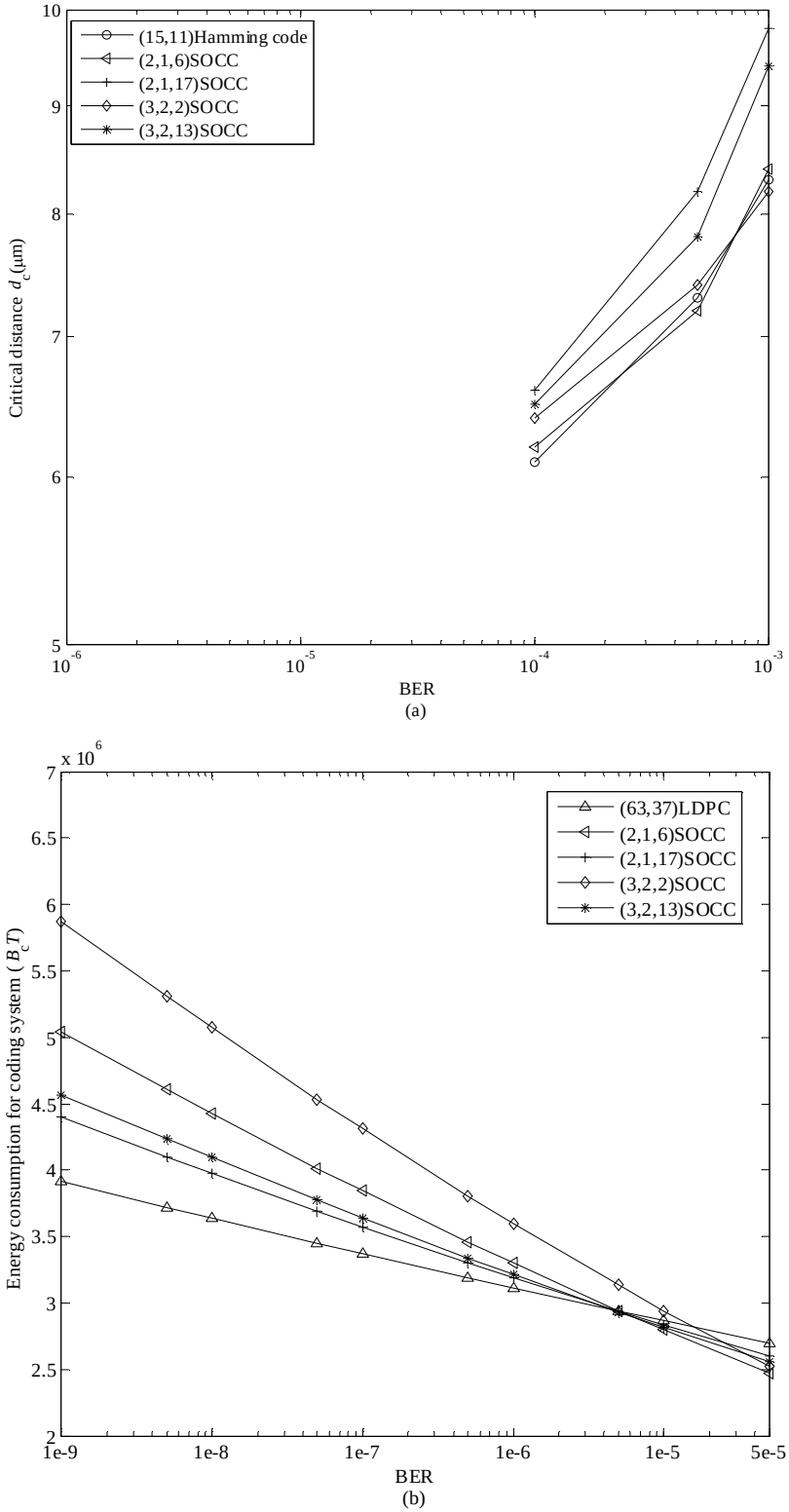

Figure 4.15: (a) critical distance and (b) energy consumption comparisons between the best-fit block code and (2,1,6), (2,1,17), (3,2,2), (3,2,13)SOCC codes when considering N2M communication.

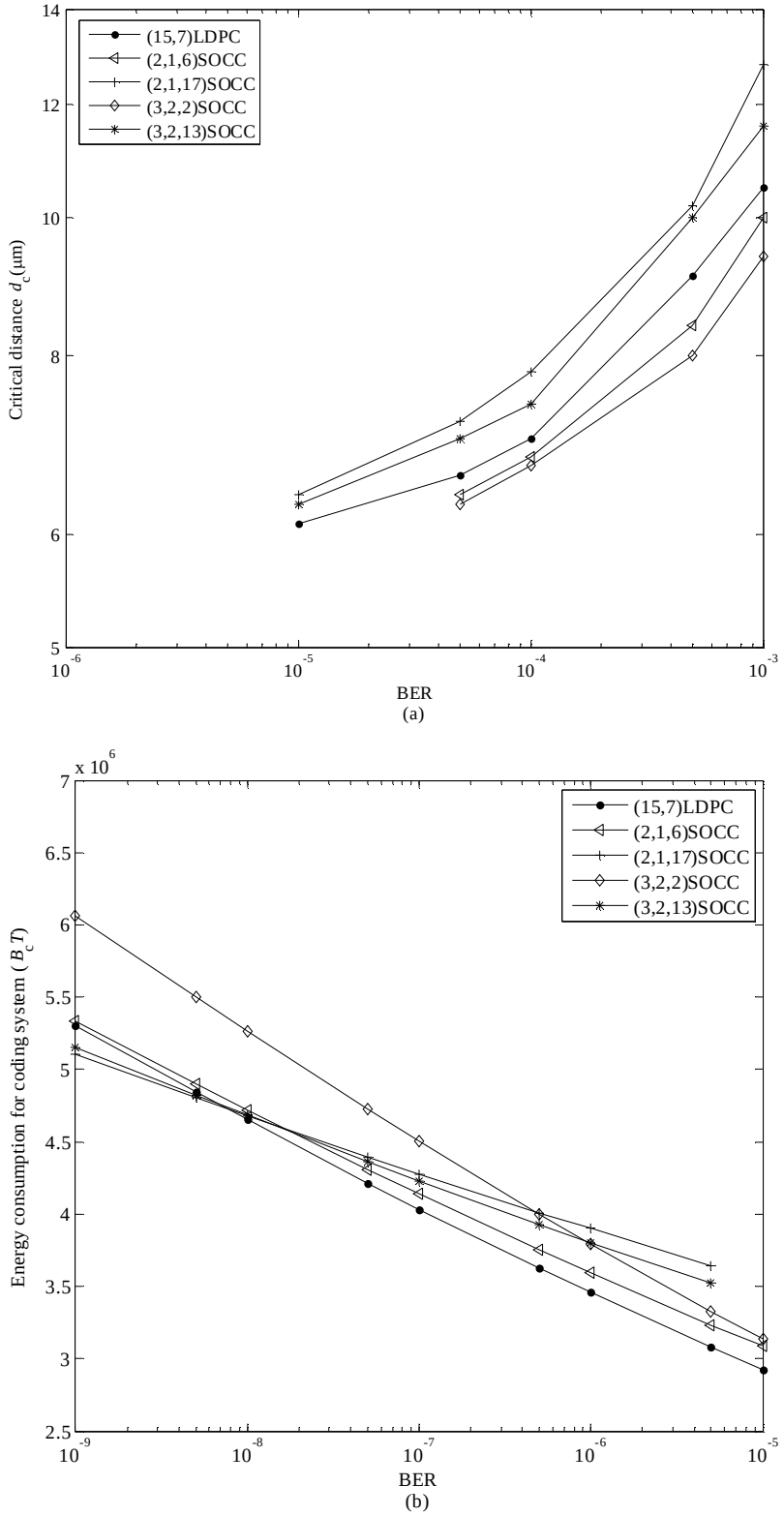

Figure 4.16: (a) critical distance and (b) energy consumption comparisons between the best-fit block codes and (2,1,6), (2,1,17), (3,2,2), (3,2,13)SOCC codes when considering M2N communication.

4.8.3 Results discussion

Given the above analyzation and comparison. A summary of the best-fit ECCs for different communication scenarios is given in Table 4.4 and Table 4.5. Here, the operating BER (from 10^{-9} to 10^{-3}) of the system is separated into two parts. One is the region that the best-fit ECCs can be determined by measuring critical distance, which is the higher operating BER region, and another region is the best-fit ECCs can be determined by measuring total energy cost, which is called the lower operating BER region.

Table 4.4: Defined operating BERs for different communication scenarios.

Communication scenario	Lower operating BER region	Higher operating BER region
N2N	$10^{-9} \sim 5\times10^{-7}$	$10^{-6} \sim 10^{-3}$
N2M	$10^{-9} \sim 5\times10^{-5}$	$10^{-4} \sim 10^{-3}$
M2N	$10^{-9} \sim 5\times10^{-6}$	$10^{-5} \sim 10^{-3}$

Table 4.5: Best-fit codes for different MC scenarios.

Communication scenario	Lower BER operating region	Higher BER operating region
N2N	(2,1,6)SOCC	(3,2,2)SOCC
N2M	(63,37)LDPC	(15,11)Hamming/(2,1,6)SOCC
M2N	(15,7)LDPC	(3,2,2)SOCC

Based on Table 4.4, the fitting ECCs for different MC scenarios are shown in Table 4.5. The table indicates that the (255,175)LDPC which has the best BER performance is not the best-fit codes for any of the MC system due to the highly complexity of the encoder and decoder design. On the contrary, the codes which did not have the best BER performance but have a simpler encoder or decoder circuits are super. Thus, a simpler circuits design for coding techniques in MC systems is very important.

4.9 Conclusions

In this chapter, the selected block codes which are Hamming, C-RM and LDPC codes and the selected convolutional code which is SOCC have been introduced into

the MC system, and the performance has been compared among them with regards to both coding gain and energy requirements. Both theoretical and simulation results of BER for the coded system are analysed and compared. The results show that the coding techniques do enhance the performance of the molecular communication system.

With a strong emphasis on not hiding the cost of this gain, this work has further analysed, under three different scenarios, how much energy these gains cost, by defining the distances at which the use of coding becomes beneficial. Furthermore, the energy costs for the coded systems under these scenarios are also taken into account when the critical distance does not exist. It has been indicated that an increase of the operating BER results in a longer critical distance and lower energy cost. For N2M and M2N communication scenarios, the critical distance decreases in comparison with the N2N communication scenario. Moreover, for a system with a specific operating BER and transmission distance, the most suitable code can be selected by analysing these performance metrics.

Chapter 5
A Refined PTP DBMC Model

5.1 Introduction and related work

As mentioned in Section 2.4, an accurate and efficient channel model is paramount for analysing the performance of communication systems. In the MC system, the most popular way is to approximate the number of received molecules as a Binomial distribution and consider the capture probability of those molecules as the success probability for information transmission. The key work can be found in [23], where the model was present under the assumption that the number of molecules transmitted in one time slot, but received in different successive time slots was independent. This prevailing assumption was carried forward and considered in numerous key papers such as [54, 100, 139-144]. The channel model introduced in Chapter 3 is also investigated under this assumption.

However, through careful consideration of the actions of an absorbing receiver, the assumption of independence between the numbers of molecules arriving in different time slots cannot accurate estimate the channel performance, as the removal of the molecule means they cannot be present later. That is, the number of molecules arriving in the previous time slots will reduce the possible number of molecules in the next and thus the number of molecules received in one time slot does affect that in the following time slots and they are dependent events.

The authors of [145], [146] have already presented a model which does consider the number of molecules received in the current time slot, taking into account those absorbed in the previous slots. However, they only presented the observation and subsequent model without much theoretical derivation. Furthermore,

no direct comparisons were presented to previously work. Thus no bounds exist on how ‘correct’ or ‘accurate’ their newer dependent model is. The work in this chapter aims to fulfil this insufficient investigation of the refined channel model.

In order to simplify the description and give a clear distinction between the refined model and the model introduced in Chapter 3. Here, the refined model is denoted as the R-Model and the previous model is denoted as the P-Model.

In this chapter, a more realistic performance of a molecular communication assuming correlated events is analysed and following achievements are made. Firstly, a comprehensive analysis of the system performance in terms of BER under the consideration of correlation between numbers of molecules in different time slots is presented. This analysis includes an explanation of dependence along with a full proof from the first principles of 3D diffusion propagation. Secondly, an arbitrary ISI length is introduced during the theoretical derivation to maximize the generality of the analysis. Thirdly, under the consideration of the R-Model, the Binomial distribution is then approximated by both the Poisson and Normal distributions such that the BER expressions for both approximations can be provided. The suitable approximation for a proposed system can be determined by measuring the Root Mean Squared Error (RMSE) [145]. In addition, the comparisons between approximations, and between the P-Model and the R-Model are also presented. The simulation results are also produced for verifying the accuracy of these channel models. These contributions allow the reader to clarify the theory behind the correlation between events as well as being able to quantify the accuracy of work using any of the approximations.

The remainder of this chapter is organised as follows. The R-Model is presented in Section 5.2. In Section 5.3, the system performance with regards to BER and channel capacity is analysed for both approximations. The simulation process is given in Section 5.4. Section 5.5 gives the key results for this chapter, and finally, Section 5.6 concludes the chapter.

5.2 R-Model

As in Chapter 3, the propagation model used for the R-Model is also the 3D diffusion based model with a molecule capture probability that is shown in (3.5). The

difference between the P-Model and the R-Model is the mathematic analysis of the arriving model.

5.2.1 Comparisons between P-Model and R-Model with the use of Normal approximation

Consider that N_{tx} molecules are released at the start of the current time slot, and that the numbers of molecules received in the current time slot for the P-Model and the R-Model are represented as $N_{p,0}$ and $N_{r,0}$. Similarly, the numbers of molecules received from the previous i^{th} symbol in the current time slot are represented as $N_{p,i}$ and $N_{r,i}$ respectively, and where $i = 1, 2, \ldots, I$.

The analysis of $N_{p,0}$ and $N_{r,0}$ is the same, where they all follow a Binomial distribution [23]:

$$N_{p,0} = N_{r,0} \sim \mathbf{B}\left(N_{tx}, P_{ca,0}\right), \tag{5.1}$$

if N_{tx} is large enough, the Binomial distributions $N_{p,0}$ and $N_{r,0}$ can be approximated by a Normal distribution $N_{pN,0}$ and $N_{rN,0}$ thus:

$$N_{pN,0} = N_{rN,0} \sim \mathbf{N}\left(N_{tx}P_{ca,0}, N_{tx}P_{ca,0}\left(1-P_{ca,0}\right)\right). \tag{5.2}$$

For the P-Model, the number of molecules received in different time slots from the same transmission was considered as independent. Under this assumption, the Normal approximation for $N_{p,i}$ can be derived as (3.10):

$$\begin{aligned} N_{pN,i} &= N_{0,i} - N_{0,i-1} \\ &\sim \mathbf{N}\left(N_{tx}\left(P_{ca,i} - P_{ca,i-1}\right), N_{tx}\left(P_{ca,i}\left(1-P_{ca,i}\right) + P_{ca,i-1}\left(1-P_{ca,i-1}\right)\right)\right) \\ &= \mathbf{N}\left(\eta_i, \varsigma_i\right), \end{aligned} \tag{5.3}$$

where $N_{0,i}$ is the number of molecules absorbed by the R_X during $(0, (i+1)\cdot t_s)$.

As mentioned in Section 5.1, the number of molecules received in different time slots from the same transmission cannot be independent due to absorption. Thus, for the R-Model, the probability density function of $N_{r,i} = y$ is given by:

$$
\begin{aligned}
\mathrm{P}\left(N_{\mathrm{r},i}=y\right) &= \sum_{x=0}^{N_{\mathrm{tx}}} \mathrm{P}\left(N_{\mathrm{r},i}=y \mid N_{\mathrm{r0},i-1}=x\right)\mathrm{P}\left(N_{\mathrm{r0},i-1}=x\right) \\
&= \sum_{x=0}^{N_{\mathrm{tx}}} \binom{N_{\mathrm{tx}}-x}{y} q^{y}(1-q)^{N_{\mathrm{tx}}-x-y} \binom{N_{\mathrm{tx}}}{x} p^{x}(1-p)^{N_{\mathrm{tx}}-x} \\
&= \left(q(1-p)\right)^{y} \sum_{x=0}^{N_{\mathrm{tx}}-y} \binom{N_{\mathrm{tx}}-x}{y} \binom{N_{\mathrm{tx}}}{x} p^{x}\left((1-p)(1-q)\right)^{N_{\mathrm{tx}}-y-x} \\
&= \left(q(1-p)\right)^{y} \sum_{x=0}^{N_{\mathrm{tx}}-y} \binom{N_{\mathrm{tx}}}{y} \binom{N_{\mathrm{tx}}-y}{x} p^{x}\left((1-p)(1-q)\right)^{N_{\mathrm{tx}}-y-x} \\
&= \binom{N_{\mathrm{tx}}}{y} \left(q(1-p)\right)^{y} \sum_{x=0}^{N_{\mathrm{tx}}-y} \binom{N_{\mathrm{tx}}-y}{x} p^{x}\left((1-p)(1-q)\right)^{N_{\mathrm{tx}}-y-x},
\end{aligned}
\tag{5.4}
$$

and then by applying Binomial theorem [147], the above equation can be replaced by:

$$
\begin{aligned}
\mathrm{P}\left(N_{\mathrm{r},i}=y\right) &= \binom{N_{\mathrm{tx}}}{y} \left(q(1-p)\right)^{y} \left(p+(1-p)(1-q)\right)^{N_{\mathrm{tx}}-y} \\
&= \binom{N_{\mathrm{tx}}}{y} \left(q(1-p)\right)^{y} \left(1-q(1-p)\right)^{N_{\mathrm{tx}}-y},
\end{aligned}
\tag{5.5}
$$

where $N_{\mathrm{r0},i\text{-}1}$ is the number of molecules received by $\mathrm{R_X}$ during $(0, i{\cdot}t_s)$ for the R-Model, $p = P_{\mathrm{ca},i\text{-}1} = P_{\mathrm{ca}}(d, i{\cdot}t_s)$, and $q = (P_{\mathrm{ca},i} - P_{\mathrm{ca},i\text{-}1})/(1 - P_{\mathrm{ca},i\text{-}1})$.

It obviously shows that $N_{\mathrm{r},i}$ follows a Binomial distribution:

$$
\begin{aligned}
N_{\mathrm{r},i} &\sim \mathbf{B}\left(N_{\mathrm{tx}}, q(1-p)\right) \\
&= \mathbf{B}\left(N_{\mathrm{tx}}, P_{\mathrm{ca},i} - P_{\mathrm{ca},i\text{-}1}\right).
\end{aligned}
\tag{5.6}
$$

The corresponding Normal approximation $N_{\mathrm{rN},i}$ can be computed as:

$$
\begin{aligned}
N_{\mathrm{rN},i} &\sim \mathbf{N}\left(N_{\mathrm{tx}}\left(P_{\mathrm{ca},i} - P_{\mathrm{ca},i-1}\right), N_{\mathrm{tx}}\left(P_{\mathrm{ca},i} - P_{\mathrm{ca},i-1}\right)\left(1 - P_{\mathrm{ca},i} + P_{\mathrm{ca},i-1}\right)\right) \\
&= \mathbf{N}\left(\varpi_i, \gamma_i\right),
\end{aligned}
\tag{5.7}
$$

where $\varpi_i = N_{\mathrm{tx}}(P_{\mathrm{ca},i} - P_{\mathrm{ca},i\text{-}1})$ and $\gamma_i = N_{\mathrm{tx}}(P_{\mathrm{ca},i} - P_{\mathrm{ca},i\text{-}1})(1 - P_{\mathrm{ca},i} + P_{\mathrm{ca},i\text{-}1})$.

It can clearly be seen that there is a difference between (5.3) and (5.7). Thus, in this chapter, (5.6) gives the refined expression which will be used in the analysis of the rest of this chapter.

The total number of information molecules received in one time slot for the P-Model is given in equation (3.11). For the R-Model, the expression of total number of molecules received in one time slot, $N_{\mathrm{rN,T}}$ is given as:

$$N_{\mathrm{rN,T}} = a_{\mathrm{c}} N_{\mathrm{r},0} + \sum_{i=1}^{I} a_{\mathrm{c}-i} N_{\mathrm{rN},i} \sim \mathbf{N}\left(a_{\mathrm{c}} N_{\mathrm{tx}} P_{\mathrm{ca},0} + \sum_{i=1}^{I} a_{\mathrm{c}-i} \varpi_i,\ a_{\mathrm{c}} N_{\mathrm{tx}} P_{\mathrm{ca},0}\left(1 - P_{\mathrm{ca},0}\right) + \sum_{i=1}^{I} a_{\mathrm{c}-i} \gamma_i \right). \tag{5.8}$$

5.2.2 R-Model with Poisson approximation

There is another commonly used approximation of the Binomial distribution which is called the Poisson distribution. The use of Poisson distribution to approximate the R-Model is detailed in this section.

$N_{\mathrm{r},0}$ and $N_{\mathrm{r},i}$ can be approximated using the Poisson approximation $N_{\mathrm{rP},0}$, $N_{\mathrm{rP},i}$, respectively:

$$N_{\mathrm{rP},0} \sim \mathbf{P}\left(N_{\mathrm{tx}} P_{\mathrm{ca},0} \right). \tag{5.9}$$

$$N_{\mathrm{rP},i} \sim \mathbf{P}\left(N_{\mathrm{tx}} \left(P_{\mathrm{ca},i} - P_{\mathrm{ca},i-1} \right) \right). \tag{5.10}$$

As the transmission symbols are in binary form, the value of $a_{\mathrm{c}\text{-}i}$ can only be 0 or 1, thus total number of molecules received in one time slot for the Poisson approximation, $N_{\mathrm{rP,T}}$ can be obtained as:

$$N_{\mathrm{rP,T}} = a_{\mathrm{c}} N_{\mathrm{rP},0} + \sum_{i=1}^{I} a_{\mathrm{c}-i} N_{\mathrm{rP},i} \sim \mathbf{P}\left(a_{\mathrm{c}} N_{\mathrm{tx}} P_{\mathrm{ca},0} + \sum_{i=1}^{I} a_{\mathrm{c}-i} N_{\mathrm{tx}} \left(P_{\mathrm{ca},i} - P_{\mathrm{ca},i-1} \right) \right). \tag{5.11}$$

5.3 BER and capacity analysis for the system with R-Model

The modulation technique used here is also the OOK. Thus, at $\mathrm{R_X}$, a pre-design threshold, τ, exists to decided which '1' or '0' is obtained. If the total number of received information molecules exceed τ, then the information is demodulated as '1', otherwise demodulated as '0'.

A. BER analysis

The condition metrics for the R-Model with the Normal and Poisson approximations can be rewritten as $\mathrm{T_{rN,c}}$ and $\mathrm{T_{rP,c}}$, respectively:

$$\begin{aligned} \mathrm{T}_{\mathrm{rN,c}} &= N_{\mathrm{rN,T}} - \tau \\ &\sim \mathbf{N}\left(a_{\mathrm{c}} N_{\mathrm{tx}} P_{\mathrm{ca},0} + \sum_{i=1}^{I} a_{\mathrm{c}-i} \varpi_i - \tau,\ a_{\mathrm{c}} N_{\mathrm{tx}} P_{\mathrm{ca},0}\left(1 - P_{\mathrm{ca},0}\right) + \sum_{i=1}^{I} a_{\mathrm{c}-i} \gamma_i \right). \end{aligned} \tag{5.12}$$

$$\begin{aligned} \mathrm{T}_{\mathrm{rP,c}} &= N_{\mathrm{rP,T}} - \tau \\ &\sim \mathbf{P}\left(a_{\mathrm{c}} N_{\mathrm{tx}} P_{\mathrm{ca},0} + \sum_{i=1}^{I} a_{\mathrm{c}-i} N_{\mathrm{tx}}\left(P_{\mathrm{ca},i} - P_{\mathrm{ca},i-1}\right)\right) - \tau. \end{aligned} \tag{5.13}$$

The corresponding metrics for each error pattern j can be obtained as $\mathrm{T}_{\mathrm{rN,c}j}$ and $\mathrm{T}_{\mathrm{rP,c}j}$:

$$\begin{aligned} \mathrm{T}_{\mathrm{rN,c}j} &= N_{\mathrm{rN,T}j} - \tau \\ &\sim \mathbf{N}\left(a_{\mathrm{c}} N_{\mathrm{tx}} P_{\mathrm{ca},0} + \sum_{i=1}^{I} a_{\mathrm{c}-i,j} \varpi_i - \tau,\ a_{\mathrm{c}} N_{\mathrm{tx}} P_{\mathrm{ca},0}\left(1 - P_{\mathrm{ca},0}\right) + \sum_{i=1}^{I} a_{\mathrm{c}-i,j} \gamma_i \right). \end{aligned} \tag{5.14}$$

$$\begin{aligned} \mathrm{T}_{\mathrm{rP,c}j} &= N_{\mathrm{rP,T}j} - \tau \\ &\sim \mathbf{P}\left(a_{\mathrm{c}} N_{\mathrm{tx}} P_{\mathrm{ca},0} + \sum_{i=1}^{I} a_{\mathrm{c}-i,j} N_{\mathrm{tx}}\left(P_{\mathrm{ca},i} - P_{\mathrm{ca},i-1}\right)\right) - \tau. \end{aligned} \tag{5.15}$$

The errors occur when there is a discrepancy between the transmitter and receiver signals. For a binary transmission, there are two cases, firstly, when a '0' is transmitted, but a '1' is received. Secondly, when a '1' is transmitted, but a '0' is received.

For this first case, the error probability of the Normal and Poisson approximations for the error pattern j, $P_{\mathrm{rN\_e01},j}$, $P_{\mathrm{rP\_e01},j}$ can be obtained as:

$$\begin{aligned} P_{\mathrm{rN\_e01},j} &= p_{\mathrm{tx}}{}^{\alpha_j}\left(1 - p_{\mathrm{tx}}\right)^{I-\alpha_j} \mathrm{P}\left(\mathrm{T}_{\mathrm{rN,c}j} > 0\right) \\ &= p_{\mathrm{tx}}{}^{\alpha_j}\left(1 - p_{\mathrm{tx}}\right)^{I-\alpha_j} \Phi\left(\frac{\mu_{\mathrm{r01},j}}{\sigma_{\mathrm{r01},j}}\right), \end{aligned} \tag{5.16}$$

$$\begin{aligned} P_{\mathrm{rP\_e01},j} &= p_{\mathrm{tx}}{}^{\alpha_j}\left(1 - p_{\mathrm{tx}}\right)^{I-\alpha_j} \mathrm{P}\left(\mathrm{T}_{\mathrm{rP,c}j} > 0\right) \\ &= p_{\mathrm{tx}}{}^{\alpha_j}\left(1 - p_{\mathrm{tx}}\right)^{I-\alpha_j} \left(1 - \mathrm{Q}\left(\tau + 1, \lambda_{\mathrm{r01},j}\right)\right), \end{aligned} \tag{5.17}$$

where:

$$\begin{aligned} \mu_{\mathrm{r01},j} &= \sum_{i=1}^{I} a_{\mathrm{c}-i,j} \varpi_i - \tau,\ \sigma_{\mathrm{r01},j} = \sqrt{\sum_{i=1}^{I} a_{\mathrm{c}-i,j} \gamma_i}, \\ \lambda_{\mathrm{r01},j} &= \sum_{i=1}^{I} a_{\mathrm{c}-i,j} N_{\mathrm{tx}}\left(P_{\mathrm{ca},i} - P_{\mathrm{ca},i-1}\right), \end{aligned} \tag{5.18}$$

where p_{tx} is the transmission probability of '1'. α_j is the number of '1's in the error pattern j. $P(T_{rP,cj} > 0)$ is the probability of $T_{rP,cj} > 0$. $\Phi(\cdot)$ is the cumulative distribution function of a standard Gaussian distribution, and $Q(x, y)$ is the regularized gamma function which is defined as:

$$Q(x,y) = e^{-y} \sum_{i=0}^{\lfloor x-1 \rfloor} \frac{y^i}{i!}. \tag{5.19}$$

For the second case, the error probability of the Normal and Poisson approximations for the error pattern j, $P_{rN\_e10,j}$, $P_{rP\_e10,j}$ can be obtained as:

$$\begin{aligned} P_{rN\_e10,j} &= p_{tx}^{\alpha_j} (1-p_{tx})^{I-\alpha_j} P(T_{rN,cj} \le 0) \\ &= p_{tx}^{\alpha_j} (1-p_{tx})^{I-\alpha_j} \Phi\left(-\frac{\mu_{r10,j}}{\sigma_{r10,j}}\right), \end{aligned} \tag{5.20}$$

$$\begin{aligned} P_{rP\_e10,j} &= p_{tx}^{\alpha_j} (1-p_{tx})^{I-\alpha_j} P(T_{rP,cj} \le 0) \\ &= p_{tx}^{\alpha_j} (1-p_{tx})^{I-\alpha_j} Q(\tau+1, \lambda_{r10,j}), \end{aligned} \tag{5.21}$$

where:

$$\begin{aligned} &\mu_{r10,j} = N_{tx} P_{ca,0} + \sum_{i=1}^{I} a_{c-i,j} \varpi_i - \tau, \quad \sigma_{r10,j} = \sqrt{N_{tx} P_{ca,0}(1-P_{ca,0}) + \sum_{i=1}^{I} a_{c-i,j} \gamma_i}, \\ &\lambda_{r10,j} = N_{tx} P_{ca,0} + \sum_{i=1}^{I} a_{c-i,j} N_{tx} (P_{ca,i} - P_{ca,i-1}). \end{aligned} \tag{5.22}$$

Thus, the average BER of the system with R-Model, P_{re}, can be derived as:

$$\begin{aligned} P_{re} &= p_{tx} P_{re10} + (1-p_{tx}) P_{re01} \\ &= p_{tx} \sum_{j=1}^{2^I} P_{rN/P\_e10,j} + (1-p_{tx}) \sum_{j=1}^{2^I} P_{rN/P\_e01,j}, \end{aligned} \tag{5.23}$$

where $P_{rN/P\_e10,j} = P_{rN\_e10,j}$ or $P_{rP\_e10,j}$ and $P_{rN/P\_e01,j} = P_{rN\_e01,j}$ or $P_{rP\_e01,j}$. The selection is based on the approximation model that will be used for the analysis in the designed system.

Table 5.1 and Table 5.2 give the error patterns and the corresponding error probabilities for the Normal approximation and the Poisson approximation, respectively.

Table 5.1: Error patterns and the corresponding error probabilities for I = 2 for Normal approximation.

The previous symbols		Error Pattern index	Error probabilities Transmit '0', receive '1'	Error probabilities Transmit '1', receive '0'
a_{c-2}	a_{c-1}	j	$P_{rN\_e01,j}$	$P_{rN\_e10,j}$
0	0	1	0	$(1-p_{tx})^2\,\Phi\left(\frac{\tau - N_{tx}P_{ca,0}}{\sqrt{N_{tx}P_{ca,0}(1-P_{ca,0})}}\right)$
0	1	2	$p_{tx}(1-p_{tx})\Phi\left(\frac{N_{tx}(P_{ca,1}-P_{ca0})-\tau}{\sqrt{N_{tx}(P_{ca,1}-P_{ca0})(1-P_{ca,1}+P_{ca0})}}\right)$	$p_{tx}(1-p_{tx})\Phi\left(\frac{\tau-N_{tx}P_{ca,1}}{\sqrt{N_{tx}((P_{ca,1}-P_{ca0})(1-P_{ca,1}+P_{ca0})+P_{ca0}(1-P_{ca0}))}}\right)$
1	0	3	$p_{tx}(1-p_{tx})\Phi\left(\frac{N_{tx}(P_{ca,2}-P_{ca,1})-\tau}{\sqrt{N_{tx}(P_{ca,2}-P_{ca,1})(1-P_{ca,2}+P_{ca,1})}}\right)$	$p_{tx}(1-p_{tx})\Phi\left(\frac{\tau-N_{tx}(P_{ca2}-P_{ca1}+P_{ca0})}{\sqrt{N_{tx}((P_{ca2}-P_{ca1})(1-P_{ca2}+P_{a1})+P_{ca0}(1-P_{ca0}))}}\right)$
1	1	4	$p_{tx}^2\Phi\left(\frac{N_{tx}(P_{ca2}-P_{ca0})-\tau}{\sqrt{N_{tx}(P_{ca2}-P_{ca0}-(P_{ca1}-P_{ca0})^2-(P_{ca2}-P_{ca1})^2)}}\right)$	$p_{tx}^2\Phi\left(\frac{\tau-N_{tx}P_{ca,2}}{\sqrt{N_{tx}(P_{ca,2}-P_{ca,0}^2-(P_{ca,1}-P_{ca,0})^2-(P_{ca,2}-P_{ca,1})^2)}}\right)$

Table 5.2: Error patterns and the corresponding error probabilities for I = 2 for the Poisson approximation.

The previous symbols		Error Pattern index	Error probabilities Transmit '0', receive '1'	Error probabilities Transmit '1', receive '0'
a_{c-2}	a_{c-1}	j	$P_{rP\_e01,j}$	$P_{rP\_e10,j}$
0	0	1	0	$(1-p_{tx})^2\,Q(\tau+1, N_{tx}P_{ca,0})$
0	1	2	$p_{tx}(1-p_{tx})(1-Q(\tau+1, N_{tx}(P_{ca,1}-P_{ca,0})))$	$p_{tx}(1-p_{tx})Q(\tau+1, N_{tx}P_{ca,1})$
1	0	3	$p_{tx}(1-p_{tx})(1-Q(\tau+1, N_{tx}(P_{ca,2}-P_{ca,1})))$	$p_{tx}(1-p_{tx})Q(\tau+1, N_{tx}(P_{ca,2}-P_{ca,1}+P_{ca,0}))$
1	1	4	$p_{tx}^2(1-Q(\tau+1, N_{tx}(P_{ca2}-P_{ca0})))$	$p_{tx}^2Q(\tau+1, N_{tx}P_{ca,2})$

B. Capacity analysis

The theoretical analysis of the capacity for the R-Model is the same as the analysis shown in Chapter 3. Thus, the capacity for thsystem with the R-Model can be obtained as:

$$\begin{aligned} \mathrm{C_r} &= \max_{p_{\mathrm{tx}}} \left(\mathbf{I}\left(X_{I+1}; Y_{I+1}\right)\right) \\ &= \max_{p_{\mathrm{tx}}} \left(\mathbf{H}\left(\left(1-p_{\mathrm{tx}}\right)\left(1-P_{\mathrm{re01}}\right)+p_{\mathrm{tx}}P_{\mathrm{re10}}\right) - p_{\mathrm{tx}}\mathbf{H}\left(1-P_{\mathrm{re10}}\right) - \left(1-p_{\mathrm{tx}}\right)\mathbf{H}\left(1-P_{\mathrm{re01}}\right)\right) \\ &= \max_{p_{\mathrm{tx}}} \Bigg(-\log_2\left(\left(\left(1-p_{\mathrm{tx}}\right)\left(1-P_{\mathrm{re01}}\right)+p_{\mathrm{tx}}P_{\mathrm{re10}}\right)^{\left(\left(1-p_{\mathrm{tx}}\right)\left(1-P_{\mathrm{re01}}\right)+p_{\mathrm{tx}}P_{\mathrm{re10}}\right)}\right. \\ &\qquad \left. \times\left(1-\left(1-p_{\mathrm{tx}}\right)\left(1-P_{\mathrm{re01}}\right)-p_{\mathrm{tx}}P_{\mathrm{re10}}\right)^{\left(1-\left(1-p_{\mathrm{tx}}\right)\left(1-P_{\mathrm{re01}}\right)-p_{\mathrm{tx}}P_{\mathrm{re10}}\right)}\right) \\ &\qquad + p_{\mathrm{tx}}\log_2\left(\left(1-P_{\mathrm{re10}}\right)^{\left(1-P_{\mathrm{re10}}\right)}P_{\mathrm{re10}}{}^{P_{\mathrm{re10}}}\right)+\left(1-p_{\mathrm{tx}}\right)\log_2\left(\left(1-P_{\mathrm{re01}}\right)^{\left(1-P_{\mathrm{re01}}\right)}P_{\mathrm{re01}}{}^{P_{\mathrm{re01}}}\right)\Bigg). \end{aligned} \tag{5.24}$$

where:

$$P_{\mathrm{re01}} = \sum_{j=1}^{2^I} P_{\mathrm{rN/P\_e01},j},\ P_{\mathrm{re10}} = \sum_{j=1}^{2^I} P_{\mathrm{rN/P\_e10},j}. \tag{5.25}$$

5.4 Simulation process

In this section, the simulation process for verifying the results obtained through theoretical analysis is described.

In the simulation, the random walk is used to describe the molecular diffusion process. If the Cartesian coordinates of the k^{th} molecule at time t are ($x_k(t)$, $y_k(t)$, $z_k(t)$), then the coordinates of this molecule at time $t+\Delta t$ are given by [148]:

$$x_k(t+\Delta t) = x_k(t) + \zeta_1\sqrt{2D\Delta t}, \tag{5.26}$$

$$y_k(t+\Delta t) = y_k(t) + \zeta_2\sqrt{2D\Delta t}, \tag{5.27}$$

$$z_k(t+\Delta t) = z_k(t) + \zeta_3\sqrt{2D\Delta t}, \tag{5.28}$$

where ζ_1, ζ_2 and ζ_3 are independent random numbers sampled from a Normal distribution with mean 0 and variance 1. D is the diffusion coefficient and Δt is the time step.

Consider a specific number of information molecules that are released as an impulse at the beginning of each time slot from coordinates (0, 0, 0). For the diffusion process, each molecule executes a random walk in three-dimensional space that following (5.26)-(5.28), where for each dimension, the molecule moving to the

right or left once every Δt s. The probabilities of the molecule going right or left are 0.5 and 0.5 respectively, and each one moves independently and does not interact with other molecules [148]. For the reception process, a molecule is absorbed if it is within R_X at the end of a time step. Once it has been absorbed, it is eliminated. R_X can demodulate the information by counting the number of received molecules at the end of the time slot. In this work, it is assumed that the receiver can count the number of received molecules during a time slot [149].

Figure 5.1 shows the number of information molecules received at R_X over the simulation time for different distances and Figure 5.2 presented the number of molecules received in the i^{th} time slot due to one transmission. These figures illustrate both simulation and theoretical analysis for an initial transmission with N_{tx} = 1000. During the simulation process, 1000 molecules were simulated for 10000 trials, and the number of average information molecules received at the receiver is measured. In order to get an accurate result, information molecules are tracked every $\Delta t = 10^{-6}$s.

Figure 5.1 indicates that the increase in the transmission distance leads to decreasing of the number of received information molecules at R_X. This is because the increase in transmission distance cause decrease of the capture probability of the receiver (see Figure 3.3). The results in Figure 5.2 show that the number of received information molecules is gradually decreasing with the increase of the time slot index. In addition, both figures show that the simulation results are consistent with the analytical results with tiny deviation.

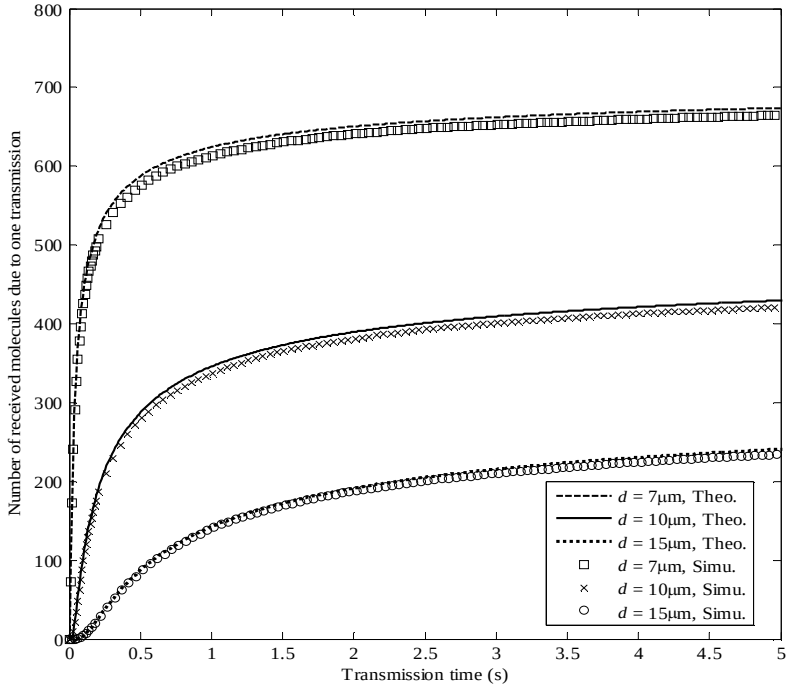

Figure 5.1: Number of received molecules at R_X over simulation time for different distance, and N_{tx} = 1000, D = 79.4μm^{2}s^{-1}. 'Theo.' represents theoretical results, 'Simu.' represents simulation results.

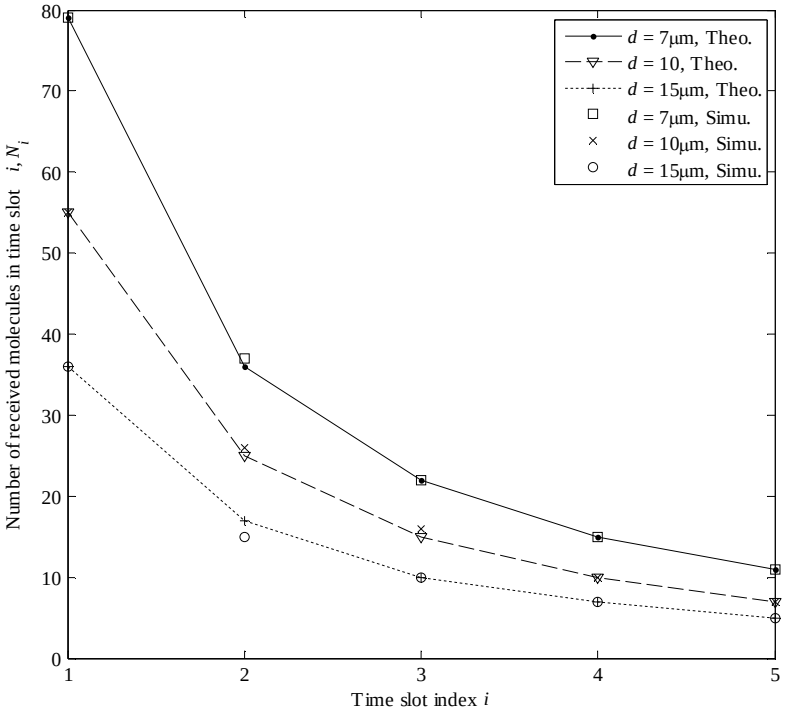

Figure 5.2: Number of received molecules in the i^{th} time slot for different distances, and N_{tx} = 1000, D = 79.4μm^{2}s^{-1}.

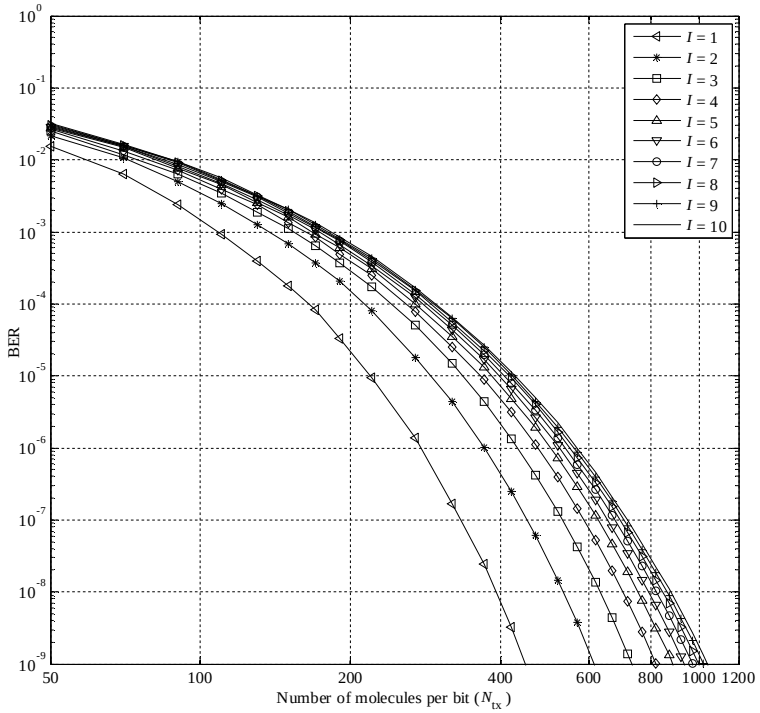

Figure 5.3: BER vs number of molecules per bit for I from 1 to 10. d = 15μm, D = 79.4μm^2/s and R = 5μm.

5.5 Numerical results

In this section, both analytical and simulation results for the PTP DBMC system with the R-Model are given. The results are presented in three parts: first, the BER and channel capacity are given Section 5.5.1. Then, in Section 5.5.2, the RMSE is introduced to determine the suitable approximation for a proposed system. Finally, a performance comparison between the P-Model and the R-Model is given in Section 5.5.3, where the simulation analysis is also presented to verify the theoretical results.

In order to make sure I = 10 is still an accurate choice for analysing the system performance, the BER for different I is also investigated for the system with the R-Model.

Figure 5.3 gives the BER performance for different values of I. The results show that the longer the ISI length, the higher the BER. As the conclusion given in Figure 3.5, the BER value begins to converge with increasing I. Thus, for analysing the performance of the system with the R-Model, the value of I is also selected as 10.

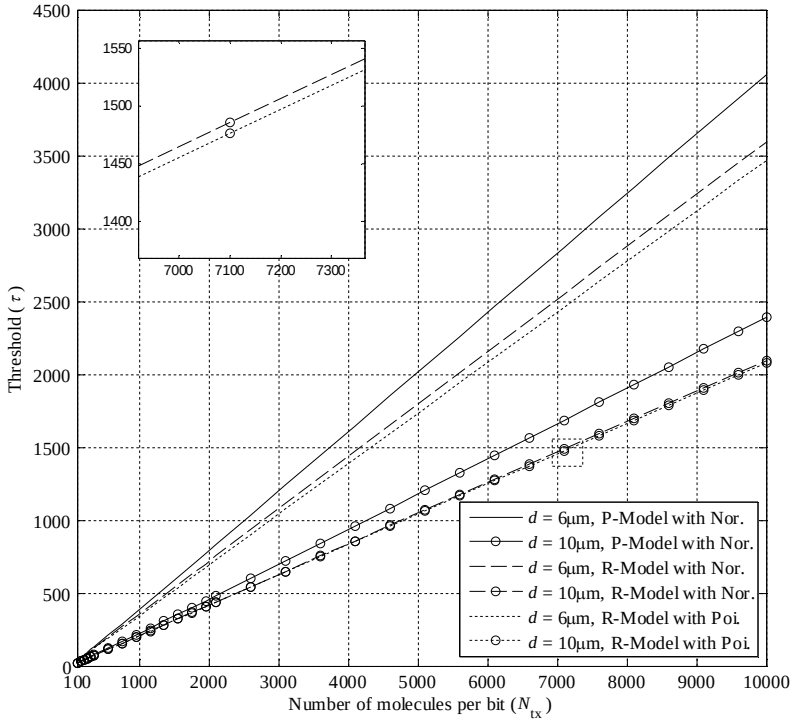

Figure 5.4: The comparison of thresholds between different models with different *d*. Nor. and Poi. denote as the Normal approximation and the Poisson approximation, respectively.

The method used to get the suitable values of τ is the same as the method described in Chapter 3. The comparison of thresholds for different models is given in Figure 5.4. The results indicate that the threshold decreases with the increasing of *d* for all models. For a fixed distance, the threshold of the system with the R-Model is lower than the threshold of the system with the P-Model. In addition, considering the system with the R-Model, the threshold of the system with the Normal approximation is slightly lower than the threshold of the system with the Poisson approximation.

The parameters setting for analytical and simulation results are given in Table 5.3 and Table 5.4, respectively.

Table 5.3: Parameter setting for analytical results.

Parameter	Definition	Value
R	Radius of the R_X	5μm
d	Transmission distance	{6, 8, 10, 12}μm
D	Diffusion coefficient	$79.4\mu m^2 s^{-1}$
N_{tx}	Number of molecules per bit	$50 \sim 10^3$
I	ISI length	10

Table 5.4: Parameter setting for simulation results.

Parameter	Definition	Value
R	Radius of the R_X	5μm
d	Transmission distance	{6 ~ 20}μm
D	Diffusion coefficient	$79.4\mu m^2 s^{-1}$
N_{tx}	Number of molecules per bit	50 ~ 2000
I	ISI length	10
Δt	Time step	10^{-6}s
Q	Number of transmitted bits	10^{15}

5.5.1 Analytical results of BER and capacity performance

Figure 5.5 shows the BER with the number of information molecules per bit for the R-Model that used different approximations. As shown in Figure 5.5, with the increasing of the number of information molecules and transmission distance, the BER decreases for the system with both approximations. For each distance, the BER for the system with the Normal approximation is lower than the BER for the system with the Poisson approximation.

Figure 5.6 shows the mutual information of the R-Model with the Normal and Poisson approximations. With the transmission probability increases, the MI increase at first and when it reaches the maximum value at p_{tx} = 0.5, it starts to decrease. Thus, the maximum MI occurs when p_{tx} = 0.5, which is also the channel capacity. The increase in d and N_{tx} will cause a decrease in capacity for all approximations.

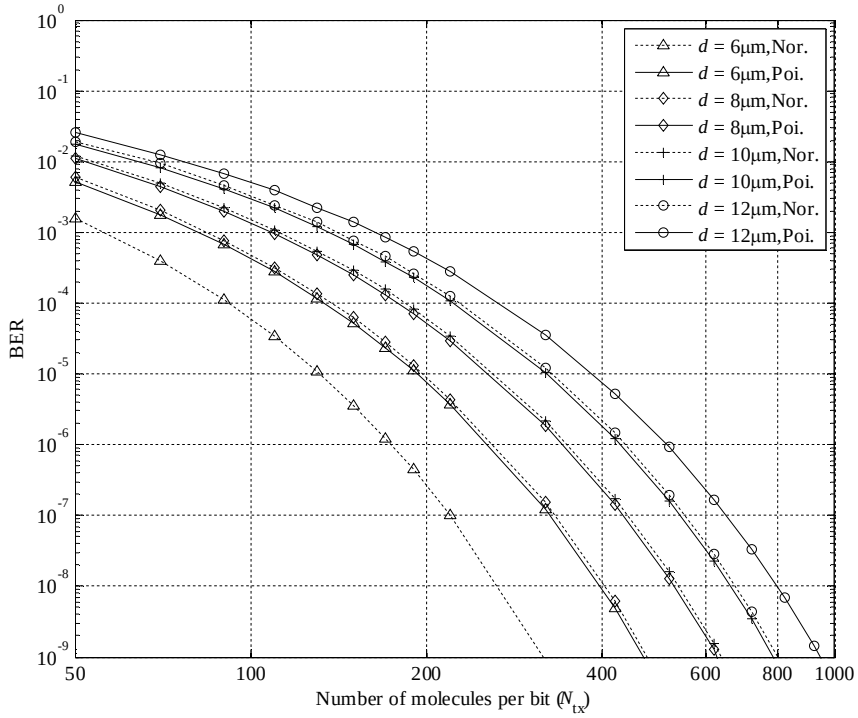

Figure 5.5: BER vs number of molecules per bit for R-Model with different approximations. Nor. and Poi. denote as the Normal approximation and the Poisson approximation, respectively, and $p_{tx} = 0.5$.

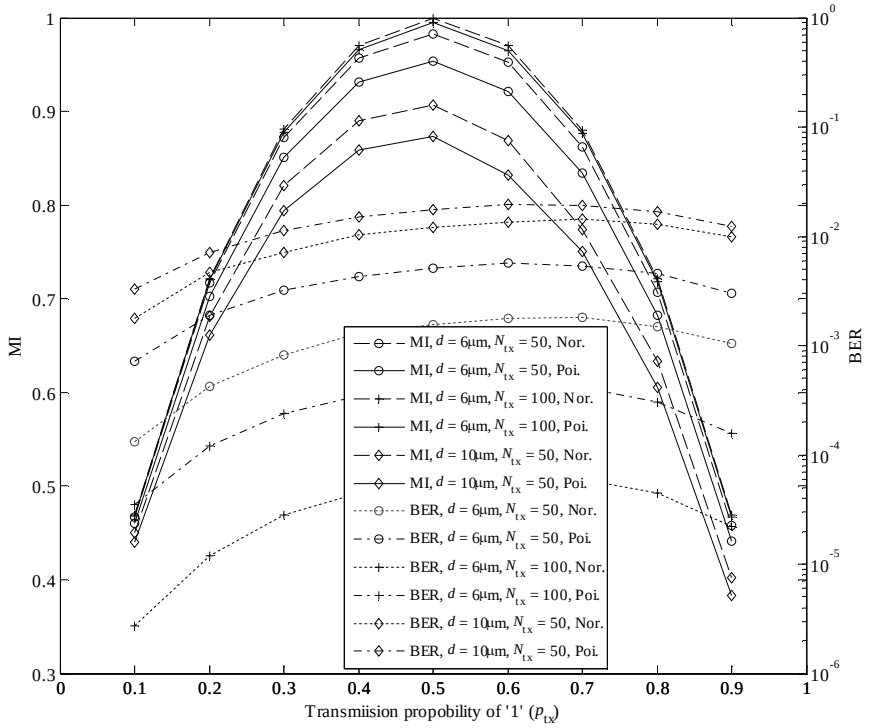

Figure 5.6: BER and MI of the system with R-Model versus p_{tx} for different d and N_{tx}.

As same as the analysis in Chapter 3, Figure 5.6 also shows that the the maximum MI does not signify the minimum BER. Thus, a optimal, p_{tx} can be obtained by:

$$\begin{aligned} C_{rMR} &= \max_{p_{tx}} \left(\mathbf{I}\left(X_{I+1}; Y_{I+1}\right)\left(1-P_{re}\right)\right) \\ &= \max_{p_{tx}} \Bigg[\Bigg(-\log_2 \Big(\left((1-p_{tx})(1-P_{re01}) + p_{tx} P_{re10}\right)^{\left((1-p_{tx})(1-P_{re01})+p_{tx}P_{re10}\right)} \\ &\quad \times \left(1 - (1-p_{tx})(1-P_{re01}) - p_{tx}P_{re10}\right)^{\left(1-(1-p_{tx})(1-P_{re01})-p_{tx}P_{re10}\right)} \Big) \\ &\quad + p_{tx} \log_2 \left(\left(1-P_{re10}\right)^{(1-P_{re10})} P_{re10}^{\ P_{re10}} \right) + (1-p_{tx}) \log_2 \left(\left(1-P_{re01}\right)^{(1-P_{re01})} P_{re01}^{\ P_{re01}} \right) \Big) \\ &\quad \times \left(1 - p_{tx}P_{re10} - (1-p_{tx})P_{re01}\right) \Bigg]. \end{aligned} \tag{5.29}$$

Using MATLAB programming, when p_{tx} = 0.5, the maximum reliable transmission rate can be achieved for the system with d = 6μm, N_{tx} = {50, 100} and a system with d = 10μm, N_{tx} = 100 for both Poisson and Normal apporximation. Thus, 0.5 is the optimal value of p_{tx} for the systems with above settings.

5.5.2 The suitable approximation for a proposed PTP MC system

In Section 5.2, the R-Model with the Normal and Poisson approximations is analysed. In this section, the RMSE is introduced as a metric to determine the suitable approximation that could be employed for analysing a given MC system. The method used here is to calculate the cumulative density functions (CDFs) of the number of received molecules for the Normal and Poisson models and compared with the CDF of the simulation results.

Using the simulation process introduced in Section 5.4, the number of received molecules during (t, $t + \Delta t$) can be obtained. After 10000 trails, the CDF of the simulation results can be evaluated. The RMSE is introduced as follows:

$$\text{RMSE} = \sqrt{\frac{1}{N_{tx}+1} \sum_{x_i=0}^{N_{tx}} \left(\text{CDF}_{sim}\left(x_i\right) - \text{CDF}_{N/P}\left(x_i\right)\right)^2}, \tag{5.30}$$

where CDF_{sim} and $\text{CDF}_{N/P}$ are CDFs of the simulation results and the Normal or Poisson model results, respectively.

Figure 5.7 shows the RMSE of CDFs for PTP MC system with different transmission distances and number of released molecules per bit. The results indicate

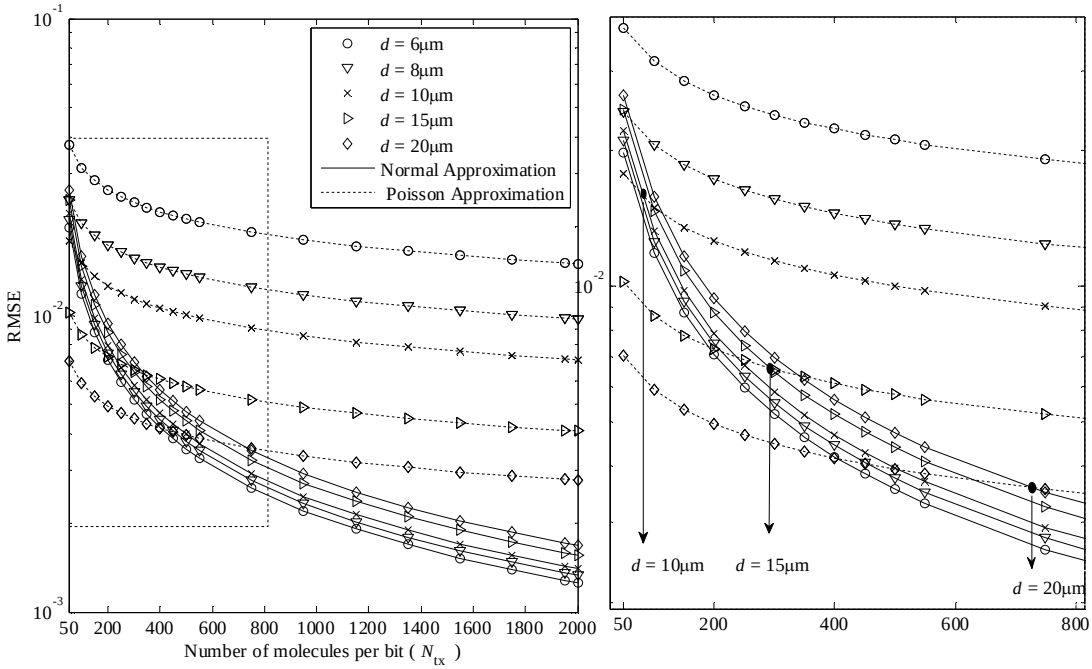

Figure 5.7: RMSE of CDFs for PTP MC systems with d = {6, 8, 10, 15, 20}μm and N_{tx} = {50 ~ 2000}.

that the RMSE of the Poisson model is more stable as N_{tx} varies. However, the Normal model obviously improves with the increasing N_{tx}. For the system with the d = {6, 8, 10, 15, 20}μm and N_{tx} = {50 ~ 2000}, the results show that when d = {6, 8}μm, the system with Normal approximation is more accurate than the system with Poisson approximation. The enlarges figure shows in Figure 5.7 also indicates that considering the transmission distances d = {10, 15, 20}μm, the Normal curves cross with Poisson curves at N_{tx} = {82, 292, 729} respectively. When N_{tx} is smaller than these points, the Poisson is better than the Normal, otherwise the system with the Normal approximation wins.

Above results illustrate the increase in N_{tx} leads to a right shift of the Normal distribution curve which can reduce the effects of the negative part of the distribution. Thus the Normal approximation is more accurate for a system with larger N_{tx}. On another hand, with the increasing of d, the capture probability at R_X decreases, the Poisson model becomes better since that the Poisson approximation is normally used for modelling the rare events.

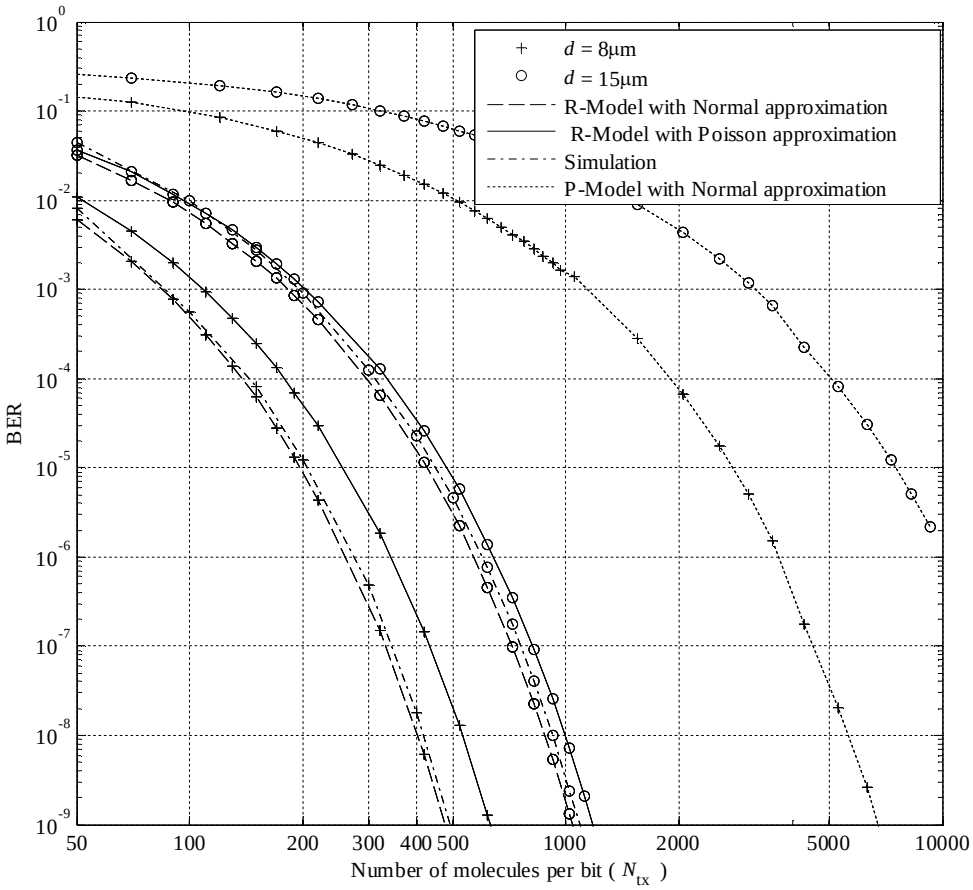

Figure 5.8: BER vs the number of molecules per bit for different channel models and simulation with $d = \{8, 15\}$μm.

5.5.3 BER comparisons between P-Model and R-Model

In this section, the BER comparisons between the P-Model and the R-Model with different approximations are given.

The simulation results are obtained based on the simulation process introduced in Section 5.4. During the simulation process, the number of times of simulation trials or the number of transmitted bits, Q, is 10^{15}.

Figure 5.8 shows the BER with the number of molecules per bit for the system that uses different models. As with previous analysis, BER decreases with the increasing for N_{tx} and decreasing of d for all models introduced. It clearly shows that the P-Model overestimates the error rate. For example, for the system with transmission distance $d = 15$μm and $N_{tx} = 500$, the P-Model predicts an error rate of

10^{-1}, almost 1000 times larger than the error rate predicted by more accurate R-Model and verified by simulation.

In addition, considering the BER comparison between the R-Model with different approximations and the simulation, it is consistent with the result given in Section 5.5.2, where the Normal approximation is more accurate for a larger N_{tx}, and the Poisson approximation is more accurate for rare events.

5.6 Conclusions

In this chapter, an R-Model which includes the dependence of the numbers of received molecules between slots has been investigated and then compared with the incumbent model which assumes the independent events. This model is further evaluated at arbitrary ISI length and with both the Normal and Poisson approximations. A decision metrics called RMSE is also applied to determine which approximation is better for a system. The results indicate that the system with the R-Model gives a more accurate estimation than the P-Model which was introduced in Chapter 3. Based on the calculation of the RMSE, the designer can decide which model approximations should be used based on their system design.

The update to the model shows that the P-Model overestimates the number of errors that can occur in the channel, and this is verified by the simulation results. It indicates that the system with P-Model will most likely deliver a higher performance in practice. This observation is thus critical to those works which deal with energy use at this nano-scale as with this assumption of dependence, less energy will be needed to attain the desired BER. In the following chapters, the theoretical results are obtained based on the system with the R-Model.

Chapter 6
A Revised look at ECCs in PTP DBMC Systems

6.1 Introduction

In Chapter 4, a full analysis of ECCs in PTP MC systems was presented based on the analysis of the P-Model. However, due to the imprecise assumption that was used in the P-Model, the error rate of the system is overestimated. Thus, a refined model, R-Model, was presented in Chapter 5. By comparing the performance of the uncoded system with different models, the R-Model does provide a more realistic prediction of the system performance. Therefore, using the P-Model to analysing the coded system (i.e. the analysis in Chapter 4) should not be accurate. Therefore, the use of ECCs in PTP MC systems should be re-investigated by applying the R-Model into the system analysis.

In this chapter, a revised look at the performance of the coded system performance is presented by applying the ECCs into the refined communication model. The system performance respects to BER and critical distance is given and compared with the results obtained in Chapter 4. This chapter aims to illustrate a more accurate estimation of the performance of the coded system. The difference in performance should be clearly seen by comparing the performance between the P-Model and the R-Model. Furthermore, in this chapter, all the results are generated by theoretical analysis.

Given the high similarity of the analysis process in Chapter 4 and this chapter, the description of coding techniques and the study of BER, energy consumption of

the coded system are not repeated here. The only difference is the communication model that be used during the analysis process, and this can be done by replacing the value of P_e^* used in (4.51) and in (4.53) with P_{re}^*. The P_{re}^* used in this chapter is the one bit error probability of an uncoded system that applied the R-Model. Aiming to use the same number of molecules as an uncoded system, the number of molecules used for the calculation of P_{re}^* for the coded system should be evaluated with a reduction of the number of information molecules used for an uncoded system, (5.23), by multiplying with the code rate. Beyond that, all the expressions are same as Chapter 4.

The remainder of this chapter is organised as follows. The BER and critical distance are presented in Section 6.2 and Section 6.3, respectively. Section 6.4 gives the comparison between results that obtained in Chapter 4 and in this chapter. Finally, this chapter is concluded in Section 6.5.

6.2 BER performance for the coded system with R-Model

In this section, the BER performance of the coded system with the R-Model is presented. As it mentioned in Section 4.8.1, the (1,3)C-RM, (2,4)C-RM and (3,5)C-RM are exactly same as (7,4)Hamming code, (15,11)Hamming code and (31,26)Hamming code respectively. Thus, for C-RM code family, only (1,4)C-RM and (2,5)C-RM are considered in this section. The BER results are obtained based on a set of parameters in Table 6.1.

Table 6.1: Parameter Setting for BER.

Parameter	Definition	Value
R	Radius of R_X	5μm
d	Transmission distance	6μm
D	Diffusion coefficient	$79.4\mu m^2 s^{-1}$
I	ISI length	10
N_{tx}	Number of molecules per bit	10 ~ 400

Figure 6.1 shows the BER results for the coded system with the R-Model. Figure 6.1(a) gives the BER comparison between the system with block codes and the uncoded system, and Figure 6.1(b) shows the BER comparison between the system with SOCCs and the uncoded system. The values of coding gain are shown

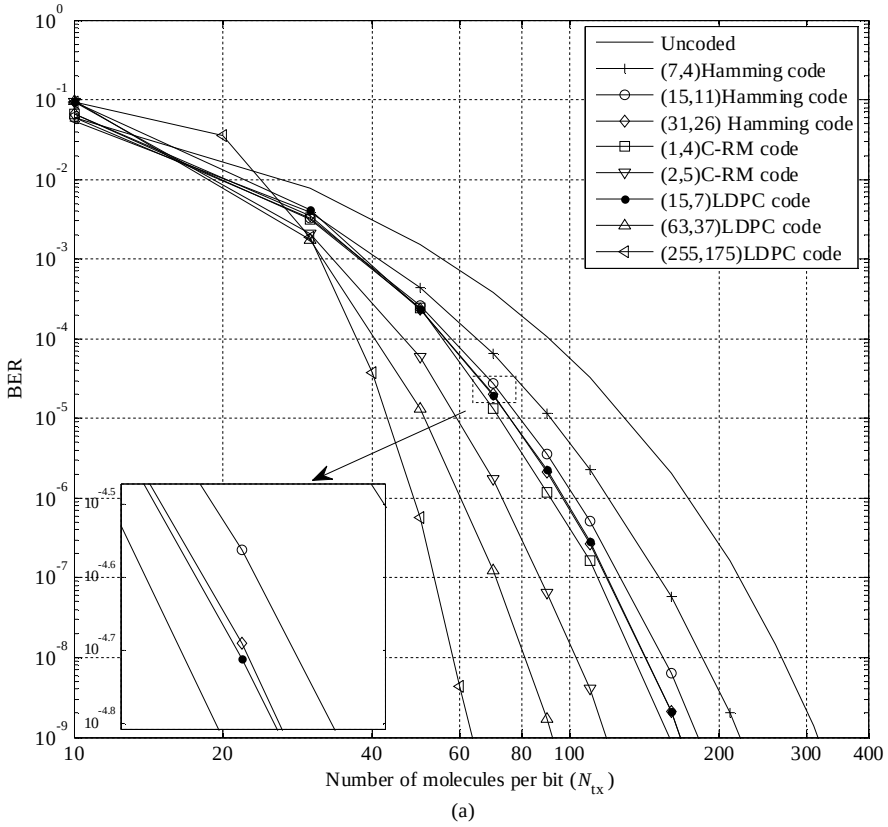

(a)

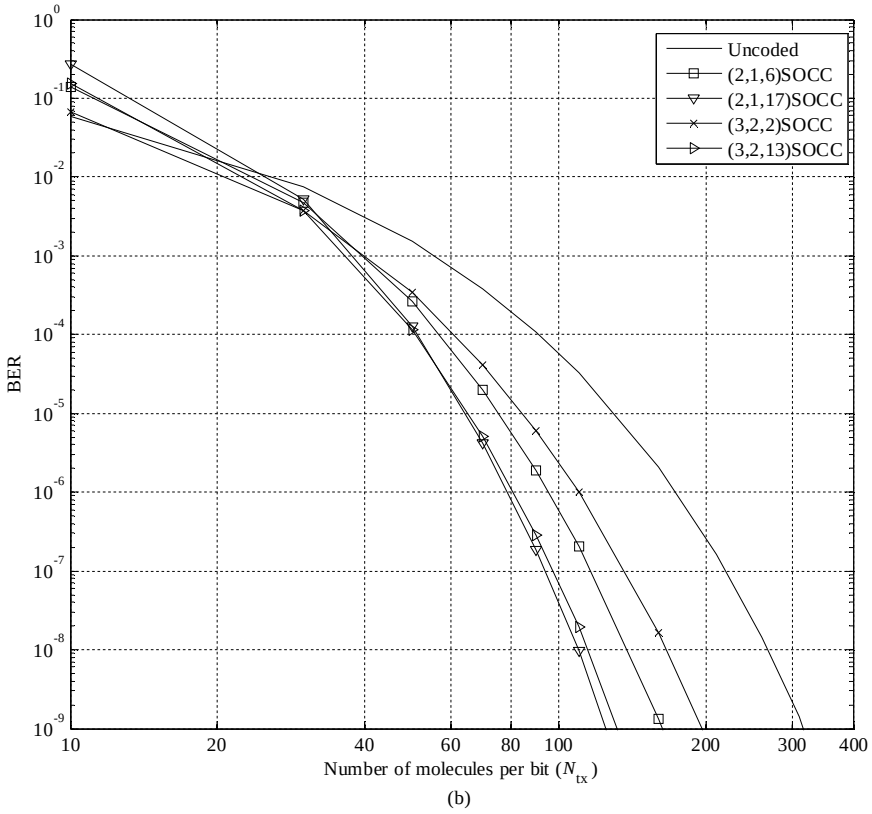

(b)

Figure 6.1: (a) BER comparison for a coded system with block codes and uncoded system. (b) BER comparison for a coded system with SOCCs, and uncoded system.

to be 1.35dB, 1.68dB, 1.68dB, 1.68dB, 2.30dB, 1.68dB, 2.43dB, 2.57dB, 1.46dB, 1.68dB, 1.47dB, 1.90dB for (7,4)Hamming, (15,11)Hamming, (31,26)Hamming, (1,4)C-RM, (2,5)C-RM, (15,7)LDPC, (63,37)LDPC, (255,175)LDPC, (2,1,6)SOCC, (2,1,17)SOCC, (3,2,2)SOCC and (3,2,13)SOCC respectively at the BER level of 10^{-3}. And for a BER level of 10^{-9}, the coding gain for above codes are 1.59dB, 2.43dB, 2.78dB, 2.30dB, 4.29dB, 2.76dB, 5.33dB, 6.95dB, 2.89dB, 4.04dB, 2.09dB and 3.80dB, respectively. It can be seen that (15,11), (31,26)Hamming codes, (1,4)C-RM code, (15,7)LDPC code and (2,1,17)SOCC have the same coding gain at 10^{-3}, this is because the number of molecules used for achieving that BER level is the same. The results also clearly show that the (255,175)LDPC code gives the largest coding gain compared to other codes.

6.3 Critical distance for the coded system with the R-Model

In this section, the critical distance is recomputed based on the BER performance shown in Section 6.2. The three communication scenarios, N2N communication, N2M communication and M2N communication which were introduced in Section 3.2.2 are also considered here. Figure 6.2 to Figure 6.7 show the analytical results of critical distance for different ECCs and communication scenarios. When applying the R-Model into system analysis, the critical distance exists for all of the considered codes and it is reflected in Figure 6.2 to Figure 6.7. Thus, the metric called total energy consumption for the coded system is no more needed here. All the results indicate that with the increasing of operating BERs, the critical distance also increases.

Figure 6.2 to Figure 6.4 show the critical distance of the system with block codes. The results that presented in Figure 6.2 are considered the N2N communication scenario. Under this scenario, the (15,7)LDPC gives the lowest critical distance, and the code from the same code family called (255,175)LDPC presents the longest critical distance based on the high complexity of the circuit design. Figure 6.3 and Figure 6.4 illustrate the critical distance for the system when considering N2M and M2N communication scenarios respectively. In these cases, the (31,25)Hamming and (15,7)LDPC codes win with the lowest critical distance.

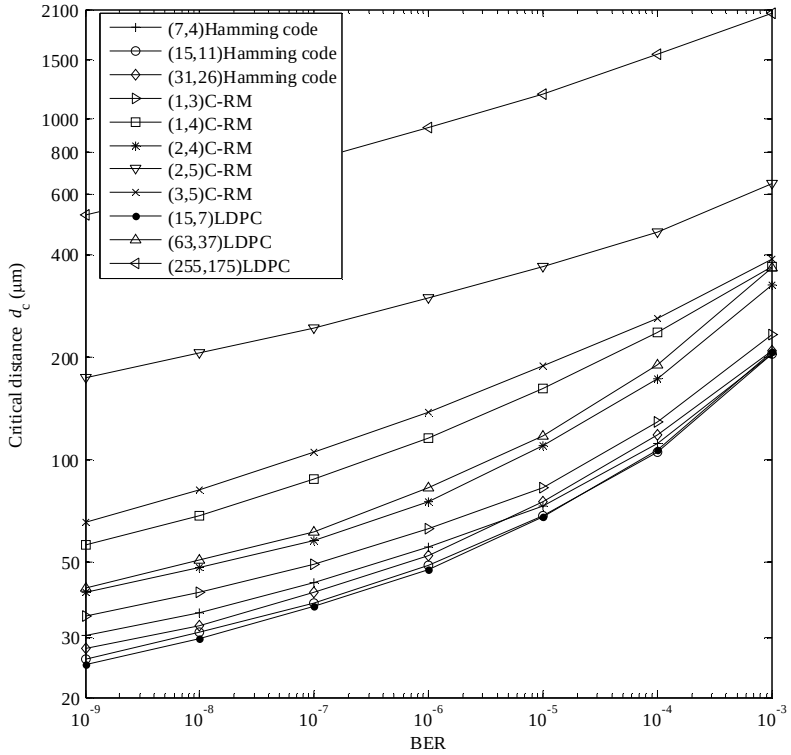

Figure 6.2: Critical distance with BER for block codes when considering N2N communication.

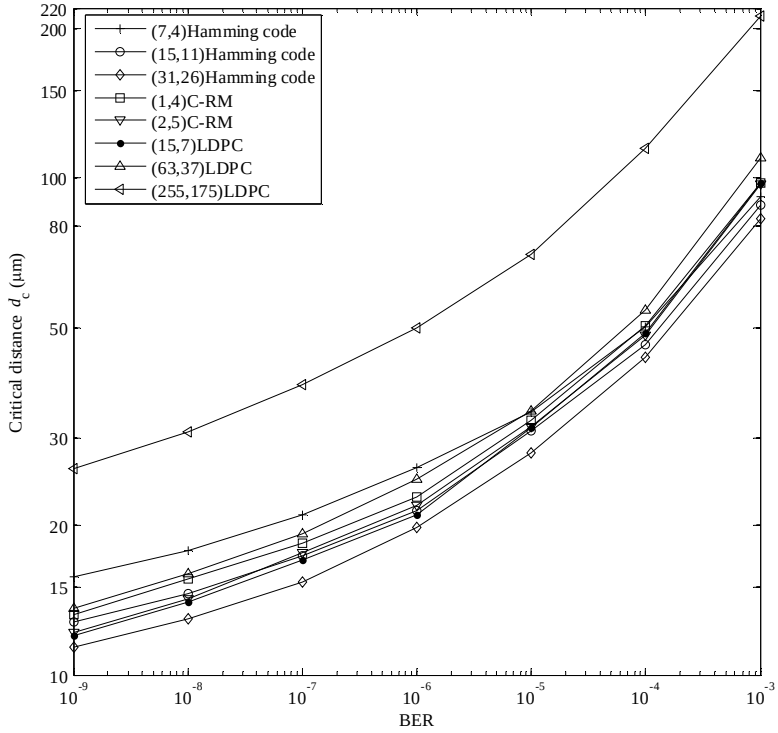

Figure 6.3: Critical distance with BER for block codes when considering N2M communication.

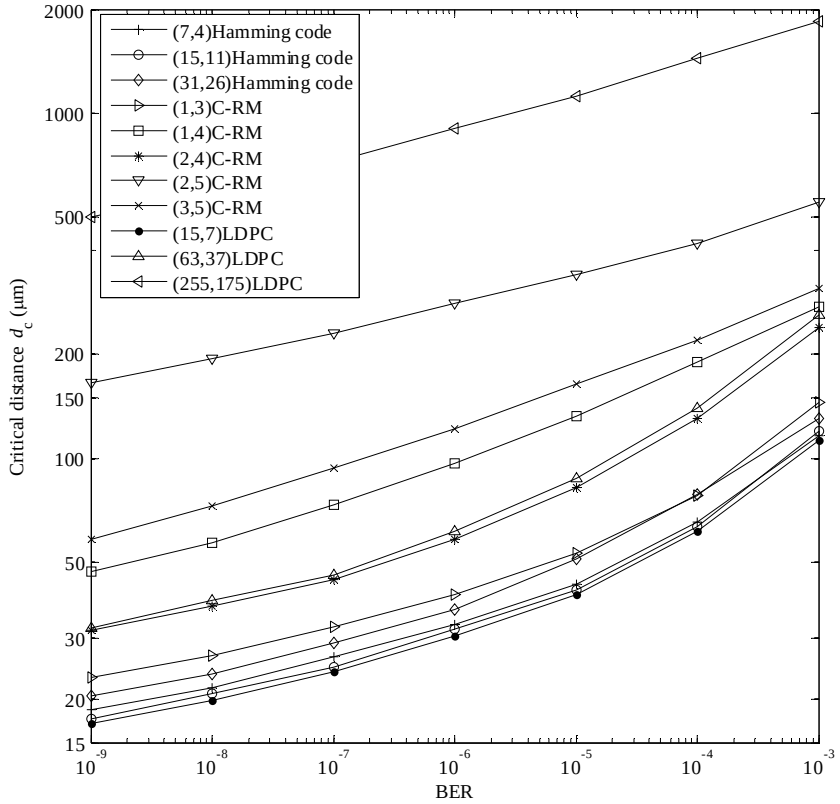

Figure 6.4: Critical distance with BER for block codes when considering M2N communication.

Using the concept of 'best-fit ECC' introduced in Chapter 4. For the results obtained based on the application of the R-Model, the best-fit block codes for N2N, N2M and M2N communication scenarios are (15,7)LDPC, (31,26)Hamming code and (15,7)LDPC, respectively. These codes are compared with SOCCs and the results are illustrated in Figure 6.5, Figure 6.6 and Figure 6.7.

Figure 6.5 considers the critical distance comparison for N2N communication scenario. In this case, the energy consumption for both encoder and decoder circuits need to be considered. The lowest critical distance is given by the use of the (3,2,2)SOCC, which means under this communication scenario, the (3,2,2)SOCC has a wider application range.

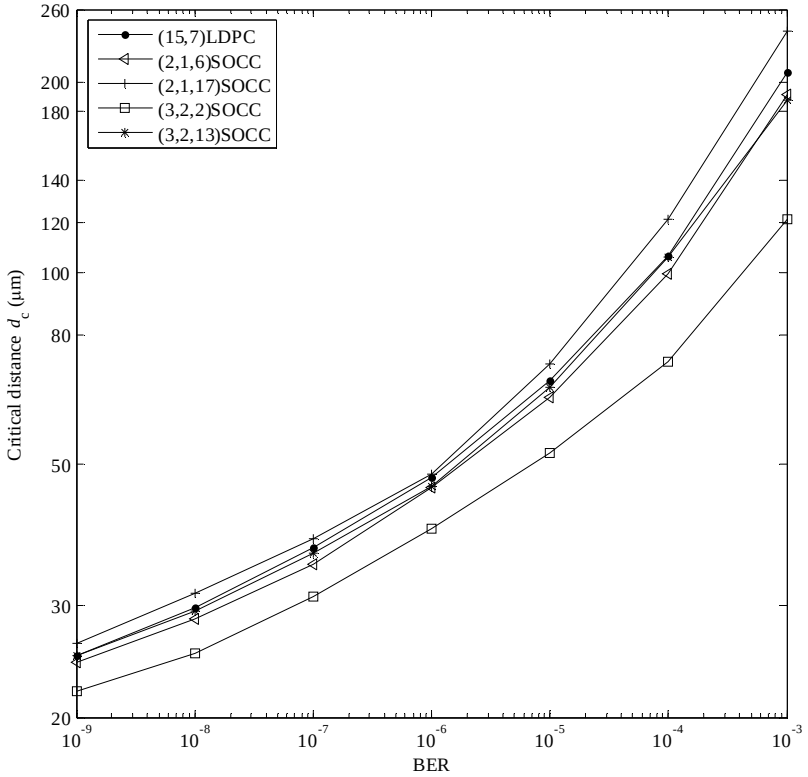

Figure 6.5: Critical distance comparisons between (15,7)LDPC and selected SOCCs when considering N2N communication.

Figure 6.6 and Figure 6.7 show other scenarios which are N2M and M2N communications. When considering N2M communication, the energy cost only includes the consumption caused by the operating of the encoder circuit. On the contrary, for M2N communication, the energy cost only include the consumption caused by the operating of the decoder circuit. The lowest critical distance belongs to (31,26)Hamming code and (3,2,2)SOCC for N2M communication scenario, and (3,2,2)SOCC for M2N communication scenario.

In addition, all the results indicate that the level of critical distance for N2M communication scenario lower than the levels of critical distance for N2N and M2N communication scenarios. This means the encoder design for all selected ECCs is simpler than the decoder design. Through the comparison, the (3,2,2)SOCC is selected as the best-fit ECCs for all three communication scenarios except N2M communication system with an operating BER level from 10^{-9} to 10^{-6}.

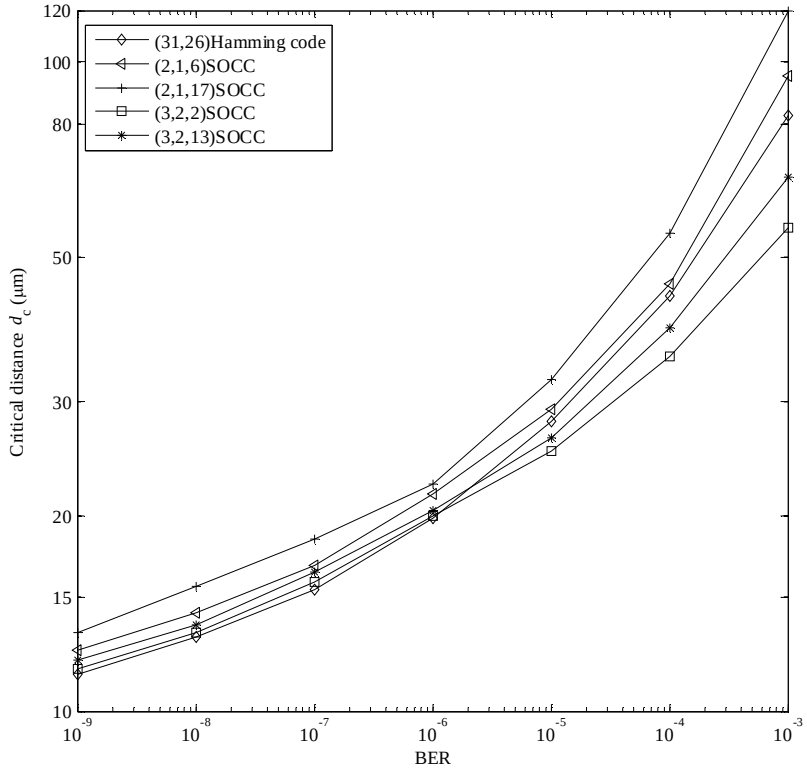

Figure 6.6: Critical distance comparisons between (31,26)Hamming code and selected SOCCs when considering N2M communication.

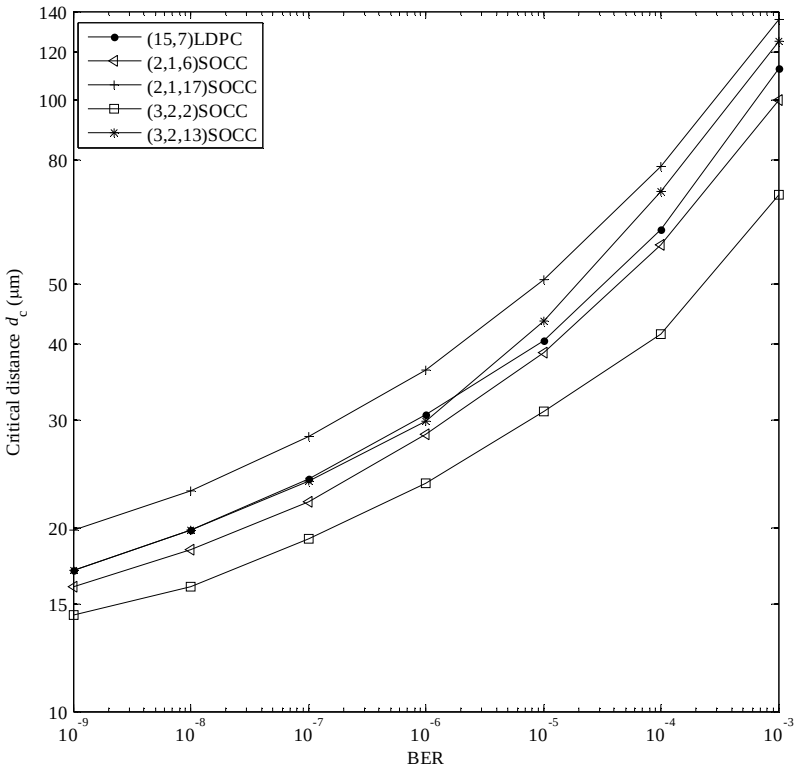

Figure 6.7: Critical distance comparisons between (15,7)LDPC and selected SOCCs when considering M2N communication.

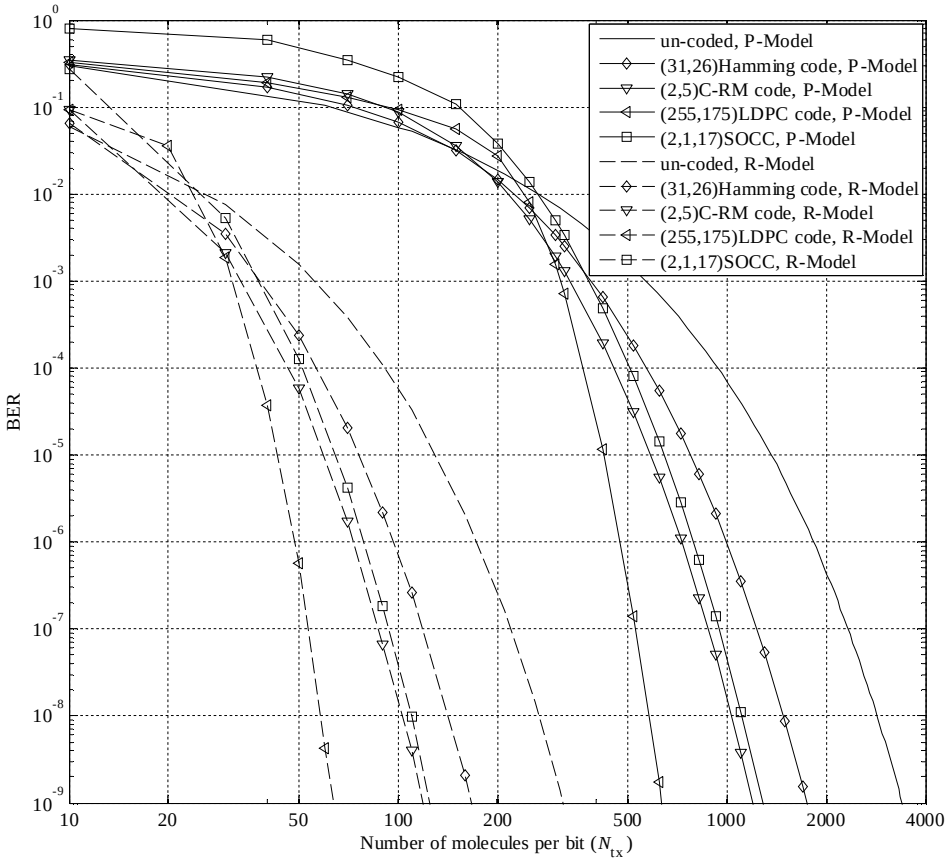

Figure 6.8: BER comparison between the systems that analysis with the P-Model and the R-Model.

6.4 Results comparison and discussion

In this section, the system performance that obtained by considering the P-Model compares the performance that obtained by considering the R-Model. The comparison and discussion are given from the following two aspects: BER and critical distance. Each one will be given in turn.

A. BER comparison

Figure 6.8 shows the analytical BER results for the system with the P-Model and the R-Model. In this comparison, only the code with the highest BER performance among their family are selected. The results present that the (255,175)LDPC still gives the best BER performance when applying the refined model into the system analysis. However, the coding gains at d = 6μm for the coded system with the R-Model is lower than the coding gains obtained for the system with the P-Model.

The results have once again proven the analysis: the use of the P-Model in the PTP MC system overestimated the BER of the system. For example, considering (255,175)LDPC code, about 60 molecules per bit can reach a 10^{-8} BER level when using the R-Model into the analysis. However, about 600 molecules need to be used per bit to achieve the same BER level when applying the P-Model.

B. Energy efficiency – critical distance

The results shown in Chapter 4 indicated that there are some cases where the use of ECCs is always beneficial for applications with transmission distance equal to or longer than 6μm (here, the minimum transmission distance is considered as 6μm), and this means no critical distance exist in those cases. However, the results presented in this chapter show that the critical distance exists in all cases. In each communication scenario, the critical distances are higher than those distances shown in Chapter 4. The reason of this is considering the same communication scenario under the same coding techniques, the system that applied the P-Model gives a larger coding gain compared to the system that applied the R-Model which is verified by Figure 6.8. Thus, for the system with the P-Model, a shorter distance can generate enough coding gain to match the extra energy required by the operating of the encoding and decoding process.

Table 6.2: Best-fit ECC for different MC scenarios with the R-Model.

Communication scenario	Lower BER operating region	Higher BER operating region
N2N	(3,2,2)SOCC	
N2M	(31,26)Hamming code	(3,2,2)SOCC
M2N	(3,2,2)SOCC	

Table 6.2 gives the best-fit ECCs for different communication scenarios with the R-Model. The lower BER operating region for N2M communication scenario is from 10^{-9} to 10^{-6}, and the higher BER operating region is from 10^{-6} to 10^{-3}. As shown in this table, the (3,2,2)SOCC is the superior code as it is the best-fit ECC for N2N, M2N communications and also N2M communication system with a higher operating BER level.

6.5 Conclusions

In order to get a more accurate estimation of the performance of the coded system, in this chapter, the use of ECCs in PTP MC system is reconsidered by applying the ECCs into a system with the R-Model. The new performance of the coded PTP MC system is presented regards to the BER and critical distance. In addition, the performance comparison between the system with the P-Model and the system with the R-Model is also presented. Through the comparison, the difference between the performance of a system that applies the P-Model and the R-Model can be clearly seen. Similar to the uncoded system, the BER of the coded system also be overestimated when applying the P-Model into the system analysis.

Although, there exists the best-fit ECC which has a wider application range, this is not the only choice for the designer. For example, when several codes are worthwhile to be applied to a proposed system. In this case, the designer can balance the energy consumption and also the BER performance based on the application of the system, i.e. a system need a low-level energy consumption, or a low-level BER.

Chapter 7
The Effect of Two-receiver on Broadcast DBMC Systems

7.1 Introduction and related work

To date, there have been several studies that address the characteristics of the channel for PTP DBMC systems, for example [17, 23, 25, 94, 141, 150, 151]. The study of the PTP DBMC system is also presented in this thesis with Chapter 3 through Chapter 6. However, scenarios where multiple transmitters communicate with multiple receivers, such as the multi-access channel or the broadcast channel in MC, have not yet received as much attention as the topic deserves. Existing papers on this subject include [84, 149, 152-154]. Given the scale of work regarding the broadcast channel in conventional communication systems, and the prevalence of multiple-input-multiple-output in natural molecular communication system [153], [149], this knowledge gap within molecular communication systems is thus important to redress.

The research in [152] and [154] aims to analyse the broadcast channel where a single transmitter communicates with multiple receivers and the system performance such as channel capacity has been studied. However, the current literature assumes that the signal at each receiver is independent, receiving molecules as if other receivers were not present, i.e. effectively treating the system as multiple PTP communication channels. For a MC system with multiple absorbing receivers, the receivers do interfere with each other as the absorbed molecule cannot be captured by any other receivers.

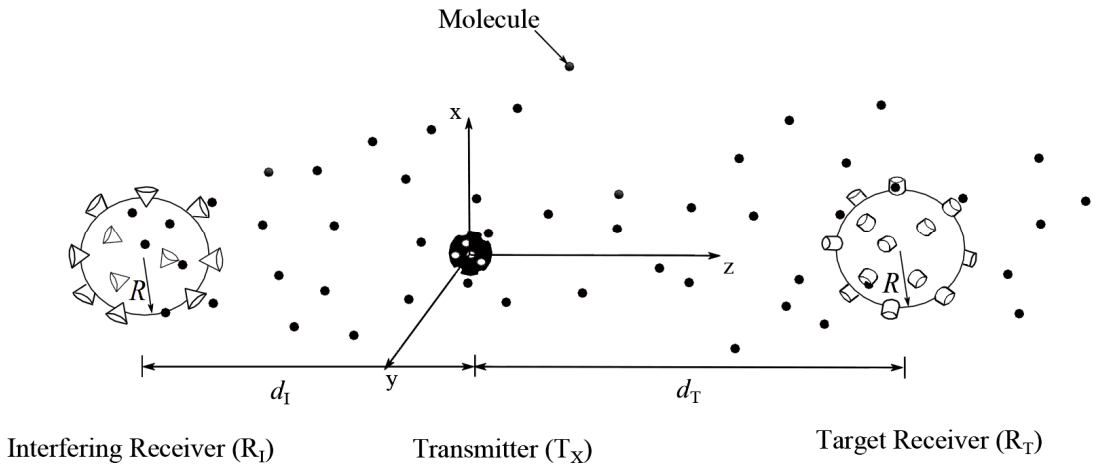

Figure 7.1: MC system with two absorbing receivers.

In this chapter, in order to investigate how the receivers influence each other, a DBMC system with one transmitter and two receivers is considered. As shown in Figure 7.1, one transmitter, T_X emits molecules into a channel with two identical receivers that can absorb the same type of molecule. One receiver is defined as the target receiver, R_T, whilst the other is defined as the interfering receiver, R_I. The d_I and d_T are the transmission distances between T_X and R_I and between T_X and R_T, respectively. The T_X, R_I and R_T are centered on the same line, i.e. fixed *x* and *y* coordinates. If the independence assumptions of [152] and [154] are considered, then there would be no molecule 'sink' or 'absorption' component caused by the presence of the interferer. This further implies the performance of the system with respect to the target receiver is likely overestimated.

This work aims to investigate the influence of R_I on R_T as a function of their relative positions. Each receiver's location is defined by the *z*-coordinate of its center. Considering a fixed position of T_X and R_T (locates to the right of T_X), three positions of R_I will be studied. Scenario 1 considers that R_I is located to the left of both T_X and R_T. Scenario 2 considers that R_I is between T_X and R_T. Finally, Scenario 3 considers that R_I is located to the right of both T_X and R_T. In each of these positions the impact on the BER and channel capacity of the communication link between T_X and R_T which can be represented as the target link will be shown.

In this chapter, a two-receiver broadcast communication channel with a 3D diffusion-based propagation model is simulated. One of the fundamental parameters of performance analysis, capture probability, can be obtained via this simulation. The

scenario that R_I, R_T and T_X are aligned on the same line is studied. The impact of the introduction of the interfering receiver with respect to its relative location is investigated by analysing the BER and channel capacity of the target communication link. Furthermore, by employing the RMSE introduced in Chapter 5, the suitable channel model of the proposed system can be determined.

The remainder of this chapter is organised as follows. The propagation construction is given in Section 7.2. The analysis of the MC broadcast channel with regards to both BER and capacity is investigated in Section 7.3. In Section 7.4, the numerical results are presented. The chapter is then concluded in Section 7.5.

7.2 Propagation construction

In Chapter 5, a simulation process is introduced for PTP DBMC systems. In this work, 3D random walk is also used to describe the molecular diffusion process for the two-receiver broadcast channel.

Considering that a number of molecules are released as an impulse at the beginning of each time slot from coordinates (0, 0, 0). For the diffusion process, each molecule executes a random walk in 3D space that follows (5.26) - (5.28) in each dimension. For the reception process, a molecule is absorbed if it is within one of the receivers at the end of a time step. Once it has been absorbed, it is eliminated. The receiver can decode the information by counting the number of received molecules at the end of the time slot.

7.2.1 Capture probability

The ability for a molecule to be captured by the receiver is denoted as the capture probability. The expression of the capture probability for a PTP DBMC system is given in (3.5). However, the expressions of the capture probability with respect to time for the multi-receiver system is still a problem. Therefore, here, the capture probability for each receiver is obtained via simulation process.

In the simulation, the number of received molecules at each receiver in 10^5 trials can be obtained by taking a large time slot duration, t_s, (5000s).

An example is given by considering the location of R_I based on Scenario 1, where R_I is located to the left of both T_X and R_T with transmission distance $d_I = 2\mu m$

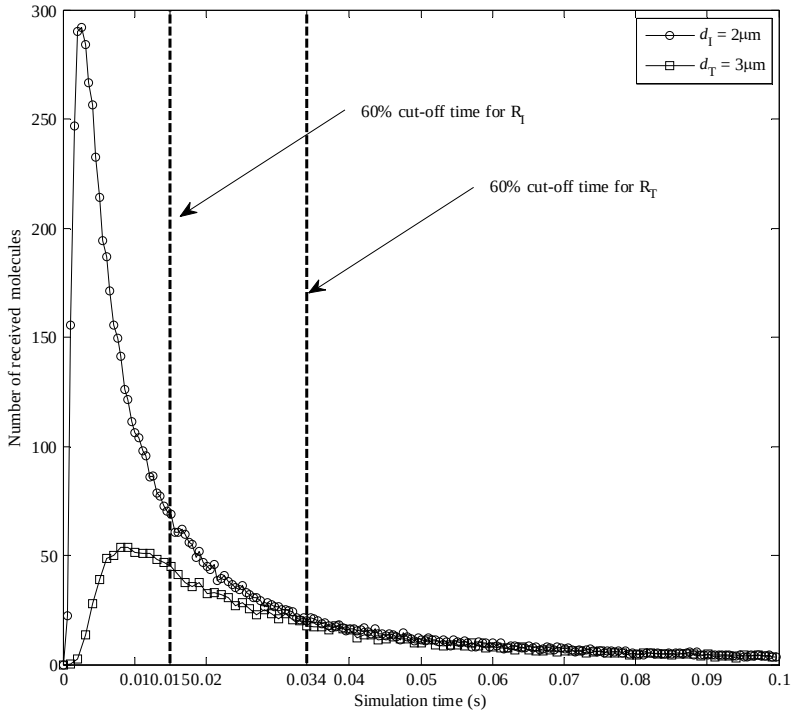

Figure 7.2: Number of received molecules of R_I and R_T for N_{tx} = 100000. Simulation with D = 79.4μm^2/s, R = 1μm.

and d_T = 3μm. Under this condition, Figure 7.2 gives the number of received molecules for the two-receiver MC system with d_I = 2μm and d_T = 3μm. The results indicate that with the increase of the propagation time, the number of received molecules increases first, and reaches the maximum value, and then it begins to decrease. It can also be seen that, for the two-receiver system, most of information molecules will be absorbed by the receiver that closer to T_X. Figure 7.3 shows the comparison of capture probability between the PTP DBMC system with transmission distance, d_S = {2, 3}μm and the two-receiver DBMC system with d_I = 2μm and d_T = 3μm. The results indicate that the capture probability increases when the receiver is closer to the transmitter for both systems. In addition, it clearly shows that with the same transmission distance, the capture probabilities of the two-receiver system are smaller than the capture probabilities of the PTP system. Thus, treating the broadcast channel as multiple PTP communication channels is not accurate and will overestimate the BER performance of the two-receiver DBMC system.

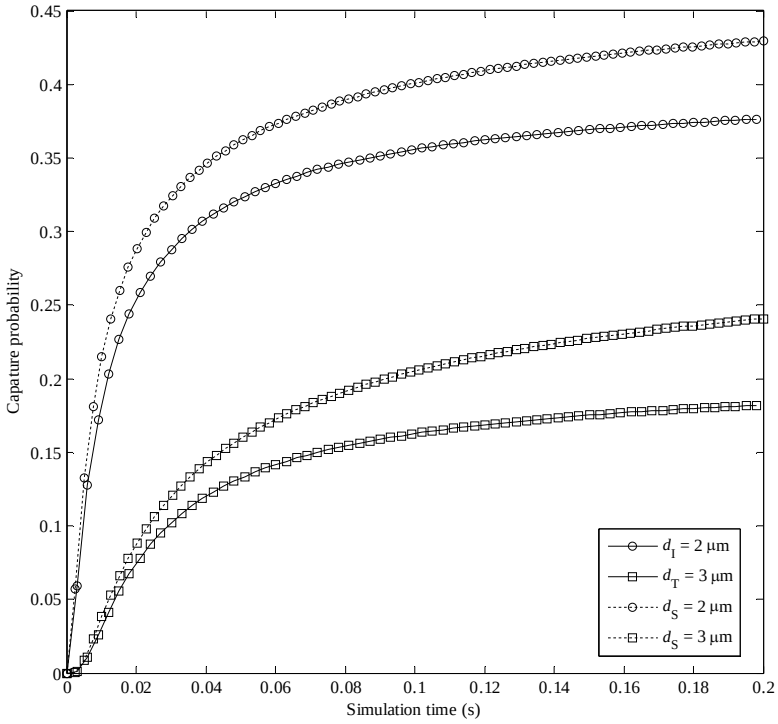

Figure 7.3: Capture probability for the PTP and two-receiver systems.

7.2.2 Comparisons between simulation and analytical results

The simulation process has been compared with the model for two absorbing spheres in [155] to validate the correct behavior of the simulation process. There, the author introduced a scenario where molecules located at coordinates (0, 0, *z*) diffuse to a pair of receivers S_1 and S_2 located at (0, 0, *l*/2) and (0, 0, -*l*/2) respectively, where *l* is an arbitrary distance. For this scenario, the analytical and approximated capture probabilities for S_1 and S_2 are given when the diffusion time is large enough (i.e., as $t \to \infty$). Comparisons in [155] show a strong agreement between the analytical and the approximated results. Thus, only the capture probabilities found using the approximate expressions are compared with the simulation in this work.

The approximations for capture probability $P_{\mathrm{ca1,ap}}$ with S_1 and $P_{\mathrm{ca2,ap}}$ with S_2 are introduced as [155]:

$$p_{\mathrm{ca1,ap}} = R \Big/ \left(d_1 \times \left(1 - \left(R/l \right)^2 \right) \right) - R^2 \Big/ \left(d_2 \times l \times \left(1 - \left(R/l \right)^2 \right) \right), \tag{7.1}$$

$$p_{\mathrm{ca2,ap}} = R \Big/ \left(d_2 \times \left(1 - \left(R/l \right)^2 \right) \right) - R^2 \Big/ \left(d_1 \times l \times \left(1 - \left(R/l \right)^2 \right) \right). \tag{7.2}$$

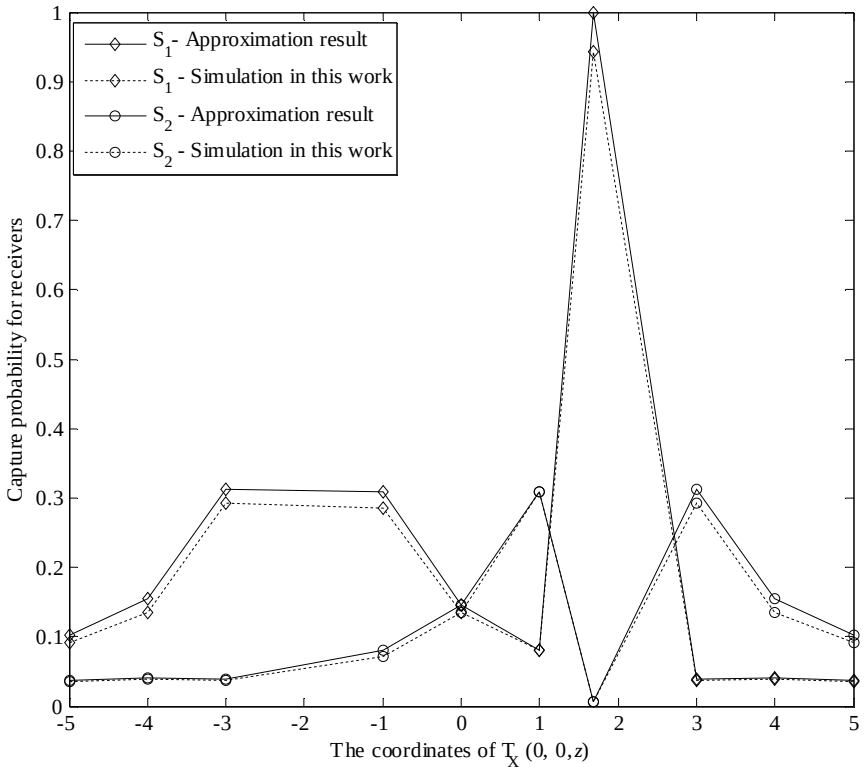

Figure 7.4: Comparisons of capture probabilities between approximation and simulation results with a large simulation time.

where R is the radius of the receivers, d_1 and d_2 are the distances between the releasing point (T_X) and the centers of the S_1 and S_2.

As shown in Figure 7.4, the capture probabilities found using the approximate expressions (7.1) and (7.2) are compared with the simulation results. The parameters used in this comparison agree with [3] and [155], where $l = 4\mu m$, $R = 0.31487\mu m$, and $D = 79.4\mu m^2 s^{-1}$.

The R-square coefficient [156] of determination is introduced to measure the quality of fit between results from simulation and results from approximations. The closer that this value is to 1, the better the fit of the simulation is, and is given by:

$$R_s^2 = 1 - SSE/SST, \tag{7.3}$$

where SSE is the sum of squared errors of prediction and SST is the sum of squares of the difference of the dependent variable and its mean. The R-square for S_1 and S_2 are 0.9935 and 0.9910 respectively. This comparison confirms that the results from this simulation process are accurate.

7.3 Channel analysis

The influence of R_I on R_T can be reflected in the performance of the target communication link. Thus, the focus here is the analysis of the target link.

The value of t_s used in Section 7.2.1 is too large to use in a communication system. Thus, this value can be determined by finding the time at which 60% of the information molecules arrives at the R_T [3]. Figure 7.2 illustrates the 60% cut-off time for the R_I and R_T. It indicates that the 60% cut-off time increases with increasing distance between T_X and R_X. Thus, the capture probability of R_T within one time slot, $P_{ca,T}(d_T, t_s)$, can be recomputed via the same simulation process introduced in Section 7.2.1.

Following the theoretical analysis introduced in Chapter 5 and applying $P_{ca,T}(d_T, t_s)$ into the refined communication model, the BER and channel capacity of the target link, P_{Te} can be obtained.

7.4 Numerical results

In this section, the capture probability of R_T, and the BER and capacity of the target link are given based on the simulation and theoretical analysis, and the results also compared to the performance of a PTP communication system with a single receiver R_S and $d_S = 7\mu m$. A set of simulation parameters is shown in Table 7.1.

Table 7.1: Parameter setting.

Parameter	Definition	Value
R	Radius of receivers	1μm
d_T	Distance between T_X and R_T	7μm
d_I	Distance between T_X and R_I	{2, 4, 7, 10, 12, 14}μm
d_S	Distance between T_X and R_S	7μm
D	Diffusion coefficient	$79.4\mu m^2 s^{-1}$
N_{tx}	Number of molecules per bit	100~10000
I	ISI length	10
(x_0, y_0, z_0)	Coordinate of T_X	(0, 0, 0)
$(0, 0, z_I)$	Coordinate of R_I	z_I = {-7, -4, -2, 2, 4, 10, 12, 14}μm
$(0, 0, z_T)$	Coordinate of R_T	(0, 0, 7μm)

The T_X and R_T are placed in fixed positions (0, 0, 0) and (0, 0, 7μm), and the coordinates of R_I (0, 0, z_I,) are variable with the changing of z_I, where $z_I \in$ {-7, -4, -2, 2, 4, 10, 12, 14}μm. d_I-, d_I+ and d_I++ are denoted as the distance between the T_X and R_I in Scenarios 1, 2, and 3, respectively.

7.4.1 The suitable approximation for analysing the proposed two-receiver MC system

In Section 5.5.2, the RMSE is introduced as a metric to determine the suitable approximation used for analysing a proposed system. Here, this metric is also applied to the two-receiver DBMC system with a set of parameters shown in Table 7.1.

Figure 7.5 (a) and (b) show the RMSE of CDFs for PTP system with d_S = 7μm and the two-receiver system with d_T = 7μm, respectively. The results indicate that the RMSE of the Poisson approximation is more stable as N_{tx} varies. However, the Normal approximation obviously improves with increasing N_{tx}. As shown in Figure 7.5(a), the Poisson approximation is more accurate for N_{tx} < 4000, above which the Normal approximation is better. The BER against the number of molecules per bit is also presented in this figure. When N_{tx} < 4000, a BER level as low as 10^{-9} can be measured for both the Normal and Poisson approximations. In this case, the Poisson approximation is preferred for a PTP communication system based on the lower RMSE values. For the target link of the two-receiver system in Figure 7.5(b), the RMSEs are measured for different distances of R_I. The results show that the values of RMSE of the Poisson approximation are always lower than the values obtained from the Normal approximation for N_{tx} = 0 ~ 10000. In the remainder of this chapter, only the Poisson approximation is considered.

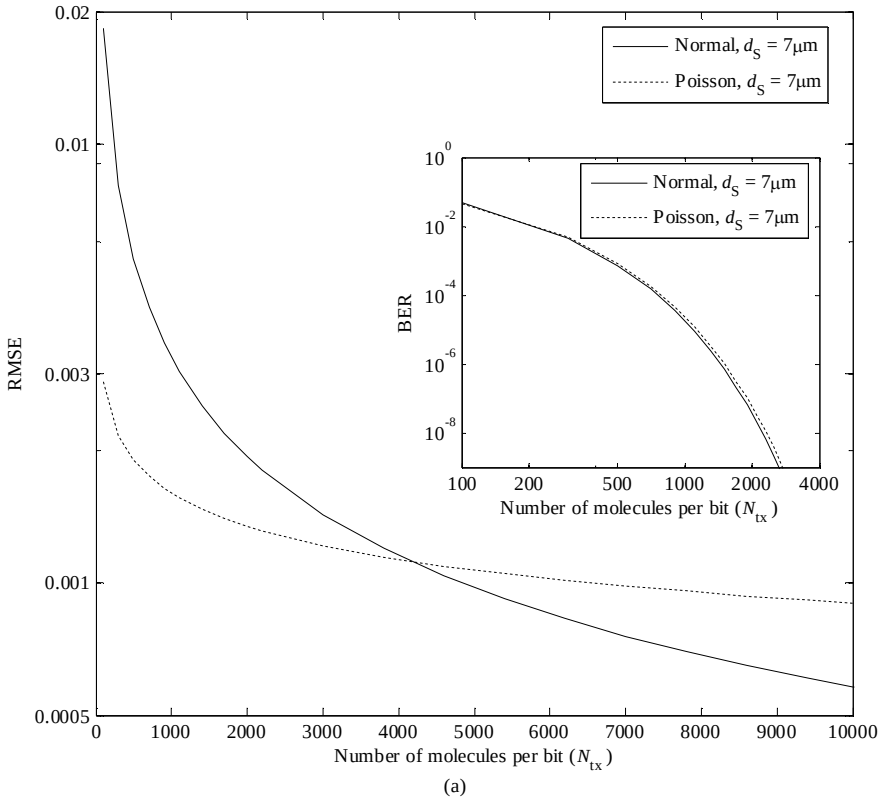

(a)

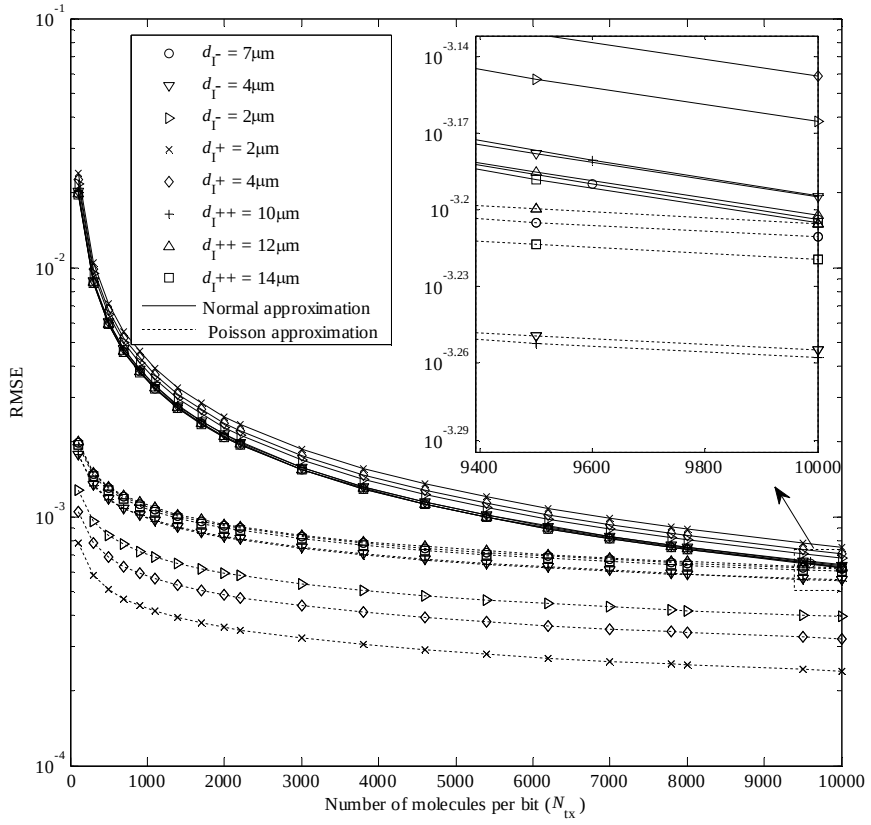

(b)

Figure 7.5: RMSE of CDFs for (a) PTP system with d_S = 7μm (b) Two-receiver system with d_T = 7μm.

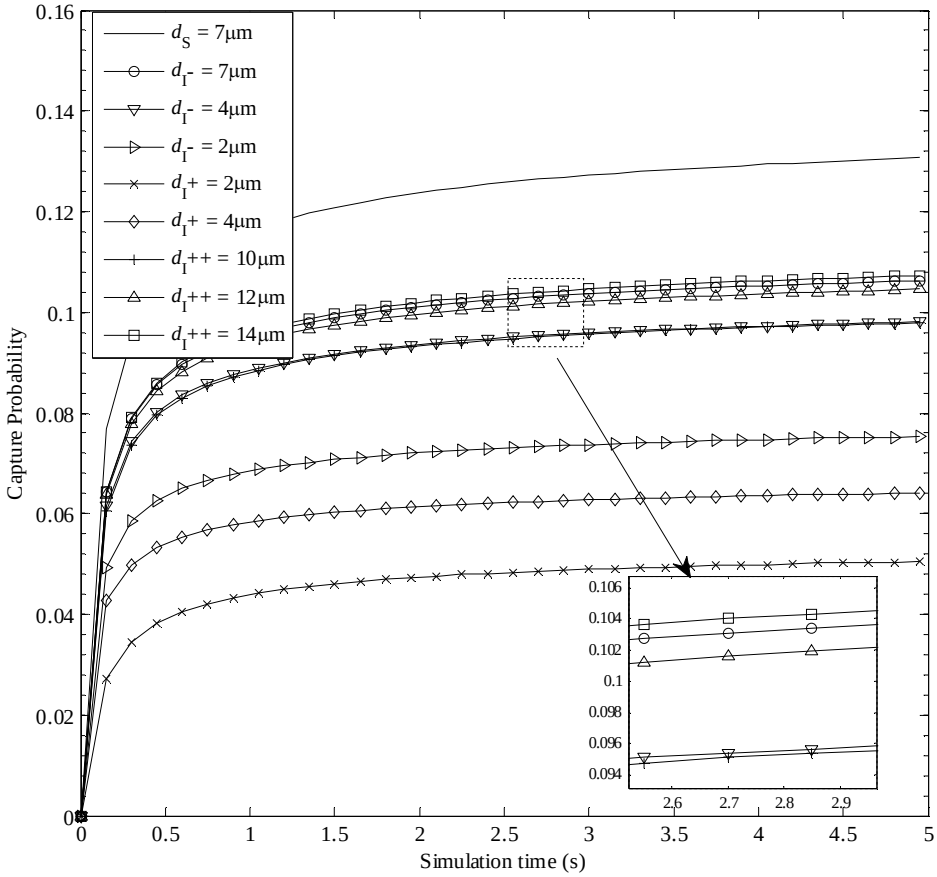

Figure 7.6: The comparisons of capture probabilities between R_T and R_S.

7.4.2 BER and channel capacity

Before presenting the system performance with BER and capacity, the comparisons of the capture probabilities between R_T with different positions of R_I and R_S is illustrated in Figure 7.6.

The results show that all capture probabilities increase with increasing simulation time. When the simulation time is long enough, the capture probability appears to converge. It can also be seen that for different positions of R_I, the capture probabilities of R_T are different, and all smaller than the capture probability of the R_S. For the two-receiver system, the maximum and minimum values of capture probabilities of R_T occur in Scenario 3 with r_I++ = 14μm, and Scenario 2 with r_I+ = 2μm respectively. These results illustrate that the capture ability of R_T is weakened and have thus shown the different levels of impact due to the existence of R_I. This is because R_I may have absorbed the information molecules that could have arrived at

R_T. Furthermore, for different positions of R_I, the ability to absorb the information molecules is different which is also reflected in the values of capture probabilities of R_T. Finally, the R_I will have the greatest impact when it is literally blocking the R_T. In this case, the capture ability of R_I and R_T reach their highest level and lowest level, respectively.

The BERs and capacities of the target link of the two-receiver system with d_T = 7μm and the PTP system with d_S = 7μm are presented in Figure 7.7(a) and Figure 7.8. The numerical results clearly show that increasing the number of molecules leads to a lower BER and higher capacity. The performance ranking is consistent with the capture probabilities show in Figure 7.6. Thus, the lowest BER and also the highest capacity is provided by the PTP system, and the lowest and highest BERs of the target link occur in Scenario 3 with d_I++ = 14μm and Scenario 2 with d_I+ = 2μm, respectively. The BERs at N_{tx} = 5000 for different values of z_I are shown in Figure 7.7(b). O_1 and O_2 are the regions that R_I overlaps with the T_X and R_T respectively. The overlap between R_I and T_X or R_I and R_T is physically unrealizable. Thus, the positions of R_I in these two regions are not taken into account. This figure directly shows the BER trend of the target link with varying positions of R_I. As R_I changes position from Scenario 1 to Scenario 2 to Scenario 3, the BER increases at first, and when it arrives at the closest position to T_X in Scenario 2, the BER reaches a maximum, and then the BER decreases. Both BER and capacity imply that the R_I's existence does reduce the reliability of the target link, and due to the significant impact, the positions of the R_I in Scenario 2 are especially undesirable for R_T, where the reliability of the target link is the worst of the three Scenarios. The impact of R_I in Scenario 1 and Scenario 3 are very similar, except when d_I- = 2μm, i.e., when the R_I is very close to the T_X. The distance variations of R_I in Scenario 3 and Scenario 2 cause the smallest and the biggest change in both BER and capacity respectively.

The increase of the distance between R_I and T_X leads to decreasing and increasing of the capture probability of R_I and R_T respectively. Thus, in each Scenario, the further the distance between the R_I and T_X, the less the impact on R_T.

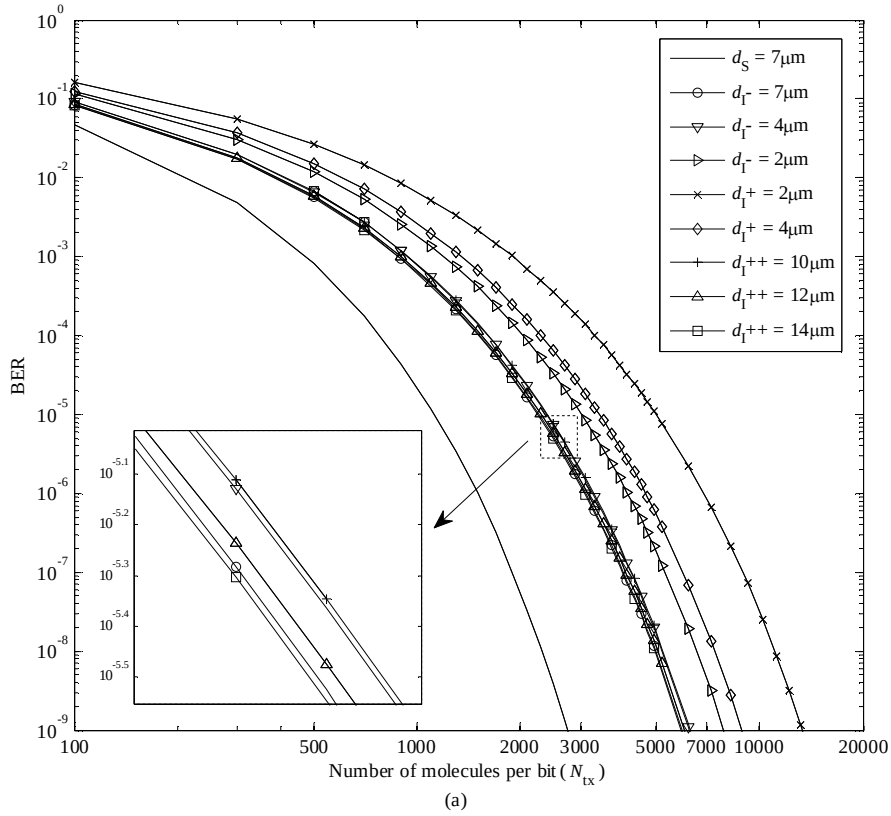

(a)

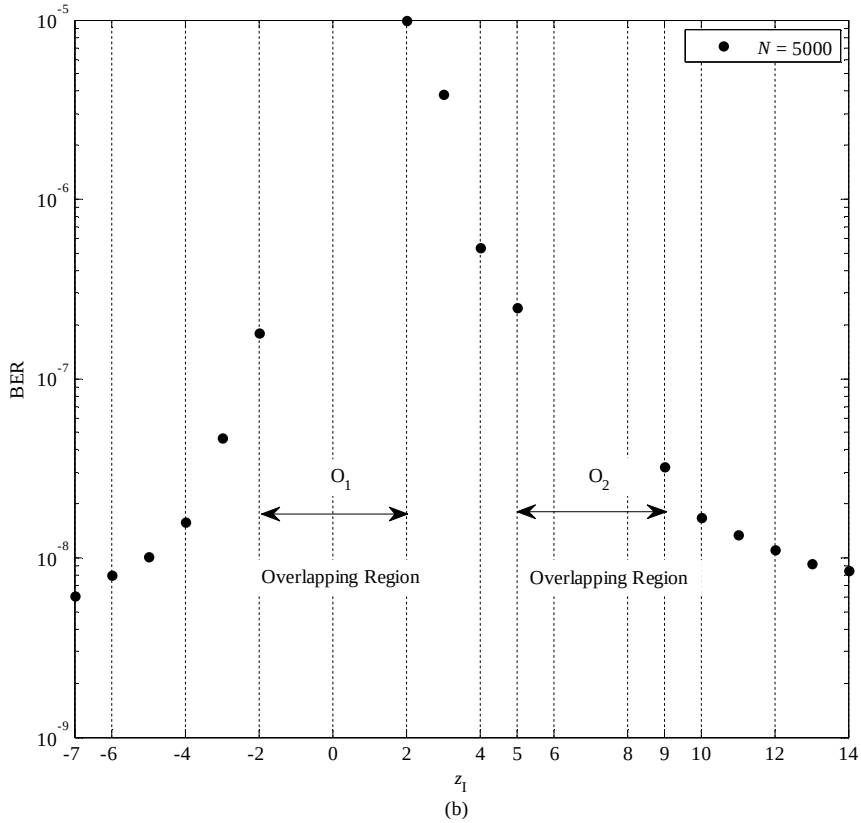

(b)

Figure 7.7: (a) BER comparisons between the target link with different positions of R_I and the PTP system, p_{tx} = 0.5 (b) BER with different values of z_I at N = 5000.

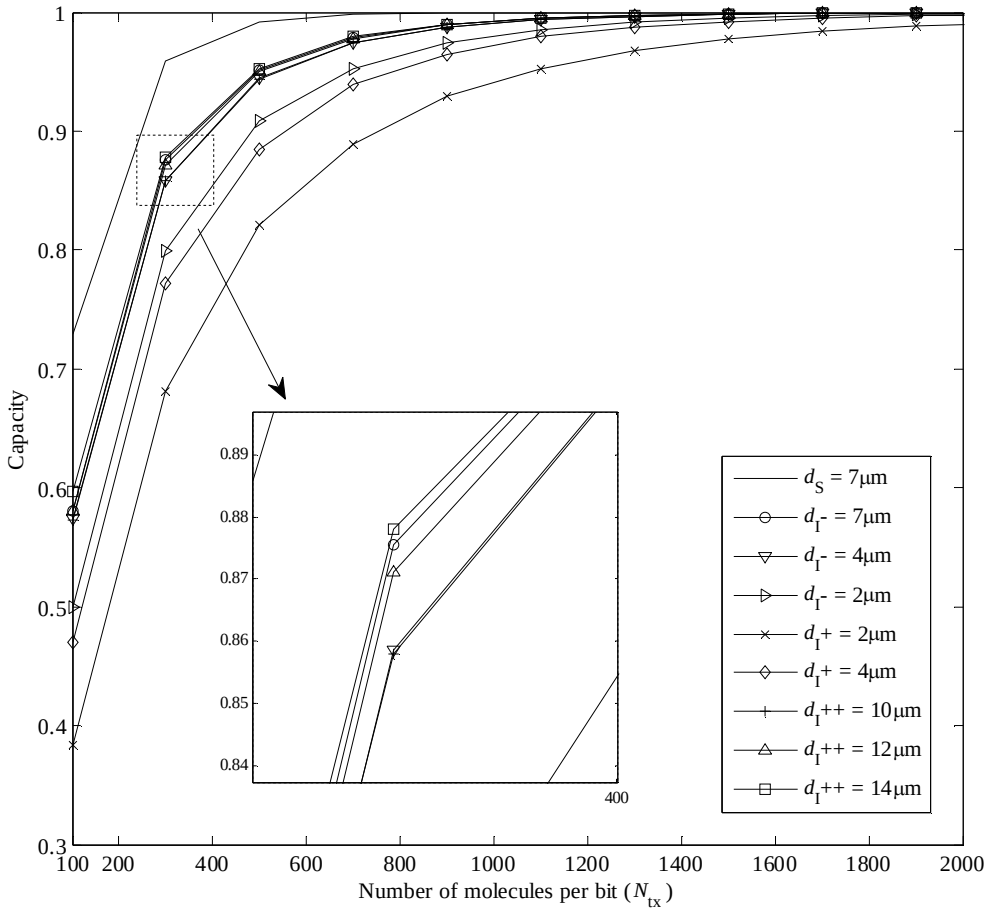

Figure 7.8: Channel capacity comparisons between the target link with different positions of R_I and the PTP system.

7.5 Conclusions

In this chapter, the two-receiver broadcast channel for MC systems has been simulated and the concept of an interferer node R_I and the effect of its location on R_T are introduced. Through the simulation and previous derived results, the impact of the position of R_I on R_T is shown via the BER and channel capacity of the target link. The results indicate that different positions of R_I relative to T_X and R_T have varying effects on R_T, especially when the R_T is completely blocked by R_I, i.e. Scenario 2. Thus, for a system with a given number of molecules released per bit, the positions of R_I in Scenario 2 cause a higher BER to the target link than those positions in the other Scenarios. In addition, for all scenarios, the further the R_I is away from T_X, the better performance of the target link can be achieved. Furthermore, the performance

of the target link of the two-receiver system is always worse than the performance of the PTP system when considering same parameters. Therefore, the use of the PTP approximation should not be used for a broadcast system with absorbing receivers as it can not guarantee, or predict, the reliability of the signal at a given receiver.

Chapter 8
Conclusions and Future Research

Molecular communications (MC) is one of the most modern communication paradigms that uses molecules as the information carrier to transmit message between nano-machines.

This thesis focused on the study of diffusion-based molecular communication (DBMC), where, the information molecules transmitted from the transmitter (T_X) to the receiver (R_X) can be realized by Brownian diffusion. The information is modulated by the presence or absence of a single type of information molecules at T_X, which is known as the On-off keying (OOK) modulation scheme. As one of the main objectives of this thesis, the performance of DBMC system was investigated for the uncoded point to point (PTP) DBMC system, the coded PTP DBMC system that employed Error Correction Codes (ECCs), i.e. Hamming codes, Cyclic-Reed Muller (C-RM) codes, Euclidean Geometry Low-density Parity-check (EG-LDPC) codes and Self-orthogonal Convolutional Codes (SOCCs) and the two-receiver DBMC system. Furthermore, in-depth investigations for characteristics of the DBMC system, the communication and propagation models, the suitable ECCs for a proposed PTP DBMC system and energy efficiency of the coded system were also presented in this thesis.

This research aimed to provide a fundamental investigation of DBMC systems and presented related theoretical and simulation results that may be beneficial for the future practical implementation.

In Section 8.1, the achievements for main chapters and the conclusions of the thesis are summarized. Future research topics are discussed in Section 8.2.

8.1 Conclusions

A. Summary of the results in main chapters

- **Chapter 3: Point to Point Model of the Diffusion-based Molecular Communications System.** In this chapter, a PTP model of a 3D DBMC system (also can be treated as a nano-to-nano machine (N2N) communication system) has been established. Additionally, two other communication scenarios called nano-to-macro/micro machine (N2M) communication and macro/micro-to-nano machine (M2N) communication were also proposed where the propagation and communication channel models were considered as same as N2N communication. The closed-form expressions of BER and channel capacity were derived for the proposed system with a consideration of Intersymbol Interference (ISI). The influence of parameters such as the number of information molecules N_{tx}, diffusion coefficient, D, transmission distance, d, time slot duration, t_s, ISI length, I, and pre-designed threshold, τ, on the system performance were also discussed. During the performance analysis, the ISI was considered as the main noise source. The results of Bit Error Rate (BER) versus ISI length indicated that the first previous symbol has the significant effect on the current symbol, and with the increases in ISI length, the influence begins to converge. For simulation, the ISI length was set to be a length of 10 to produce high precision results. The system performance showed that with a fixed diffusion medium, T_X and R_X, the increases in transmission distance causes an increasing of BER and decreasing of Mutual Information (MI) and channel capacity. The relationship between the transmission probability (the probability of transmitting '1') and the MI was also investigated in this chapter. The results illustrated that with the increasing of the transmission probability, the MI increases first, and then reaches the maximum value after that it starts decreasing. The maximum value as known as the channel capacity. The research described in Chapter 4 is based on this PTP uncoded DBMC system model.

- **Chapter 4: Error Correction Codes in PTP DBMC System.** The study in Chapter 4 focused on enhancing the reliability of the MC system by employing ECCs. Two families of ECCs called block codes and convolutional codes were considered to be used in the MC system. For block codes, the Hamming, C-RM and EG-LDPC codes were selected for the use of the system analysis. For convolutional codes, the SOCCs were selected. The propagation and communication channel used for analysing the coded MC system was based on the uncoded channel model introduced in Chapter 3. The BER performance indicated that the introduction of ECCs into MC system does improve the reliability of the MC system. For the proposed system, the (255,175)LDPC code provided the largest coding gain compared to other ECCs. Besides the analysis of BER, the energy consumptions during the encoding and decoding processes were also taken into account under the consideration of three different communication scenarios. The cascade cycle was considered as a basic element to build the logic circuits and the Adenosine triphosphate (ATP) was considered as the basic energy unit to be used to calculate the energy requirements for a proposed system. The energy consumption of the encoder or decoder was supported came from two parts: the energy consumption for operating of logic gates and the energy consumption for synthesizing substrate molecules. The energy efficiency of the MC system was illustrated in two ways, the critical distance and the total energy consumption for a proposed coded system. The critical distance is defined as the real transmission distance when the energy consumption for the uncoded system equals to the energy consumption for the coded system. Thus, when the transmission distance is longer than the critical distance, the ECC is worth appling to the MC system. The energy performance of different coding techniques under different communication scenarios indicated that the critical distance increases and the energy consumption for coded system decreased with increasing operating BER. The most suitable ECC can be selected by analysing the BER and energy efficiency, for a system with a specific operating BER and transmission distance.

- **Chapter 5: A Refined PTP DBMC Model.** In this chapter, a refined PTP DBMC model (R-Model) was presented, where the dependence of number of molecules in different time slots was taken into account. The Binomial distribution of the R-Model was approximated by both the Normal and the Poisson distribution, and the corresponding expressions of BERs were derived. The suitable approximation for a proposed MC system can be determined by measuring the Root Mean Squared Error (RMSE). Furthermore, in this chapter, a comparison between the previous model (P-Model) introduced in Chapter 3 and the R-Model has been illustrated. A simulation process by considering the molecules random walk was also provided to verify the accuracy of these models. The BER performance clearly showed that employing the P-Model into the analysis process can not obtain an accurate estimation of the system performance. Actually, the use of the P-Model overestimates the BER. This has been verified by simulation results. In addition, for the MC system with the specific T_X and R_X, and propagation environment, the suitable approximation that used in performance analysis is dependent on the transmission distance and the number of information molecules that are released from T_X. Generally, for a system that uses a large number of molecules per transmission (N_{tx}), the Normal distribution is more suitable to be used for the analysis. For those systems with a longer transmission distance, the Poisson distribution is more suitable.
- **Chapter 6: A Revised Look at ECCs in PTP DBMC Systems.** In this chapter, the performance of the coded system has been re-investigated by employing the R-Model into the theoretical analysis process. The aim of this chapter was to give a revised look at the use of ECCs in PTP DBMC systems. The BER results indicated that employing the P-Model into the analysis also overestimated the BER of the coded system. Moreover, for a specific transmission distance, the coding gains obtained from the system with the R-Model is smaller than the coding gains from the system with the P-Model. This occurs for all ECCs. Under this case, the energy performance has also been modified. The new results indicated the values of critical distances exist

for all of operating BER levels, and they are higher than the previous results for all communication scenarios.

- **Chapter 7: The Effect of Two-receiver on Broadcast DBMC Systems.** Chapter 7 aimed to investigate the broadcast channel in two-receiver MC systems in two aspects. The first aspect was the investigation of capture probability for each receiver. As was shown in previous chapters (i.e. Chapter 3 and Chapter 5), the capture probability is an important parameter for analysing the system performance, and the expression of the capture probability for the PTP DBMC system exists. However, for a two-receiver system with absorbing receivers, this expression is not valid anymore. In this chapter, a detailed simulation process for capture probabilities of two-receiver broadcast MC has been illustrated and the approximate simulated capture probability (the value when the simulation time is large enough) for each receiver was also compared with the theoretical results. Thus, the behaviour of the simulation was validated. The second aspect was the investigation of the interference between receivers on a broadcast MC system. Here, a system with one T_X and two identical R_Xs that can absorb the same type of information molecules was proposed. One of the R_Xs was considered as an interfering receiver (R_I) and another one was considered as a target receiver (R_T). Considering a system with a fixed position of T_X and R_T, three different positions of R_I were studied. Scenario 1 considered that R_I was located to the left of both T_X and R_T. Scenario 2 considered that R_I was between T_X and R_T. Scenario 3 considered that R_I was located to the right of both T_X and R_T. The effect of the position of R_I on R_T can be reflected in the BER and channel capacity of the target link (communication between T_X and R_T). The results indicated that the positions of R_I in Scenario 2 give the highest impact on the target link than those positions in the other scenarios. In addition, for any scenario, the closer R_I to T_X, the higher impact on R_T.

B. Summary of the conclusions

The main contributions of the thesis come from two aspects: ***Establishing and analysing the performance of the PTP and the two-receiver DBMC systems***

and ***employing ECCs into the PTP DBMC system to enhance the reliability of transmission***.

For the first aspect, the diffusive PTP and two-receiver broadcast MC systems were designed and studied. In this thesis, two channel models were studied for PTP DBMC system, which can be denoted as the P-Model and the R-Model. The Binomial distribution used to model the number of arriving molecules was approximated as the Normal and the Poisson distribution to simplify the calculation process. The RMSE as a decision metric was also introduced to determine which approximation is more suitable for a proposed system. Considering a memory limited channel with an arbitrary ISI length, the closed-form expressions for BER and channel capacity based on both P-Model and R-Model have been derived. The simulation of the random walk of the molecule in a 3D environment was also presented in this thesis to verify the behaviour of the propagation model. The study of the two-receiver DBMC system was focused on the interference between R_I and R_T. By analysing different positions of the R_I, the effects of R_I on R_T in terms of the BER and channel capacity of the target link were shown. Above studies presented a way to analysing the PTP DBMC system, and how to determine the related parameters and the suitable analytic channel model. The related results provided an overview of the performance of the PTP DBMC system based on different parameter settings.

The second aspect, the ECC, as an efficient way to enhance the system performance has been employed into the MC system. There, three of block codes, i.e., Hamming codes, LDPC codes and C-RM codes, and one of the convolutional codes, i.e., SOCC were selected for the use in the PTP DBMC system. Considering different communication scenarios, the performance of the coded DBMC system with regards to BER and energy efficiency were also investigated. The BERs of the coded systems were generated and compared with the uncoded system to show that employing ECCs can enhance the reliability of the MC system. During the investigation of the energy efficiency process, the critical distance was introduced as a metric to determine at which transmission distance, the employment of ECCs into the MC system become beneficial. Through the analysis of BER and critical distance

of the coded system, the system designer can determine if or which ECC should be employed into the proposed MC system.

8.2 Future research

The description of the MC system and the presentation of the related results in this thesis show that the MC has vast potential applications and will benefit lots of manufacturing processes. However, this area is very new, and still has lots of open problems, and new topics which can be investigated in the future. In this section, the future research in this area is presented.

The first direction of the future research is the extension of the current work from the following area:

- **Communication model analysis:**

In this thesis, the primary noise was from the ISI. Thus, all the communication processes introduced in this work only suffer from previous transmission symbols. However, considering MC, many internal and external noises exist, e.g. temperature, environment flow, or other unwanted molecules. These should be considered in the analysis of the channel to avoid an imprecise estimation of the system performance. For this, a noise model which can select different noise sources should be considered in the future. For a specific application environment, a specific noise model can be generated by selecting the corresponding noise sources.

As shown in Chapter 3 and Chapter 5, many channel models had been proposed, and the accuracy of these channel models is an important issue for future development. During the analysis, the consideration of assumptions is a way to simplify the complexity of the analysis process, but it may cause an accuracy reduction of channel estimation. Thus, avoiding the unreliable assumptions is the next step of this work.

Simulating the behaviour of the environment and the random walk of molecules is an efficient way to verify the theoretical analysis. However, the simulation method used in this thesis lacks efficiency. The computation becomes very slow when processing high resolution. Thus, future work may focus on the development of a new method to make the simulation process more efficient.

Furthermore, the detection technique is another key point for the reliability of the transmission process. The OOK as a basis modulation technique that was used for all of the works presented this thesis, and the detection scheme used in here is counting the number of received molecules at the end of each time slot and comparing with the pre-designed threshold to determine the information that was sent at the T_X. Due to the simplicity of this scheme, it can not enhance the accuracy of the detection process. Therefore, more functional detection schemes i.e. ones that contain ISI elimination can be considered as a future research direction.

- **Broadcast channel analysis:**

In this research, a simulation process of the capture probabilities for the two-receiver system has been proposed. There exist opportunities in the research of investigating the closed-form expressions of capture probability for each receiver in a multiple-receiver system. An idea to deal with this problem is modelling the simulation results using a specific general function with several undetermined coefficients of the channel parameters. These coefficients can be estimated by using different approaches methods, i.e. Bayesian approaches.

In this thesis, R_I, R_T and T_X are considered to be centred on the same line, and by changing the positions of R_I along this line, the effect of the R_I on R_T is investigated. This work can be extended by considering more scenarios, for example, when R_I, R_I and T_X are not located on the same line. Furthermore, the investigation of the system with more than one R_I should be considered in the future.

- **Coding techniques:**

As mentioned in Chapter 4, the control and correction of errors that introduced in transmission process are the key points for any communication systems. Here, ECCs have been introduced into the MC system, and the results indicate that the introduction of ECCs does improve the performance of the MC system. Although the technique for building biological circuits is in the process of being developed, there are many issues that may take more time to resolve. Thus, new codes for MC should be investigated. The design of this kind of codes should focus on the simplicity of the construction and ability to correct error. On the other hand, the network coding that normally is used in wireless communication systems

may also be considered as a next work step for enhancing the MC system performance.

The second direction of the future research is experimental research. The experimental research in MC is another important direction for the future work. The experimental work should focus on the construction of the biological environment by using biological cells e.g. bacteria, and through the control of this environment, the DBMC should be studied. Experimental research is the most direct way to verify the theoretical analysis, and can ensure a high level of accuracy of the theoretical results for modelling the future application. However, the experimental research is still in the early stage, so the interdisciplinary collaborations are required for the next step investigation.

Finally, with the rise of the nanotechnology, the DBMC will become a feasible and efficient communication scheme that can benefit lots of applications in the future. Therefore, it is strongly believed that the research presented in this thesis will help system designers to understand the DBMC system and evaluate a more functional MC system.

Bibliography

[1] I. F. Akyildiz, F. Brunetti, and C. Blázquez, "Nanonetworks: A new communication paradigm," *Computer Networks*, vol. 52, pp. 2260-2279, 2008.

[2] R. P. Feynman, "There's plenty of room at the bottom," in *Feynman and computation*, J. G. H. Anthony, Ed., Perseus Books, 1999, pp. 63-76.

[3] N. Taniguchi, "On the basic concept of nanotechnology," in *Proceedings of the International Conference on Production Engineering, Tokyo, Part II, Japan Society of Precision Engineering*, 1974, pp. 18-23.

[4] K. E. Drexler, "Molecular engineering: An approach to the development of general capabilities for molecular manipulation," in *Proceedings of the National Academy of Sciences*, vol. 78, pp. 5275-5278, 1981.

[5] T. Suda, M. Moore, T. Nakano, R. Egashira, A. Enomoto, S. Hiyama, *et al.*, "Exploratory research on molecular communication between nanomachines," in *Genetic and Evolutionary Computation Conference (GECCO), Late Breaking Papers*, 2005, pp.1-5.

[6] A. A. Tseng, K. Chen, C. D. Chen, and K. J. Ma, "Electron beam lithography in nanoscale fabrication: recent development," *IEEE Transactions on Electronics Packaging Manufacturing*, vol. 26, pp. 141-149, 2003.

[7] J. L. Wilbur, A. Kumar, H. A. Biebuyck, E. Kim, and G. M. Whitesides, "Microcontact printing of self-assembled monolayers: applications in microfabrication," *Nanotechnology*, vol. 7, pp. 452 - 457, 1996.

[8] M. Meyyappan, J. Li, J. Li, and A. Cassell, "Nanotechnology: An overview and integration with MEMS," in *Proceedings of the 19th IEEE International Conference on Micro Electro Mechanical Systems (MEMS'06)*, 2006, pp. 1-3.

[9] V. Balzani, A. Credi, S. Silvi, and M. Venturi, "Artificial nanomachines based on interlocked molecular species: recent advances," *Chemical Society Reviews*, vol. 35, pp. 1135-1149, 2006.

[10] G. M. Whitesides, "The once and future nanomachine," *Scientific American*, vol. 285, pp. 78 -83, 2001.

[11] B. Alberts, D. Bray, J. Lewis, M. Raff, K. Roberts, J. D. Watson, *et al.*, "Molecular Biology of the Cell (3rd edn)," *Trends in Biochemical Sciences*, vol. 20, pp. 210-210, 1995.

[12] G. Alfano and D. Miorandi, "On information transmission among nanomachines," *1st International Conference on Nano-Networks and Workshops*, 2006, pp. 1-5.

[13] S. F. Bush, "Wireless ad hoc nanoscale networking," *IEEE Wireless Communications*, vol. 16, pp. 6-7, 2009.

[14] R. A. Freitas, *Nanomedicine*: Landes Bioscience, 1999.

[15] T. Nakano, M. J. Moore, F. Wei, A. V. Vasilakos, and J. Shuai, "Molecular communication and networking: Opportunities and challenges," *IEEE Transactions on NanoBioscience*, vol. 11, pp. 135-148, 2012.

[16] N. Farsad, H. B. Yilmaz, A. Eckford, C.-B. Chae, and W. Guo, "A comprehensive survey of recent advancements in molecular communication," *arXiv preprint arXiv:1410.4258*, 2014.

[17] M. Pierobon and I. F. Akyildiz, "A physical end-to-end model for molecular communication in nanonetworks," *IEEE Journal on Selected Areas in Communications*, vol. 28, pp. 602-611, 2010.

[18] I. F. Akyildiz and J. M. Jornet, "The internet of nano-things," *IEEE Wireless Communications*, vol. 17, pp. 58-63, 2010.

[19] T. Nakano, M. J. Moore, F. Wei, A. V. Vasilakos, and J. Shuai, "Molecular Communication and Networking: Opportunities and Challenges," *IEEE Transactions on NanoBioscience,* vol. 11, pp. 135-148, 2012.

[20] M. J. Moore and T. Nakano, "Comparing transmission, propagation, and receiving options for nanomachines to measure distance by molecular communication," in *IEEE International Conference on Communications (ICC)*, 2012, pp. 6132-6136.

[21] T. Nakano, T. Suda, M. Moore, R. Egashira, A. Enomoto, and K. Arima, "Molecular communication for nanomachines using intercellular calcium signaling," in *5th IEEE Conference on Nanotechnology*, 2005, pp. 478-481.

[22] T. Nakano, Y. Okaie, and A. V. Vasilakos, "Throughput and efficiency of molecular communication between nanomachines," in *IEEE Wireless Communications and Networking Conference (WCNC)*, 2012, pp. 704-708.

[23] M. Ş. Kuran, H. B. Yilmaz, T. Tugcu, and B. Özerman, "Energy model for communication via diffusion in nanonetworks," *Nano Communication Networks,* vol. 1, pp. 86-95, 2010.

[24] D. Kilinc and O. B. Akan, "Receiver Design for Molecular Communication," *IEEE Journal on Selected Areas in Communications,* vol. 31, pp. 705-714, 2013.

[25] M. Ş. Kuran, H. B. Yilmaz, T. Tugcu, and I. F. Akyildiz, "Modulation Techniques for Communication via Diffusion in Nanonetworks," in *IEEE International Conference on Communications (ICC)*, 2011, pp. 1-5.

[26] F. M. Raymo, "Digital Processing and Communication with Molecular Switches," *Advanced Materials,* vol. 14, pp. 401-414, 2002.

[27] A. P. de Silva and N. D. McClenaghan, "Molecular-Scale Logic Gates," *Chemistry – A European Journal,* vol. 10, pp. 574-586, 2004.

[28] H. M. Sauro and B. N. Kholodenko, "Quantitative analysis of signaling networks," *Progress in biophysics and molecular biology,* vol. 86, pp. 5-43, 2004.

[29] K. E. Drexler, *Nanosystems: molecular machinery, manufacturing, and computation*: John Wiley & Sons, Inc., 1992.

[30] B. Atakan, *Molecular Communications and Nanonetworks*: Springer, 2014.

[31] T. Nakano, A. W. Eckford, and T. Haraguchi, *Molecular communication*: Cambridge University Press, 2013.

[32] Y. Moritani, S. Hiyama, and T. Suda, "A Molecular Communication System," in *Natural Computing: 4th International Workshop on Natural Computing*, Springer Japan, 2010, pp. 82-89.

[33] N. Rikhtegar and M. Keshtgary, "A brief survey on molecular and electromagnetic communications in nano-networks," *International Journal of Computer Applications*, vol. 79, 2013.

[34] T. Nakano, T. Suda, Y. Okaie, M. J. Moore, and A. V. Vasilakos, "Molecular communication among biological nanomachines: A layered architecture and research issues," *IEEE Transactions on NanoBioscience*, vol. 13, pp. 169-197, 2014.

[35] C. Bustamante, Y. R. Chemla, N. R. Forde, and D. Izhaky, "Mechanical Processes in Biochemistry," *Annual Review of Biochemistry*, vol. 73, pp. 705-748, 2004.

[36] M. Moore, A. Enomoto, T. Nakano, R. Egashira, T. Suda, A. Kayasuga, *et al.*, "A design of a molecular communication system for nanomachines using molecular motors," in *Pervasive Computing and Communications Workshops*, 2006, pp. 554 - 559.

[37] V. Serreli, C.-F. Lee, E. R. Kay, and D. A. Leigh, "A molecular information ratchet," *Nature*, vol. 445, pp. 523-527, 2007.

[38] B. Atakan and O. B. Akan, "Deterministic capacity of information flow in molecular nanonetworks," *Nano Communication Networks*, vol. 1, pp. 31-42, 2010.

[39] M. Pierobon and I. F. Akyildiz, "Diffusion-Based Noise Analysis for Molecular Communication in Nanonetworks," *IEEE Transactions on Signal Processing*, vol. 59, pp. 2532-2547, 2011.

[40] S. Hiyama, T. Inoue, T. Shima, Y. Moritani, T. Suda, and K. Sutoh, "Autonomous Loading, Transport, and Unloading of Specified Cargoes by Using DNA Hybridization and Biological Motor‐Based Motility," *Small*, vol. 4, pp. 410-415, 2008.

[41] M. J. Moore, T. Suda, and K. Oiwa, "Molecular communication: modeling noise effects on information rate," *IEEE Transactions on NanoBioscience*, vol. 8, pp. 169-180, 2009.

[42] T. Nakano, T. Suda, M. Moore, R. Egashira, A. Enomoto, and K. Arima, "Molecular communication for nanomachines using intercellular calcium signaling," in *5th IEEE Conference on Nanotechnology*, 2005, pp. 478-481.

[43] T. Nakano, T. Suda, T. Koujin, T. Haraguchi, and Y. Hiraoka, "Molecular communication through gap junction channels," *Transactions on Computational Systems Biology X*, Springer, 2008, pp. 81-99.

[44] T. Nakano, Y.-H. Hsu, W. C. Tang, T. Suda, D. Lin, T. Koujin, *et al.*, "Microplatform for intercellular communication," in *3rd IEEE International Conference on Nano/Micro Engineered and Molecular Systems*, 2008, pp. 476-479.

[45] L. C. Cobo and I. F. Akyildiz, "Bacteria-based communication in nanonetworks," *Nano Communication Networks*, vol. 1, pp. 244-256, 2010.

[46] M. Gregori and I. F. Akyildiz, "A new nanonetwork architecture using flagellated bacteria and catalytic nanomotors," *IEEE Journal on Selected Areas in Communications*, vol. 28, pp. 612-619, 2010.

[47] M. Gregori, I. Llatser, A. Cabellos-Aparicio, and E. Alarcón, "Physical channel characterization for medium-range nanonetworks using flagellated bacteria," *Computer Networks*, vol. 55, pp. 779-791, 2011.

[48] M. J. Berridge, "The AM and FM of calcium signalling," *Nature*, vol. 386, pp. 759-760, 1997.

[49] D. L. Nelson, A. Lehninger, M. M. Cox, M. Osgood, and K. Ocorr, *Lehninger Principles of Biochemistry / The Absolute, Ultimate Guide to Lehninger Principles of Biochemistry*: Macmillan Higher Education, 2008.

[50] L. Parcerisa Giné and I. F. Akyildiz, "Molecular communication options for long range nanonetworks," *Computer Networks,* vol. 53, pp. 2753-2766, 2009.

[51] S. Hiyama, Y. Moritani, T. Suda, R. Egashira, A. Enomoto, M. Moore, *et al.*, "Molecular communication," *Journal-Institute of Electronics Information and Communication Engineers,* vol. 89, 2006.

[52] M. U. Mahfuz, D. Makrakis, and H. T. Mouftah, "On the characterization of binary concentration-encoded molecular communication in nanonetworks," *Nano Communication Networks,* vol. 1, pp. 289-300, 2010.

[53] N. Garralda, I. Llatser, A. Cabellos-Aparicio, E. Alarcón, and M. Pierobon, "Diffusion-based physical channel identification in molecular nanonetworks," *Nano Communication Networks,* vol. 2, pp. 196-204, 2011.

[54] K. Na-Rae and C. Chan-Byoung, "Novel modulation techniques using isomers as messenger molecules for molecular communication via diffusion," in *IEEE International Conference on Communications (ICC)*, 2012, pp. 6146-6150.

[55] B. Krishnaswamy, C. M. Austin, J. P. Bardill, D. Russakow, G. L. Holst, B. K. Hammer, *et al.*, "Time-elapse communication: Bacterial communication on a microfluidic chip," *IEEE Transactions on Communications,* vol. 61, pp. 5139-5151, 2013.

[56] B. Tepekule, A. E. Pusane, H. B. Yilmaz, and T. Tugcu, "Energy efficient ISI mitigation for communication via diffusion," in *IEEE International Black Sea Conference on Communications and Networking (BlackSeaCom)*, 2014, pp. 33-37.

[57] B. Atakan, S. Galmés, and O. B. Akan, "Nanoscale communication with molecular arrays in nanonetworks," *IEEE Transactions on NanoBioscience,* vol. 11, pp. 149-160, 2012.

[58] B. Atakan and O. B. Akan, "An information theoretical approach for molecular communication," in *Bio-Inspired Models of Network, Information and Computing Systems*, 2007, pp. 33-40.

[59] A. Einolghozati, M. Sardari, and F. Fekri, "Capacity of diffusion-based molecular communication with ligand receptors," in *IEEE Information Theory Workshop (ITW)*, 2011, pp. 85-89.

[60] D. Arifler, "Capacity analysis of a diffusion-based short-range molecular nano-communication channel," *Computer Networks*, vol. 55, pp. 1426-1434, 2011.

[61] B. Atakan, "Optimal transmission probability in binary molecular communication," *IEEE Communications Letters*, vol. 17, pp. 1152-1155, 2013.

[62] T. Nakano, Y. Okaie, and J.-Q. Liu, "Channel model and capacity analysis of molecular communication with Brownian motion," *IEEE Communications Letters*, vol. 16, pp. 797-800, 2012.

[63] J. Crank, *The mathematics of diffusion*: Oxford university press, 1979.

[64] K. Srinivas, A. W. Eckford, and R. S. Adve, "Molecular communication in fluid media: The additive inverse gaussian noise channel," *IEEE Transactions on Information Theory*, vol. 58, pp. 4678-4692, 2012.

[65] H. Li, S. M. Moser, and D. Guo, "Capacity of the memoryless additive inverse gaussian noise channel," *IEEE Journal on Selected Areas in Communications*, vol. 32, pp. 2315-2329, 2014.

[66] H. ShahMohammadian, G. G. Messier, and S. Magierowski, "Nano-machine molecular communication over a moving propagation medium," *Nano Communication Networks*, vol. 4, pp. 142-153, 2013.

[67] P. Cuatrecasas, "Membrane Receptors," *Annual Review of Biochemistry*, vol. 43, pp. 169-214, 1974.

[68] M. S. Leeson and M. D. Higgins, "Forward error correction for molecular communications," *Nano Communication Networks*, vol. 3, pp. 161-167, 2012.

[69] H. Arjmandi, A. Gohari, M. N. Kenari, and F. Bateni, "Diffusion-based nanonetworking: A new modulation technique and performance analysis," *IEEE Communications Letters,* vol. 17, pp. 645-648, 2013.

[70] M. U. Mahfuz, D. Makrakis, and H. T. Mouftah, "Strength-based optimum signal detection in concentration-encoded pulse-transmitted OOK molecular communication with stochastic ligand-receptor binding," *Simulation Modelling Practice and Theory,* vol. 42, pp. 189-209, 2014.

[71] M. Pierobon and I. F. Akyildiz, "Noise analysis in ligand-binding reception for molecular communication in nanonetworks," *IEEE Transactions on Signal Processing,* vol. 59, pp. 4168-4182, 2011.

[72] E. Gul, B. Atakan, and O. B. Akan, "NanoNS: A nanoscale network simulator framework for molecular communications," *Nano Communication Networks,* vol. 1, pp. 138-156, 2010.

[73] I. Llatser, D. Demiray, A. Cabellos-Aparicio, D. T. Altilar, and E. Alarcón, "N3Sim: Simulation framework for diffusion-based molecular communication nanonetworks," *Simulation Modelling Practice and Theory,* vol. 42, pp. 210-222, 2014.

[74] L. Felicetti, M. Femminella, and G. Reali, "A simulation tool for nanoscale biological networks," *Nano Communication Networks,* vol. 3, pp. 2-18, 2012.

[75] L. Felicetti, M. Femminella, and G. Reali, "Simulation of molecular signaling in blood vessels: Software design and application to atherogenesis," *Nano Communication Networks,* vol. 4, pp. 98-119, 2013.

[76] L. Felicetti, M. Femminella, G. Reali, P. Gresele, and M. Malvestiti, "Simulating an in vitro experiment on nanoscale communications by using BiNS2," *Nano Communication Networks,* vol. 4, pp. 172-180, 2013.

[77] H. B. Yilmaz and C.-B. Chae, "Simulation study of molecular communication systems with an absorbing receiver: Modulation and ISI mitigation techniques," *Simulation Modelling Practice and Theory,* vol. 49, pp. 136-150, 2014.

[78] R. Weiss and T. F. Knight Jr, "Engineered communications for microbial robotics," *DNA Computing*, Springer, 2000, pp. 1-16.

[79] A. Tamsir, J. J. Tabor, and C. A. Voigt, "Robust multicellular computing using genetically encoded NOR gates and chemical 'wires'," *Nature*, vol. 469, pp. 212-215, 2011.

[80] W. Bacchus and M. Fussenegger, "Engineering of synthetic intercellular communication systems," *Metabolic engineering*, vol. 16, pp. 33-41, 2013.

[81] M. E. Ortiz and D. Endy, "Engineered cell-cell communication via DNA messaging," *Journal of biological engineering*, vol. 6, 2012.

[82] N. Farsad, W. Guo, and A. W. Eckford, "Tabletop molecular communication: Text messages through chemical signals," *PloS one*, vol. 8, p. e82935, 2013.

[83] S. Qiu, W. Guo, S. Wang, N. Farsad, and A. Eckford, "A molecular communication link for monitoring in confined environments," *IEEE International Conference on Communications Workshops (ICC)*, 2014, pp. 718-723.

[84] C. Lee, B. Koo, N. R. Kim, B. Yilmaz, N. Farsad, A. Eckford, *et al.*, "Molecular MIMO communication link," in *IEEE Conference on Computer Communications Workshops (INFOCOM WKSHPS)*, 2015, pp. 13-14.

[85] R. Freitasjr, "What is nanomedicine? Nanomedicine: nanotechnology," *Nanomedicine: Nanotechnology, Biology and Medicine*, vol. 1, pp. 2-9, 2005.

[86] Y. Moritani, S. Hiyama, and T. Suda, "Molecular communication for health care applications," in *4th Annual IEEE International Conference on Pervasive computing and communications workshops*, 2006, pp. 549-553.

[87] B. Atakan, O. B. Akan, and S. Balasubramaniam, "Body area nanonetworks with molecular communications in nanomedicine," *IEEE Communications Magazine*, vol. 50, pp. 28-34, 2012.

[88] T. M. Allen and P. R. Cullis, "Drug delivery systems: entering the mainstream," *Science*, vol. 303, pp. 1818-1822, 2004.

[89] D. Tessier, I. Radu, and M. Filteau, "Antimicrobial fabrics coated with nano-sized silver salt crystals," in *NSTI Nanotechnology*, 2005, pp. 762-764.

[90] J. W. Aylott, "Optical nanosensors—an enabling technology for intracellular measurements," *Analyst,* vol. 128, pp. 309-312, 2003.

[91] R. Byrne and D. Diamond, "Chemo/bio-sensor networks," *Nature Materials,* vol. 5, pp. 421-424, 2006.

[92] J. Han, J. Fu, and R. B. Schoch, "Molecular sieving using nanofilters: past, present and future," *Lab on a Chip,* vol. 8, pp. 23-33, 2008.

[93] M. S. Dresselhaus, R. E. Smalley, G. Dresselhaus, and P. Avouris, *Carbon Nanotubes: Synthesis, Structure, Properties, and Applications*: Springer Berlin Heidelberg, 2001.

[94] M. Pierobon and I. F. Akyildiz, "Capacity of a Diffusion-Based Molecular Communication System With Channel Memory and Molecular Noise," *IEEE Transactions on Information Theory,* vol. 59, pp. 942-954, 2013.

[95] S. P. Leary, C. Y. Liu, and M. L. Apuzzo, "Toward the emergence of nanoneurosurgery: part III--nanomedicine: targeted nanotherapy, nanosurgery, and progress toward the realization of nanoneurosurgery," *Neurosurgery,* vol. 62, p. E1384, 2008.

[96] D. A. LaVan, T. McGuire, and R. Langer, "Small-scale systems for in vivo drug delivery," *Nature Biotechnology,* vol. 21, pp. 1184-1191, 2003.

[97] A. G. Thombre, J. R. Cardinal, A. R. DeNoto, S. M. Herbig, and K. L. Smith, "Asymmetric membrane capsules for osmotic drug delivery: I. Development of a manufacturing process," *Journal of Controlled Release,* vol. 57, pp. 55-64, 1999.

[98] S. Nain and N. N. Sharma, "Propulsion of an artificial nanoswimmer: a comprehensive review," *Frontiers in Life Science,* pp. 1-16, 2014.

[99] J. M. Jornet and I. F. Akyildiz, "Joint energy harvesting and communication analysis for perpetual wireless nanosensor networks in the terahertz band," *IEEE Transactions on Nanotechnology,* vol. 11, pp. 570-580, 2012.

[100] Y. Lu, M. D. Higgins, and M. S. Leeson, "Comparison of Channel Coding Schemes for Molecular Communications Systems," *IEEE Transactions on Communications,* vol. 63, pp. 3991-4001, 2015.

[101] Verdu, x, S., and H. Te, "A general formula for channel capacity," *IEEE Transactions on Information Theory,* vol. 40, pp. 1147-1157, 1994.

[102] T. Nakano, Y. Okaie, and L. Jian-Qin, "Channel Model and Capacity Analysis of Molecular Communication with Brownian Motion," *IEEE Communications Letters,* vol. 16, pp. 797-800, 2012.

[103] J. J. Kim and K. Park, "Modulated insulin delivery from glucose-sensitive hydrogel dosage forms," *Journal of Controlled Release,* vol. 77, pp. 39-47, 2001.

[104] C. C. Miller, "The Stokes-Einstein Law for Diffusion in Solution," *Proceedings of the Royal Society of London. Series A, Containing Papers of a Mathematical and Physical Character,* vol. 106, pp. 724-749, 1924.

[105] K. Pin-Yu, L. Yen-Chi, P. C. Yeh, L. Chia-han, and K. C. Chen, "A new paradigm for channel coding in diffusion-based molecular communications: Molecular coding distance function," in *IEEE Global Communications Conference (GLOBECOM)*, 2012, pp. 3748-3753.

[106] S. Po-Jen, L. Chia-Han, Y. Ping-Cheng, and C. Kwang-Cheng, "Channel Codes for Reliability Enhancement in Molecular Communication," *IEEE Journal on Selected Areas in Communications,* vol. 31, pp. 857-867, 2013.

[107] B. Chenyao, M. S. Leeson, and M. D. Higgins, "Minimum energy channel codes for molecular communications," *Electronics Letters,* vol. 50, pp. 1669-1671, 2014.

[108] R. W. Hamming, "Error detecting and error correcting codes," *Bell System technical journal,* vol. 29, pp. 147-160, 1950.

[109] D. E. Muller, "Application of Boolean algebra to switching circuit design and to error detection," *Transactions of the I.R.E. Professional Group on Electronic Computers,* vol. EC-3, pp. 6-12, 1954.

[110] I. Reed, "A class of multiple-error-correcting codes and the decoding scheme," *Transactions of the IRE Professional Group on Information Theory,* vol. 4, pp. 38-49, 1954.

[111] S. Boztas and I. E. Shparlinski, *Applied Algebra, Algebraic Algorithms and Error-Correcting Codes: 14th International Symposium, AAECC-14, Melbourne, Australia, Proceedings*: Springer, 2001.

[112] W. W. Peterson and E. J. Weldon, *Error-correcting Codes*: MIT Press, 1972.

[113] T. Kasami, L. Shu, and W. Peterson, "New generalizations of the Reed-Muller codes--I: Primitive codes," *IEEE Transactions on Information Theory,* vol. 14, pp. 189-199, 1968.

[114] R. G. Gallager, "Low-density parity-check codes," *IRE Transactions on Information Theory,* vol. 8, pp. 21-28, 1962.

[115] R. M. Tanner, "A recursive approach to low complexity codes," *IEEE Transactions on Information Theory,* vol. 27, pp. 533-547, 1981.

[116] D. J. MacKay and R. M. Neal, "Near Shannon limit performance of low density parity check codes," *Electronics letters,* vol. 33, pp. 457-458, 1997.

[117] G. D. Forney, R. E. Blahut, and R. Koetter, *Codes, Graphs, and Systems: A Celebration of the Life and Career of G. David Forney, Jr. on the Occasion of His Sixtieth Birthday*: Springer US, 2002.

[118] K. Yu, L. Shu, and M. P. C. Fossorier, "Low-density parity-check codes based on finite geometries: a rediscovery and new results," *IEEE Transactions on Information Theory,* vol. 47, pp. 2711-2736, 2001.

[119] T. K. Moon, *Error Correction Coding: Mathematical Methods and Algorithms*: Wiley, 2005.

[120] J. C. Moreira and P. G. Farrell, *Essentials of Error-Control Coding*: Wiley, 2006.

[121] P. Reviriego, J. A. Maestro, and M. F. Flanagan, "Error Detection in Majority Logic Decoding of Euclidean Geometry Low Density Parity Check (EG-

LDPC) Codes," *IEEE Transactions on Very Large Scale Integration (VLSI) Systems,* vol. 21, pp. 156-159, 2013.

[122] K. Ganesan, P. Grover, and J. Rabaey, "The power cost of over-designing codes," in *IEEE Workshop on Signal Processing Systems (SiPS),* 2011, pp. 128-133.

[123] P. Grover and A. Sahai, "Green codes: Energy-efficient short-range communication," in *IEEE International Symposium on Information Theory (ISIT),* 2008, pp. 1178-1182.

[124] S. Bougeard, J. F. Helard, and J. Citerne, "A new algorithm for decoding concatenated CSOCs: application to very high bit rate transmissions," in *IEEE International Conference on Personal Wireless Communication*, 1999, pp. 399-403.

[125] S. Lin and D. J. Costello, *Error control coding: fundamentals and applications*: Prentice-Hall, 1983.

[126] M. Kavehrad, "Implementation of a self-orthogonal convolutional code used in satellite communications," *IEE Journal on Electronic Circuits and Systems,* vol. 3, pp. 134-138, 1979.

[127] R. Townsend and E. Weldon, "Self-orthogonal quasi-cyclic codes," *IEEE Transactions on Information Theory,* vol. 13, pp. 183-195, 1967.

[128] S. L. Howard, C. Schlegel, and K. Iniewski, "Error control coding in low-power wireless sensor networks: When is ECC energy-efficient?," *EURASIP Journal on Wireless Communications and Networking*, vol. 2006, pp. 1-14, 2006.

[129] J. Levine, H. Y. Kueh, and L. Mirny, "Intrinsic fluctuations, robustness, and tunability in signaling cycles," *Biophysical Journal,* vol. 92, pp. 4473-4481, 2007.

[130] S. Balasubramaniam and J. Kangasharju, "Realizing the Internet of Nano Things: Challenges, Solutions, and Applications," *Computer,* vol. 46, pp. 62-68, 2013.

[131] E. Shacter, P. B. Chock, and E. R. Stadtman, "Energy consumption in a cyclic phosphorylation/dephosphorylation cascade," *Journal of Biological Chemistry*, vol. 259, pp. 12260-12264, 1984.

[132] R. E. Blahut, *Algebraic Codes for Data Transmission*: Cambridge University Press, 2003.

[133] F. J. MacWilliams and N. J. A. Sloane, *The Theory of Error-correcting Codes*: North-Holland Publishing Company, 1977.

[134] W. Ryan and S. Lin, *Channel Codes: Classical and Modern*: Cambridge University Press, 2009.

[135] H. Min-Hsiu, Y. Wen-Tai, and H. Li-Yi, "High Performance Entanglement-Assisted Quantum LDPC Codes Need Little Entanglement," *IEEE Transactions on Information Theory*, vol. 57, pp. 1761-1769, 2011.

[136] K. Yu, L. Shu, and M. P. C. Fossorier, "Low density parity check codes: construction based on finite geometries," in *IEEE Global Telecommunications Conference (GLOBECOM '00)*, 2000, pp. 825-829.

[137] E. J. Weldon and Jr., "Euclidean geometry cyclic codes," in *Proceedings of the Symposium on Combinatorial Mathematics*, University of North Carolina, Chapel Hill, NC, 1967.

[138] P. Elias, "Coding for noisy channels," in *Proceedings of the Institute of Radio Engineers*, 1955, pp. 356-356.

[139] M. Ş. Kuran, H. B. Yilmaz, T. Tugcu, and I. F. Akyildiz, "Interference effects on modulation techniques in diffusion based nanonetworks," *Nano Communication Networks*, vol. 3, pp. 65-73, 2012.

[140] K. Na-Rae, A. W. Eckford, and C. Chan-byoung, "Symbol Interval Optimization for Molecular Communication With Drift," *IEEE Transactions on NanoBioscience*, vol. 13, pp. 223-229, 2014.

[141] A. Aijaz and A. H. Aghvami, "Error Performance of Diffusion-Based Molecular Communication Using Pulse-Based Modulation," *IEEE Transactions on NanoBioscience*, vol. 14, pp. 146-151, 2015.

[142] M. S. Leeson and M. D. Higgins, "Error correction coding for molecular communications," in *IEEE International Conference on Communications (ICC)*, 2012, pp. 6172-6176.

[143] M. S. Kuran, H. B. Yilmaz, and T. Tugcu, "A tunnel-based approach for signal shaping in molecular communication," in *IEEE International Conference on Communications Workshops (ICC)*, 2013, pp. 776-781.

[144] G. Genc, H. B. Yilmaz, and T. Tugcu, "Reception enhancement with protrusions in communication via diffusion," in *First International Black Sea Conference on Communications and Networking (BlackSeaCom)*, 2013, pp. 89-93.

[145] H. B. Yilmaz and C. Chan-byoung, "Arrival modelling for molecular communication via diffusion," *Electronics Letters*, vol. 50, pp. 1667-1669, 2014.

[146] A. Heren, H. Yilmaz, C. Chae, and T. Tugcu, "Effect of Degradation in Molecular Communication: Impairment or Enhancement?," *IEEE Transactions on Molecular, Biological and Multi-Scale Communications*, vol. 1, pp. 217-229, 2015.

[147] O. Ibe, *Fundamentals of Applied Probability and Random Processes*: Elsevier Science, 2014.

[148] H. C. Berg, *Random Walks in Biology*: Princeton University Press, 1993.

[149] B. H. Koo, C. Lee, H. B. Yilmaz, N. Farsad, A. Eckford, and C. B. Chae, "Molecular MIMO: From Theory to Prototype," *IEEE Journal on Selected Areas in Communications*, vol. 34, pp. 600-614, 2016.

[150] H. ShahMohammadian, G. G. Messier, and S. Magierowski, "Optimum receiver for molecule shift keying modulation in diffusion-based molecular communication channels," *Nano Communication Networks*, vol. 3, pp. 183-195, 2012.

[151] H. B. Yilmaz, A. C. Heren, T. Tugcu, and C. B. Chae, "Three-Dimensional Channel Characteristics for Molecular Communications With an Absorbing Receiver," *IEEE Communications Letters*, vol. 18, pp. 929-932, 2014.

[152] B. Atakan and O. B. Akan, "On molecular multiple-access, broadcast, and relay channels in nanonetworks," presented at the Proceedings of the 3rd International Conference on Bio-Inspired Models of Network, Information and Computing Sytems, Hyogo, Japan, 2008.

[153] L. S. Meng, P. C. Yeh, K. C. Chen, and I. F. Akyildiz, "MIMO communications based on molecular diffusion," in *IEEE Global Communications Conference (GLOBECOM)*, 2012, pp. 5380-5385.

[154] S. F. Bush, *Nanoscale Communication Networks*: Artech House, 2010.

[155] H. Sano, "Solutions to the Smoluchowski equation for problems involving the anisotropic diffusion or absorption of a particle," *The Journal of Chemical Physics*, vol. 74, pp. 1394-1400, 1981.

[156] W. Mendenhall, R. Beaver, and B. Beaver, *Introduction to Probability and Statistics*: Cengage Learning, 2012.